1996

The Behaviour Of Transmission Lines Under High Winds

Souza Acir Loredo

THE BEHAVIOUR OF TRANSMISSION LINES UNDER HIGH WINDS

by

Acir Mércio Loredo Souza

Faculty of Engineering Science
Department of Civil Engineering

Submitted in partial fulfilment
of the requirements for the degree of
Doctor of Philosophy

Faculty of Graduate Studies
The University of Western Ontario
London, Ontario
July 1996

ISBN 0-612-15065-8

ABSTRACT

The behaviour of transmission lines under severe winds is examined.

Firstly, the effect of scale of turbulence on the response of a line-like structure (cable model) is investigated through wind tunnel tests, and the experimental results are successfully compared with theoretical predictions made through the statistical method using influence lines. Consistency with theory allows for the development of a new modelling approach to conductor systems using a distorted horizontal (spanwise) scale to accommodate these systems in the wind tunnel. Cables with different characteristics are simulated and tested at transverse and oblique wind incidences.

The model cables are successful in reproducing full-scale behaviour of transmission lines. The results obtained demonstrate the effect of turbulence in the dynamic response. Resonant response can be important in the total response depending on the characteristics of the structure and of the wind flow. Aerodynamic damping plays an important role in the dynamic behaviour of the cables. Correlation and coherence between cable forces were found to diminish with increasing separation between cables.

Secondly, using a theoretical approach, the design procedure for the establishment of wind loading on transmission towers is reviewed and current procedures, such as Davenport's Gust Response Factor (GRF), are compared with the statistical method using influence lines (SIL), which is considered more realistic.

Peak loads calculated using SIL were larger than peak loads given by the GRF and by a typical Utility Company method by about 20% to 30%. It is found that the

dynamic response of transmission structures is strongly dependent on the turbulence intensity level and is sensitive to the structures' design parameters. For members in which there is reversal in the member forces depending on the load position, the resonant response in the second mode of vibration was bigger, even by four to five times, than the corresponding one in the first mode. This may lead to fatigue problems.

À minha família,
e em especial aos meus pais,
dedico este trabalho.

ACKNOWLEDGEMENTS

First of all, I would like to thank my supervisor Dr. Alan Garnett Davenport, from whom I have learned a great deal, for his enthusiasm, guidance and friendship throughout this research and for allowing me the privilege of studying under his supervision. Most gratifying of all was to discover the "big person" who fills up the "big name". I am very grateful for the warm treatment and hospitality extended to me and my family by Dr. Davenport and Ms. Sheila Davenport during our stay in Canada.

I would like to express my gratitude to everyone at the Boundary Layer Wind Tunnel Laboratory - faculty, staff and students. All helped me to make these past four years at the BLWTL an enjoyable and fruitful experience. Special thanks go to Dr. T. C. Eric Ho for his friendship, encouragement and for being always there when help was needed. Special thanks are extended to Mr. Mike Mikitiuk, Dr. David Surry, Ms. Karen Norman and Ms. Tanya Spruyt. The special help and abilities provided by Mr. Anthony Burggraaf during the experimental work are gratefully acknowledged. Many thanks to the several suggestions and friendship received from Mr. Yasushi Watanabe and Dr. N. Lakshmanan during their stay in the BLWTL. Fellow students and friends Juan Pablo Raggio Quintas, Robert E. Morden, Klaus P. Thiele, Rogério Noal Monteiro and Augusto Zumarraga were very generous in giving their time for that extra help needed. My chum and future Dr. Juan Pablo Raggio Quintas was very active in all the "background operation" that helped the completion of this work, and deserves a special thanks.

The financial support provided by the Brazilian National Research Council, CNPq, is gratefully appreciated. Dr. José Carlos Ferraz Hennemann and very specially Dr. Joaquim Blessmann, both from the Universidade Federal do Rio Grande do Sul in Porto Alegre, are very much thanked for providing the necessary incentive (and recommendation letters) for me to come to Western. Dr. Blessmann has always been a source of encouragement, a big and dear friend and an example to follow.

Above all, I thank my family, here and back home, for their tremendous support throughout this time. For being a very special part of me, and for all the love and encouragement provided, I deeply thank my parents, my sisters and my grandmother, who was not able to physically wait for our return home. Very specially thanked is also my wife Adriana for her love, support and encouragement, in spite of the many sacrifices, and for giving me Juliana, a precious gift who came into our lives in the course of this work.

TABLE OF CONTENTS

LIST OF TABLES

LIST OF FIGURES

NOMENCLATURE

Symbol	Units	Description
A	m^2	total area enclosed by the frame
A_c	m^2	area of cable cross section
A_s	m^2	projected area of the individual members of a frame
B_c	-	dimensionless response term corresponding to the quasi-static background wind loading on the wire (conductor or ground wire)
B_t	-	dimensionless response term corresponding to the quasi-static background wind loading on the tower
C	-	exponential decay factor for "narrow band" correlation
C_{crit}	-	critical modal damping
C_D	-	drag coefficient
C_F	-	force coefficient
C_j^*	-	modal damping at mode j
d	m	diameter of wire (conductor or ground wire)
D	m	characteristic width of a structure
E	Pa	modulus of elasticity of the material
E_x	-	exposure factor
f	Hz	structure/member natural frequency

f_{cj}	Hz	natural frequency for horizontal sway of the wire (conductor or ground wire) in mode j
f_{Tj}	Hz	natural frequency of the transmission structure in the transverse direction in mode j
F	N	wind force
g	m/s^2	gravitational acceleration, constant, 9.81
g_s	-	statistical peak factor for gust response of a component
G	-	gust response factor
G_c	-	gust response factor for the cable (conductor or ground wire)
G_t	-	gust response factor for the tower
h_o	m	effective height of structure
H	m	total height of structure above ground
H_t	N	horizontal line tension (horizontal component of T at support)
i	-	influence line
I_v	-	intensity of turbulence
j	-	mode of vibration
k	-	Von Kármán constant, 0.40
l	m	length of the cable
L	m	design wind span of the wires (conductor or ground wire), characteristic length

${}^{x}L_v$	m	transverse integral scale of turbulence
${}^{y}L_v$	m	longitudinal integral scale of turbulence
${}^{z}L_v$	m	vertical scale of longitudinal turbulence
m	kg/m	mass per unit length
M	kg	generalized mass, total mass
n	-	reduced frequency
p	Pa	wind pressure
q	Pa	dynamic velocity pressure
Q_j	N	modal generalized force
R_c	-	dimensionless resonant response term of the wire (conductor or ground wire)
R_s	N	rated strength
R_t	-	dimensionless resonant response term of the structure
R_{xx}'	-	cross-correlation coefficient
Re	-	Reynolds number
S	m	cable (conductor or ground wire) sag at midspan
S_f	-	span factor
$S_F(f)$	-	spectrum of the force
$S_Q(f)$	-	spectrum of the modal generalized force
St	-	Strouhal number
t	-	time
T	N	line tension

u_*	m/s	friction velocity
U	N	vertical line tension (vertical component of T at support)
$v(t)$	m/s	fluctuating component of windspeed
V_z	m/s	wind speed at height z
$\overline{V}$	m/s	mean wind speed
w	N/m	wire weight per unit length
w_1	m	width
$\tilde{x}_j(x)$	-	jth cable mode shape in x direction
$\tilde{y}_j(x)$	-	jth cable mode shape in y direction
$\tilde{z}_j(x)$	-	jth cable mode shape in z direction
z	m	height above ground
z_c	m	reference height for conductors
z_0	m	roughness length
α	-	power-law exponent
β	°	angle between horizontal and tangent to cable at support
γ	–	percentage of span used in the distorted model
Δl	m	change in length of cable due to T
ΔS	m	change in sag of cable
ε_j	-	nondimensional frequency parameter for cable symmetrical in-plane mode
ϕ	-	the solidity ratio (A_f/A)

ζ	-	total damping
ζ_{aj}	-	aerodynamic damping in the j^{th} mode
ζ_s	-	structural damping
κ	-	surface drag coefficient
λ	-	ratio of model and prototype quantities, scale
λ^2	-	cable stiffness parameter [after Irvine(1981)]
μ_j	-	j^{th} mode shape
ν	m^2/s	kinematic viscosity of the air
ω	rad/s	natural circular frequency of vibration ($= 2\pi f$)
ρ	kg/m^3	cable density
ρ_a	kg/m^3	air density
σ	m/s , N	standard deviation (wind speed, force)
υ	-	crossing rate

Special notation

Symbol	Description
$(\ )_m$	denotes model
$(\ )_m^*$	denotes distorted model
$(\ )_p$	denotes prototype

Units

The International System of Units (SI) is generally used in this thesis, except in a few cases where British and/or technical units are used for convenience.

Symbol	Name	Quantity
m	metre	length
kg	kilogram	mass
s	second	time
K	kelvin	temperature
rad	radian	plane angle
Hz	hertz	frequency
mb	millibar	atmospheric pressure (100Pa)
N	newton	force (kg m s^{-2})
Pa	pascal	pressure, stress (N/m^2)
°	degree	plane angle
°C	degree Celsius	temperature

CHAPTER 1

INTRODUCTION

1.1 TRANSMISSION LINES: WHY WORRY ABOUT WIND?

Probably everyone has experienced, at one time or another, some interruption in the supply of electrical energy to his/her home during a windstorm. Why? Tracy and McDonald (1989) provide a very interesting description of the problem: the wind can cause "a tree limb to brush against or fall onto a power line, causing a fuse to blow or a circuit breaker to trip", and/or directly hit towers and lines, knocking down these structures. And because transmission lines are unusual structures in so far as they cover long distances and different terrains, and the rupture of any portion puts the entire line out of service, the wind related phenomena can happen several kilometers apart and still cause the same type of problems. Fortunately this interruption does not last more than a few hours and soon the incident is forgotten (if the food in the freezer has not been spoiled). Although for the majority of the population there may be not much harm (directly), some people and some businesses cannot afford to wait in the darkness. Among others, some of the problems are:

a) Hospital life support systems hesitate for a moment (hopefully the auxiliary power supply will work).

b) Elevators stop between floors, which may or may not be serious, depending on where the elevator is and who is in it.

c) As alarms become inoperable (and if it is night darkness will prevail) theft has an increased probability of happening.

d) Street traffic lights become inoperable, causing traffic jams and possibly traffic accidents.

e) Electrically powered communication systems are disabled and all electrically operated industrial equipment stops.

f) Although not frequent, there have been deaths due to electrocution by fallen distribution lines.

These are in general the consequences for the general public. "What are the damages to the electric utility (as distinct from the public) due to high winds? The damages to the utility include the costs of repairing or replacing lines and structures damaged directly or indirectly by the wind, and the costs of power purchased from other utilities to replace temporarily lost generation or the costs of foreign utility line usage to re-route self-generated power around a line failure" (and those can also affect, financially, the general public).

Accidents & Economics

Accidents of transmission lines due to winds have been happening since these structures started to be erected and persist today.

Boudreaux (1962) reports damages of more than 1.5 million U.S. dollars to the system of the Houston Lighting & Power Company caused by Hurricane Carla in September 1961.

Shichiri (1971) reports hundreds of towers damaged by typhoons in Japan. Transmission tower failures in New Zealand are reported by Monk (1980) who also makes considerations about the possible causes of those accidents.

Blessmann (1986) comments on accidents in Brazil and Argentina and makes a comparison among towers that were designed taking into account the, at that time, 1978 edition of the new Brazilian wind code (1988), in which case the number of accidents was minimal (actually none was reported at that time), and towers designed without adopting proper wind codes, in which case structures have failed.

Saffir (1991) reports damages caused by Hurricane Hugo (September 10-22, 1989) which caused destruction from Guadalupe to Virginia. Power transmission lines were knocked out in the Virgin Islands, Puerto Rico, South Carolina and many other Caribbean Islands. The most severe damage was suffered by Montserrat that lost almost all of the high voltage transmission system and low voltage distribution system.

The American Society of Civil Engineers (1991b) cites the work done by Griffing and Leavengood (1973). More recently (April 1996) several transmission towers were knocked down by extreme winds in Ontario, Canada, as shown in Fig. 1.1.

Unfortunately, although care to take wind loads into account is practice in current design, towers still fail world-wide under these loads and, often, due to unknown reasons. As if all the loss of money, economic activity and normal life disruption involved

in the damage of transmission lines caused by the wind was not reason enough to justify further studies of these structures. another new reality, now related to the possibility of profit, launches even further the interest in such systems. The magazine Engineering News-Record (1996), in its March edition, brings as cover story: "power market faces a new day". It deals with the new world-wide opportunities for every sector of the construction industry involved with power generation and transmission, since all will be affected by the ongoing restructuring of the sector, meaning deregulation and competition.

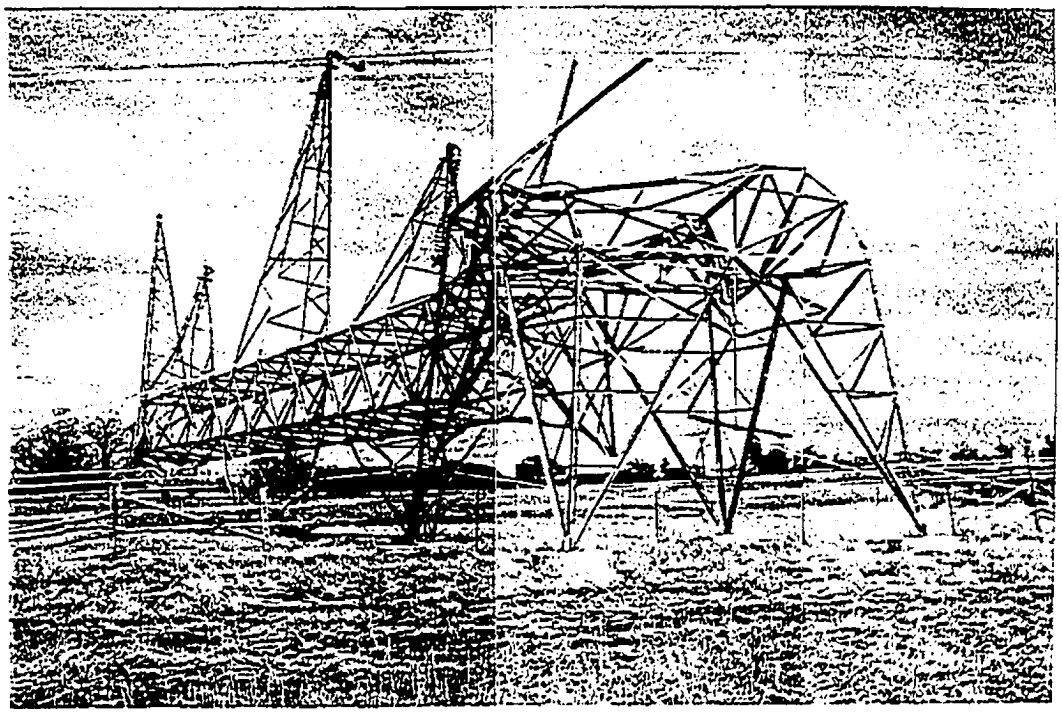

Figure 1.1 Transmission line damaged by wind in Ontario, Canada (April 1996).

1.2 DEFINITION OF TRANSMISSION LINES

This thesis deals with the behaviour of transmission lines under high winds. Some definitions regarding these structures are given by the Canadian Standards Association (1987) and are reproduced here:

Line - wires, conductors and their supporting structures located entirely outside of buildings.

Conductor - a conducting material, usually in the form of a metallic wire (solid or stranded), intended to be used for carrying electric current.

Support - a pole, tower, foundation, guy, crossarm, pin, insulator, fastening, or other component used in supporting wire or cable attachments.

These definitions are for systems such as those illustrated in Figure 1.2, in which the lines are intended to be used for carrying electric current, either for energy supply or communication purposes. The term transmission lines, therefore, is general and includes, as stated above, the towers. However, the isolated towers are also very important structures, being used for many purposes as communication, luminary, etc. It is convenient to initially study the separate effect of the wind on each of these structures: cables (conductors and shield wires) and towers.

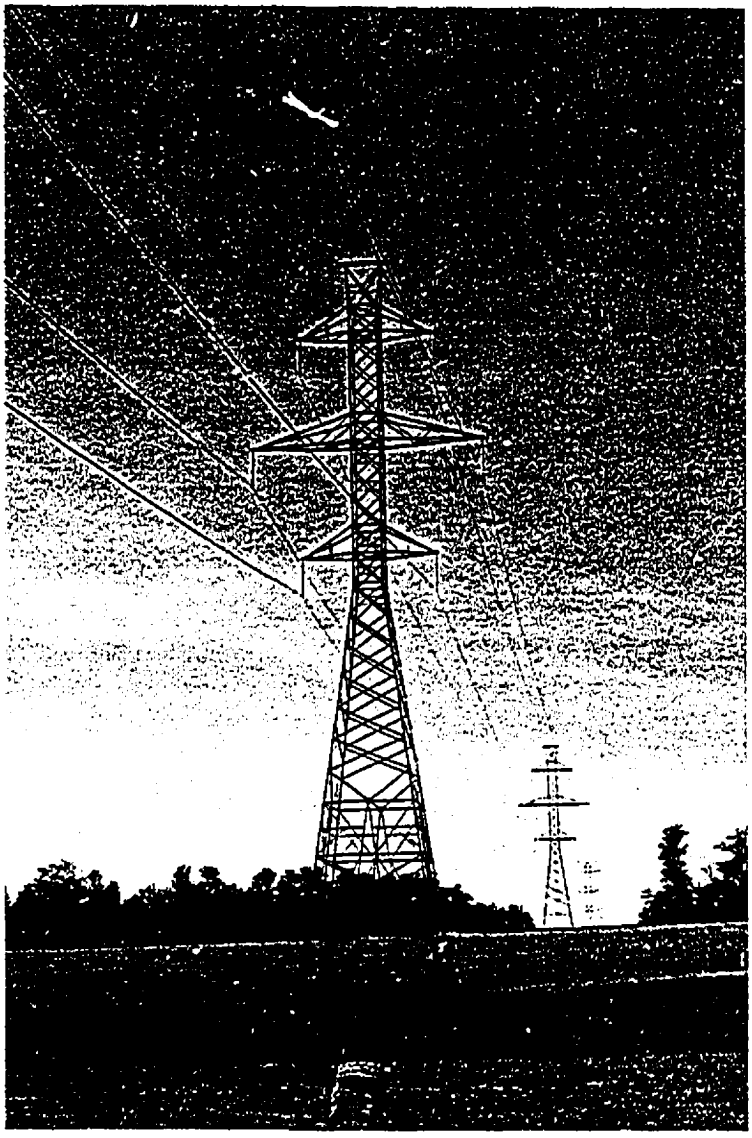

Figure 1.2 Typical transmission line configuration.

The power lines can be located in only two places: overhead or underground. The majority of the current network is overhead, the reason being the more efficient power transfer and lower costs.

Being located overhead, however, causes the transmission lines systems to be exposed to environmental loads. The wind is, generally, the most important.

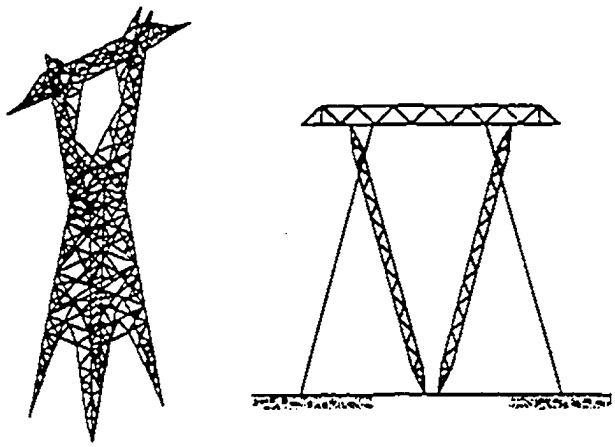

Figure 1.3 Types of transmission towers: (a) self-supporting towers, (b) guyed towers.

1.3 DESIGN OF TRANSMISSION STRUCTURES

Transmission lines appear in the most varied shapes and configurations (Fig. 1.3); the system shown in Fig. 1.2 being one of the most typical. A guide to the design of transmission structures is seldom found in the literature, some exceptions being the works of Petersen (1962), Marsh (1968), Lummis and Fiss (1971) and ASCE (1992). There is also the work by Marjerrison (1967), which describes in detail all the steps involved in the

task of designing these structures, the concepts of which are still very much in use by many utility companies. A brief outline of the procedure described by him follows:

1.3.1 Establishing the configuration

The configuration of a transmission tower is dependent on at least five factors:

1. Length of insulator assembly.

2. Minimum clearance requirements for prevention of switching surge flashovers, code requirements and safety to personnel.

3. Midspan clearance under dynamic conductor behaviour.

4. Geometric mean distance between conductors.

5. Economical use of material.

Having satisfied all of the general clearance requirements, it remains to pick a body width, bracing system and leg slope that will result in the least expensive "in place" tower.

A number of bracing systems have been used in the pedestal portion of transmission towers. A tension system can be used in which all of the diagonal members are assumed to act only in tension. Horizontal members at the junction of each tension "X" are designed for compression. This system is often found most economical where the lateral dimensions of the tower are relatively great with respect to the tower loading. This type of bracing results in large deflection values under heavy loading, since the tension members are smaller in cross sections than compression members would be for similar loading. If such a tower is overloaded, as under test, the "inactive" tension members will

appear to fail in compression although the active tension member is well able to carry the load.

A tension-compression system works very well where the lateral dimensions of the tower are not too great with respect to the tower loads. Such a system can be made up with nearly all diagonal "X" bracing. Tests show that the tension diagonal does an excellent job of supporting the compression diagonal to which it is attached at their crossover point. The system is applicable to both large and small towers. It results in better distribution of loads to the tower footings and reduces stress in the tower legs, especially that brought on by torsional loads.

Another common tension-compression system can be designed around a series of "K" braced frames. This system may be applicable to very large towers but has not been found to be competitive with either the tension system or the "X" braced tension-compression system on the usual line tower.

1.3.2 Determining Tower Loads

Vertical loads on a transmission tower arise from two sources: (1) weight of the conductor and its assumed coating of ice and (2) construction or rigging loads brought about by stringing the conductor as the line is constructed or handling the conductor in making repairs to it after the line is in service.

Dead loads. As in any other structure, the dead weight of the tower itself must be taken into account when calculating member stresses and subsequently selecting member sizes.

Longitudinal loads. Towers are required to withstand the longitudinal pull of the conductors arising from a variety of loading possibilities.

Transverse loads arise from both the wind on the bare or iced wire and changes in line direction. The wind load span on a given tower is measured between centerlines of adjacent spans (Fig. 1.4).

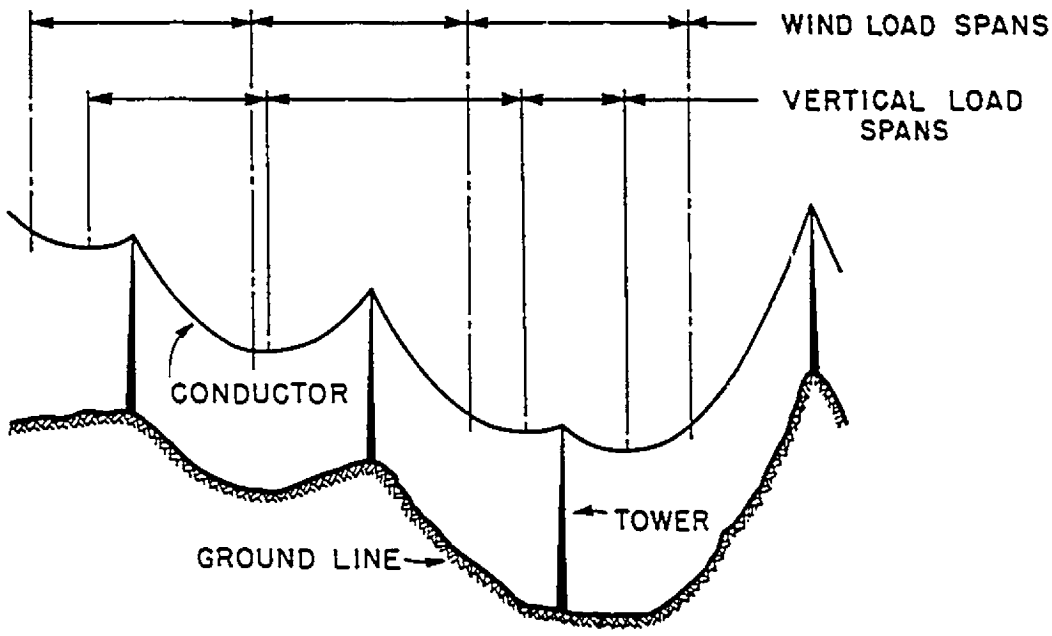

Figure 1.4 Definitions in the loading of transmission lines.

1.3.3 Stress Analysis

The calculation of tower stresses due to wind on the tower "is one of the most time-consuming and tedious jobs encountered in tower analysis". It is generally necessary to estimate the wind for a preliminary design and then calculate the more accurate values

after redundant bracing values are determined and main member sizes and sail areas are fairly well established. It is customary to apply wind loads at major panel points, not at secondary redundant bracing panel points.

After analysis is made for the various cases of loading, the forces are carefully summarised for each loading case and each tower member. It is then convenient to select the maximum force in each member and proceed with the selection of member sizes.

1.3.4 Member Selection

After the stress analysis has been completed and summarised, the maximum tensile and compressive force for each member in the tower is noted. A few members in the tower may be subjected to flexural stresses due to rigging or other loads, but most members in the superstructure will be required to resist only direct stress - tension or compression or both.

In the design of most transmission towers, structural steel angles of handbook sizes will cover 95 percent of the superstructure requirements. These may be used singly or in back-to-back combinations. For very high or very heavy towers, built-up angle sections are often useful and sometimes wide flange sections prove economical for main legs where the force is very high.

It is customary to design transmission structures of all descriptions with a lower factor of safety than is used in most other structures. Although extreme loads on a transmission line are probably less predictable than on other structures, it is common

practice to test full scale representative tower types so that errors in design and detailing can usually be caught before the tower is fabricated "en masse".

The tower members are proportioned to resist compression in accordance with a reliable column formula. Tension members are proportioned on the basis of tension on the net section - sometimes subject to modification after the detailing is complete.

1.3.5 Footings

Tower footings are subjected to three types of load (1) compressive or downward (2) tension or uplift and (3) lateral or shearing.

Transmission tower footing loads vary over a considerable range of values. The large number of footings involved, the variety of soil conditions encountered and the remoteness of many construction sites, make it necessary for the designer to use his/her ingenuity in developing the most economical footing possible.

1.3.6 Tower Testing

Ordinarily, the loads are applied through steel cables with the loads being applied by dead weights, electric winches or hydraulic cylinders. Loads are measured through load cells.

Deflection under torsional loads is generally quite apparent and is especially interesting. Bowing of compression members is easily visible, while supposedly "inactive" tension members fail in compression with no ill effects to the tower as a whole. Shortening of a whole compression face of the tower sometimes causes supposedly "active" tension

members to fall slack and bow out, the stresses apparently shifting to some other portion of the tower not considered in the static analysis.

1.3.7 Overview of the design process

From the above outline of the design procedure the main steps involved in the usual calculation of these structures were described. More concisely, in what concerns the present work:

A certain pattern of wind loading is assumed, generally a power law profile, maximum wind speed likely to occur, aerodynamic coefficients and geometric properties estimated, and from those the wind loadings are calculated. These are applied to the cables and towers and the forces determined. The tower members are then selected and the tower tested extensively (statically) for that loading, and generally a "low" factor of safety is used in the design.

Many modern codes of practice and guidelines for structural loading of transmission lines (ASCE, 1991) adopt a probability-based Load and Resistance Factor Design (LRFD) procedure. Load and Resistance factors are selected according to the nature and variability of the loads. The selection of these factors has a paramount effect on the cost and reliability of the line. The basic idea is that the nominal strength of a component of the line is multiplied by a resistance factor such that the resulting product must be larger than the effect of the estimated load (normally multiplied by a load factor). The choice of each factor depends on the desired reliability or its possible estimation.

Good overviews of such procedures are given by Billinton and Allan (1986) and Cornell (1986), and in more detail by the ASCE (1991).

In order to increase the accuracy in the loading estimate, it becomes increasingly important to establish the loading patterns as precisely as possible and, for that matter, to further explore possible loading mechanisms currently not being taken into account in the design process, especially in what concerns the response to wind loading.

1.4 RESPONSE TO WIND LOADING

In this part a brief and general overview of the methods used to calculate the response to wind loading are given. The particular procedures adopted for each kind of structure (cables and towers) are given more specifically in the proper chapters.

1.4.1 Definition of the reference coordinate system.

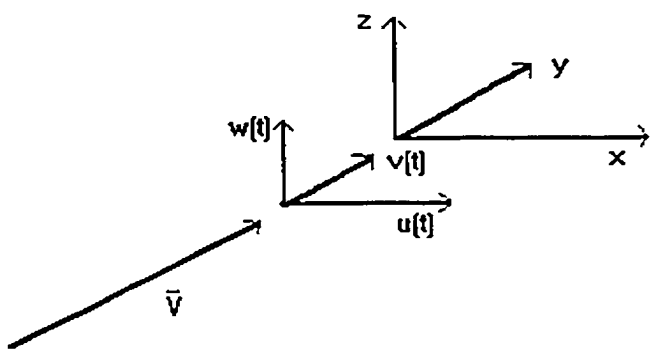

Figure 1.5 Reference coordinate system.

In what concerns this work, the diagram given in Fig. 1.5 represents the reference coordinate system adopted herein. In this, $\overline{V}$ represents the mean wind speed, and *v(t)*, *u(t)* and *w(t)* the fluctuating components of this velocity in the longitudinal or along-wind (y), lateral or horizontal cross-wind (x) and vertical cross-wind (z) directions, respectively.

1.4.2 **Current Procedure**

There are two main approaches to describing effects of wind gusts being currently used:

a) Gust Response Factor

This factor accounts for the dynamic effects of gusts on the wind response of the transmission line components. It takes into account the spatial extent of the gusts (length scales) and their correlation along the span; also, the characteristics of the structure are considered.

For design purposes, the effective peak wind forces $\hat{F}_c$ and $\hat{F}_t$ on the transmission line cable and tower, respectively, are calculated as follows:

$$\hat{F}_c = 1/2\, \rho_a \overline{V}^2\, C_{Dc}\, G_c\, d\, l \qquad (1.1)$$

$$\hat{F}_t = 1/2\, \rho_a \overline{V}^2\, C_{Dt}\, G_t\, A_t \qquad (1.2)$$

where ρ_a is the air density, $\overline{V}$ the mean wind speed, C_D the drag coefficient (subscripts c and t referring to cable and tower, respectively), G the gust factor, d the cable diameter, l the cable length and A_t the tower's effective frontal area.

This procedure is suggested by ASCE(1991) based on the work of Davenport (1979).

b) Span Factor

In this approach, a "span factor", S_f, is applied to the wind force based on the peak gust wind speed, $\hat{V}$. It is, of course, only valid for the cable (directly), the peak force being:

$$\hat{F}_c = 1/2\, \rho_a \hat{V}^2 C_{Dc}\, d\, l\, S_f \tag{1.3}$$

The span factor accounts for the correlation of the gusts along the cable span. The span factor, depending on its definition and calculation, can be dependent on almost the same parameters as the Gust Response Factor. Simulations by Matheson and Holmes (1981) gave a value of 0.685 for a 300 *m* line in open country terrain. As mentioned by Holmes (1993), this factor has a direct relationship with the Gust Response Factor derived for transmission lines by Davenport (1979).

1.4.3 **Statistical method using influence lines**

A typical form of response for structures subjected to wind loading is illustrated in Fig. 1.6. This response could represent a wide range of structural actions including resultant forces, bending moments, cable tensions, as well as deflections and accelerations.

For design purposes, the peak dynamic response, $\hat{r}$, may be expressed as:

$$\hat{r} = \bar{r} + g_s \bar{r} \tag{1.4}$$

in which $\bar{r}$ is the mean or time average response, $\tilde{r}$ is the rms of the fluctuating response, and g_r is a statistical peak factor, generally in the range of 3 to 4. At this point, it is noted that, in the following, the rms value is taken as being equal to the standard deviation (or square root of the variance), i.e., with the mean component removed.

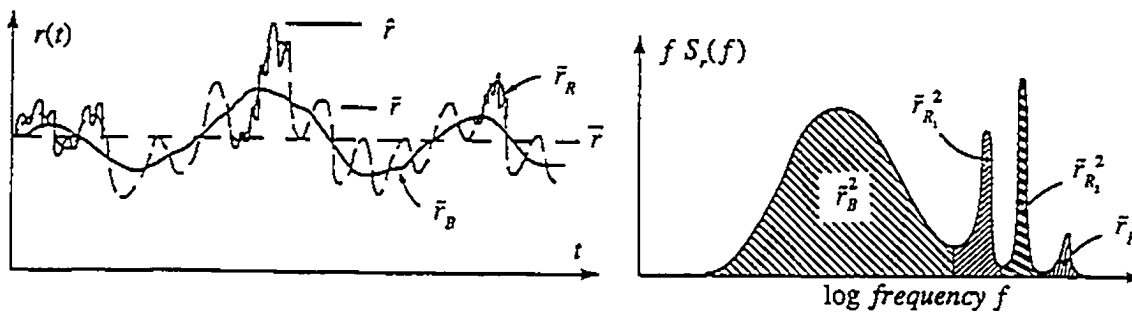

Figure 1.6 Response of a structure to wind: (a) time history, (b) power spectrum.

Figure 1.6(b) shows the manner in which the energy of the fluctuating response is distributed with frequency. The mean square response for a specified range of frequencies is represented by the area under the spectrum corresponding to that range. The fluctuating response can be divided in two distinct components: (a) Background response whose energy is spread over a broad band in the low frequency range, and (b) Resonant response which consists of a series of highly concentrated energy peaks centred on the natural frequencies of the structure.

The total mean square fluctuating response can be calculated as the sum of the background response plus the contribution from each significant vibration mode, hence

$$\bar{r} = \sqrt{\bar{r}_B^2 + \Sigma \bar{r}_{Rj}^2} \tag{1.5}$$

here, $\bar{r}_B$ is the rms background response and $\bar{r}_{Rj}$ is the rms resonant response in the jth mode of vibration.

The background response, by definition, occurs at frequencies below those at which dynamic amplification effects are significant. It can therefore be treated as a quasi-static action in response to slowly varying wind loads.

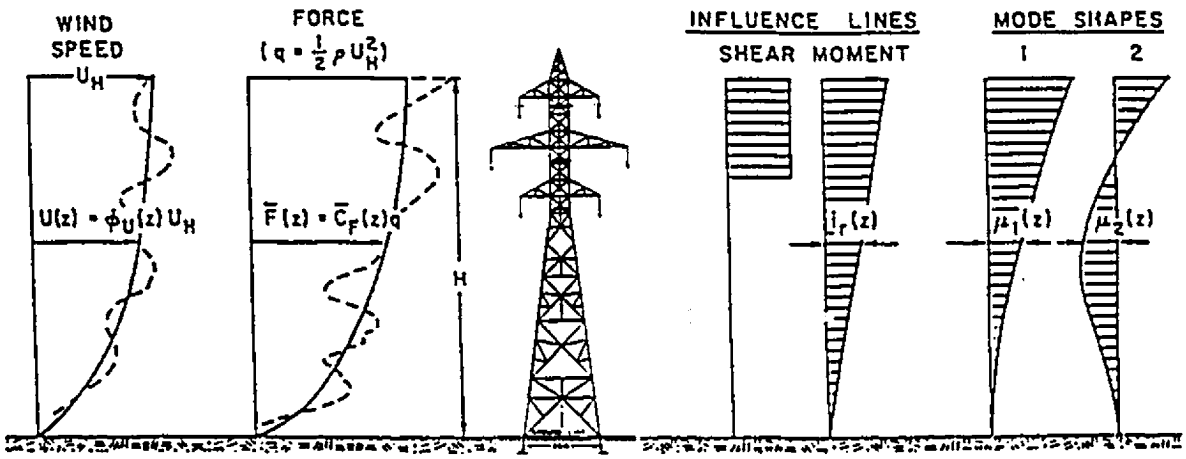

Figure 1.7 Definition sketch for wind loading.

A unified approach (Fig. 1.7) for a variety of structural responses is possible through the use of influence lines which describe the effects of moving loads acting on the

structure (Davenport, 1987). The instantaneous response at some point on the structure, $r(t)$, due to along-wind forces is given by:

$$r(t) = F(z,t)\, i_r(z)\, dz \tag{1.6}$$

where $F(z,t)$ is the instantaneous lateral force at some length or elevation, z, and some time, t, and $i_r(z)$ is the value of the influence line for that response. In what follows, δ will represent the extent of the structure: height (h) for the tower and length (l) for the cable.

(i) Mean Response: The mean response of the structure to steady winds is:

$$\bar{r} = \int_0^{\delta} \bar{F}(z)\, i_r(z)\, dz \tag{1.7}$$

in which $\bar{F}(z)$ is the time averaged lateral wind load (force per unit length) defined by:

$$\bar{F}(z) = 1/2\, \rho_a\, \bar{V}(z)^2\, C_D(z)\, D(z) \tag{1.8}$$

$C_D(z)$ is the drag coefficient, $D(z)$ is a characteristic width and $\bar{V}(z)$ the mean wind speed at a certain reference height or, in case of variation with height, the wind speed profile, which can be described by any suitable logarithmic or power law expression.

(ii) Background response: The quasi-static mean square response to partially correlated fluctuating loads can be calculated by:

$$\tilde{r}_B^2 = \int_0^\delta \int_0^\delta \overline{F'(z,t)\,F'(z',t)}\; i_r(z)\; i_r(z')\; dz\, dz' \qquad (1.9)$$

$F'(z,t)$ being the fluctuating part of the lateral load at point z and time t, and is given by:

$$F'(z,t) = \rho_a\; \bar{V}(z)\, v(z,t) C_D(z)\, D(z) \qquad (1.10)$$

in which $v(z,t)$ is the fluctuating wind speed component in the along-wind direction.

The covariance of the force at two points z and z' can be written as:

$$\overline{F'(z,t)\,F'(z',t)} = R_F(z,z')\; \tilde{F}(z)\; \tilde{F}(z') \qquad (1.11)$$

where $R_F(z,z')$ is the correlation coefficient between the fluctuating forces at the two elevations, z and z', and $\tilde{F}(z)$ the rms fluctuating wind load.

(iii) Resonant response: For the jth vibration mode, the rms resonant response can be approximated by the expression:

$$\tilde{r}_{R_j} = \sqrt{\frac{\pi}{4(\zeta_S + \zeta_{a_j})}\, f_j\, S_{Q_j}(f_j)}\; \frac{\int_0^\delta m(z)\, \mu_j(z)\, i_r(z)\, dz}{\int_0^\delta m(z)\, \mu_j^2(z)\, dz} \qquad (1.12)$$

in this, $m(z)$ is a function expressing the mass per unit length of the structure, $\mu_j(z)$ is the jth mode shape, ζ_S and ζ_{a_j} are, respectively, the structural damping and the aerodynamic damping in the jth mode, f_j the jth natural frequency of the structure and $S_Q(f)$ the spectrum of the generalized force in the jth mode.

The spectral density of the modal generalized force is (Eq. 1.13):

$$S_{Q_j}(f_j) = \rho_a^2 \int_0^\delta \int_0^\delta \overline{V}(z)\overline{V}(z')C_D(z)C_D(z')D(z)D(z')S_v(z,z',f_j)\mu_j(z)\mu_j(z')dzdz'$$

in which $S_v(z,z'f_j)$ is the cross spectral density of wind velocity.

Specific equations are developed for cables and towers and are given in Chapters 2 and 4, respectively.

Some assumptions are made in this process:

a) The modes of vibration are assumed to be uncoupled (satisfying the orthogonality conditions).

b) The spanwise correlation of force is assumed to be the same as that for the transverse correlation of the longitudinal wind component.

c) Towers and cables are treated as one-dimensional (line-like) structures, in which the smallest significant wave length is large as compared to the structure's breadth.

1.5 REVIEW OF EXISTING APPROACHES

There are several works which can be linked to transmission lines, each one approaching specific problems such as forces on cables or towers (both isolated or as a joint system) under theoretical analyses, wind tunnel tests, and/or full-scale measurements. Many Electric Power Companies have research programs as well and provide a valuable amount of data in the area. It is impossible, therefore, to report all the related work that has been done so far and only outlines of some of these works are presented below.

One of the first full-scale investigations in conductor oscillation was that done on the 275kV crossing over the Rivers Severn and Wye in Great Britain, in which the details are given by Davis et al. (1963). In many instances the oscillations were of sufficient amplitude to cause electrical flashover between conductors and consequent outage of the circuits. Instruments were installed on site to record the form of the oscillations and the meteorological conditions under which they occur. These showed that only the lowest-frequency modes were involved, and that at all times of flashover the wind speed and direction were confined within narrow limits. Besides the full-scale measurements, wind tunnel tests were also carried out on models of the stranded conductor. The wind acting at a small yaw angle to the conductor "sees" it as a non-symmetrical section, hence giving a non-symmetrical pressure distribution over the cable section, having the potential for initiating galloping. Smoothing of the conductors by wrapping with p.v.c. tape has proved successful in completely suppressing vertical oscillations.

Liebfried and Mors (1964) report full-scale tests made from 1955 to 1961 in Germany. In the Hornisgrinde Testing Station the mechanical behaviour of single and bundled conductors was tested and examined under normal as well as extraordinary loading conditions due to wind pressure and ice coating. Results show that the wind load of the conductors was smaller than those prescribed by the German VDE 0210 Specifications for the construction of overhead power lines. Reduction factors were found to vary with the wind velocity. With decreasing wind velocity the reduction factor increases. In this case the values of the wind load tend more and more to the theoretical

ones. Regarding the swinging of the cables, it was found that the deviation angles are smaller than those calculated according to the specifications.

In the same year Manuzio and Paris (1964) discuss the problems concerning wind loading on overhead line conductors making use of the statistical theories applied to wind loading already introduced by Davenport (1961). The report shows an analytical approach to such problems and gives results of computations made for several span lengths and wind velocities. Three years later Manuzio (1967) presented a paper dealing with the statistical determination of wind loadings on the end supports of suspended cables. The study had been carried out by theoretical methods and the results were given. Besides, she also reports on preliminary results obtained from experimental observations gathered at two stations especially equipped by ENEL (Italian National Electricity Board) for measurements of wind effects; the aim was to verify the theoretical findings.

In the beginning of the seventies, Cooper and Wardlaw (1970) report on a wind tunnel investigation concerning the aerodynamic stability of a twin-bundle, high-voltage, transmission line. Several models, ranging in scale from 1:12.8 to full size were tested. Sustained large amplitude vibrations of the small scale cables were observed, but the full size sectional model did not exhibit any sustained vibratory motion at the prototype spacing. Measurements of damping and amplitude were taken for the leeward cable with the windward cable fixed. The full-scale model provided sufficient data to indicate the probable cause of the instability, and to suggest a new theoretical approach to the problem. In the same year, Castanheta (1970) presented a paper in which the scope was to study the dynamic behaviour of overhead power lines in order to compute the maximum

forces of cables on towers, due to wind. The analysis was made in statistical terms. The influence of the length of the cables and the intensity of turbulence of the wind on the dynamic behaviour of the power lines was particularly emphasised. Theoretical and experimental results of the "spatial coefficient of reduction" of wind forces on long cables were also presented and interpreted.

Three years later Cojan (1973) performed dynamic analysis of data obtained from a full-scale experiment. He measured the forces transmitted to two rigid columns, due to a 500*m* length, 32*mm* diameter cable. A plot of normalized spectral amplitudes, determined as the ratio of the spectrum of horizontal support force over the spectrum of wind pressure on the cable, was presented. A value of 10 was selected for the coefficient C of the exponential coherence function.

In the mid seventies Wardlaw et al. (1975), in an analytical and wind tunnel investigation into the aeroelastic behaviour of bundled conductors, studied a three-dimensional, multi-subspan catenary. However, it was not the authors' intention that the "semi-aerolastic" model be a small scale simulation of a prototype line. In the late seventies Davenport (1979) presented a paper dealing with Gust Response Factors for transmission line wind loading. The approach is based on the statistical methods which takes account of the spatial correlation and energy spectrum of windspeed and the dynamic response of the transmission line system. The main focus is on the transverse loading; the influence of the variation in drag coefficient was also discussed.

A study on the structural failure of transmission towers under high winds was made by Monk (1980). The effect of a once-in-50-year windspeed on a typical New

Zealand transmission tower was investigated. In regard to the response of the tower to turbulent wind, the tensile stress was found to exceed the yield point of the leg material due to stress concentration at a bolted joint. The possibility of flow-induced vibration of individual members of the towers was also investigated, but no evidence in support of the theory was found. An investigation on the potential aerodynamic instability of structural angle members was also performed by Davenport et al. (1984).

Results of a full-scale study on the dynamic response of a 500 kV single circuit latticed steel transmission line tower to wind loading were presented by Kempner and Laursen (1981). The program was initiated in 1975 and the report presents the results of some of the most recent and significant recordings and summarises results that have been obtained to date (of the report). Among them we cite the ± 15% differences in tower member axial stresses between field measurements and computer analysis using static wind loads. Furthermore, the tower appears to respond in a quasi-static fashion to the types of wind observed. Typical gust response factors have ranged from 1.1 to 1.7. The corresponding stress response factors have shown typical values ranging from 1.14 to 2.0. At the same Conference, Krishnasamy (1981) also presented results of a full-scale investigation, in this case conducted by Ontario Hydro since 1975. There were indications that the use of design specifications current at that time might result in transmission structures with higher than required strength. The author stated that a more realistic assessment of the weather related loads on transmission lines, combined with improved design methods taking into account statistical variations of load and strength, would lead to eventual cost reduction. In the same year Kempner, Stroud and Smith (1981) presented results of another full-scale structural-dynamic and static tests, now performed on the

Bonneville Power Administration 1,200 kV mechanical-test line. The objectives of the test were to: (1) characterise the dynamic and static properties of the 1,200 kV eight-conductor bundle and one of the suspension towers; (2) improve / verify dynamic finite element techniques used for transmission tower modelling; and (3) investigate and develop experimental testing and analytical methods for applying structural-dynamic technology to transmission line systems. The paper presented the most significant results of the test program.

Two years later Ferraro (1983) reported on the full-scale measurements of transmission line response to turbulent winds done in two transmission line systems located in Oregon and in Ontario. The relationship between time varying mean quantities of wind speed and transverse swing angle were investigated. The data was also subjected to dynamic analysis and compared with two related models: one a simple two degree-of-freedom dynamic model proposed by Davenport, the second, a complementary two degree-of-freedom deterministic model developed in the study. Results indicated that the simplified model generally performed well when the transmission line behaviour was governed by its fundamental tower and conductor modes. The complementary model confirmed the assumptions and applications of the simplified parent model and also successfully predicted full-scale transverse swing angle and tower member stress responses.

Mehta and Norville (1985) reported the results of analyses made in a $33m$ height Delta configuration transmission tower and conductors with spans in the range of $430m$. The data were collected by the Bonneville Power Administration in the United States and

include 12-minute continuous recordings of wind speeds and directions, and signals from load cells, swing angles, and strain gages. The analyses and results include time-history, turbulence intensity, power spectrum and gust factor for wind and time-history, and power spectrum and response factor for the response of a strain gage attached to a leg of the tower structure. The results indicated a strong dependence of the gust response factor on the turbulence intensity of the wind. Four years later Mehta and Kadaba (1989) presented the results of full-scale measurements of a 35*m* high energised 500 kV transmission line. The conductor spans on the two sides of the instrumented tower were 252*m* and 450*m*. Statistical analysis of the data yielded effective force coefficient, resonant response and aerodynamic damping of the conductors. Some of the important results are: (1) the field-measured effective force coefficient for the conductor has a range of 0.48-0.74 with the mean value of 0.61; (2) the conductor response spectra show noticeable peaks near the conductor fundamental frequencies of 0.12 and 0.22 *Hz*. The spectral energy for resonant response is low, less than 15% of the total energy; (3) aerodynamic damping of the conductors, estimated from the field measured data, varied from 18% to 91%, with most of the estimated values falling between 30% and 60%.

Wind tunnel studies were performed by Bayar (1986) on two models of square self-supported latticed towers to determine appropriate drag coefficients. Those were compared with other published test results and to the ANSI A58.1 Code. Recommended equations were given for determining the drag coefficient of latticed towers with solidity ratios in a given range. For the wind direction on the diagonal axis of the tower the drag was found to be independent of the solidity ratio and, therefore, a multiplier was

recommended. A multiplier was also recommended for towers with legs that have a heel angle.

Liew and Norville (1989) presented a method for studying the response of a transmission tower structural system subjected to wind loads. The wind speeds and loads from the conductors were considered as the loads on the transmission tower structural system. The stresses in selected members were considered as the responses. The data were used to determine the frequency response functions, which would provide a measure of response. This was obtained by subjecting the system to multiple loadings. Several conclusions were made from the analyses. Among them we cite: (a) the direct effect of wind speed on the transmission tower structural system is not significant. Instead, the effects from the conductor loads are more significant. This is at variance with the findings of this thesis in the sense that this may be true in some cases, but not always; (b) the response of the transmission tower is more accurately represented by considering two loadings than a single loading; (c) the response of the transmission tower is found to be mainly linear.

A more sophisticated approach is made by Al-Bermani and Kitipornchai (1992) in which a non-linear analytical technique for predicting and simulating the ultimate structural behaviour of self-supporting transmission towers under static load conditions is presented. The method considers both the geometrical and material non-linear effects and treats the angle members in the towers as general asymmetrical thin-walled beam-column elements. The developed software, AK TOWER, was used to predict the ultimate behaviour of two full-scale towers tested in Australia. No comparison of the calculated

and the actual member forces was made due to the lack of such field data in these tests, but predictions of the ultimate loads, the nodal deflections at various points and the tower failure deflected shapes have been made. The developed software was able to predict accurately the collapse load (predominantly flexural load) for one, heavy suspension tower. As for the other (tension tower), the predicted collapse load for a test under torsional load was 16.7% lower than the test collapse load.

The Electric Power Research Institute's Transmission Line Mechanical Research Center (TLMRC) started a multi-phased research program to identify possible causes of discrepancies in "field" and "wind tunnel" conductor drag coefficients. This program was briefly reported in the Wind Engineer (1994). The first phase of the research was to build a "free-air-wind-tunnel" to measure the drag coefficients in the open air with a wind tunnel like test setup. The results showed that, for the velocity range (Reynolds No. of 89,000 or less) tested in the field, the drag coefficients agreed favourably with those obtained from quality wind tunnel tests. The conclusion is that wind tunnel drag data are sufficient to determine the drag forces on a short segment of conductor in open air. The detailed results of the first phase were reported by Shan et al. (1992). The second phase of the research was being conducted at the TLMRC and consists of a full-scale conductor wind loading experiment.

In the same subject is the study performed by Ball et al (1992). The purpose of the project was to identify errors in the wind tunnel testing technique in view of the great discrepancy existing between aerodynamic drag coefficients of electrical power conductors measured in wind tunnel experiments and those inferred from field

observations of operating lines. A series of experiments was conducted to investigate the importance of the model aspect ratio and the end conditions present at the junction of the model and the wind tunnel wall. The results show that significant errors are possible in the wind tunnel experiments due to these effects but none can account for the large discrepancy between wind tunnel and field data. Still dealing with conductors is the work done by Tabatatai et al (1992) describing a study on the drag properties of trapezoidal and circular wire conductors in a wind tunnel and under field conditions. The wind tunnel study indicates that, at high windspeeds, the trapezoidal wire conductors have lower drag coefficients than comparable standard circular wire conductors. Some typical results of the field measurements are also included, but a comparison of the sources of data had not been done yet.

An interesting study concerned with offshore structures but that can be directly related to transmission line studies was made by Holdϕ (1993). He performed an experimental investigation into the effect of Reynolds number variation on the lattice structure part of a wind tunnel model of the topside of an offshore structure. The results suggest that when global modelling considerations dictate low local lattice structure Reynolds numbers, it may be advisable to cater for the lattice structure effects separately and add or superimpose these onto the global results. He has also found wind tunnel test results on model lattice structures below a Reynolds number of 2200 based on the lattice member cross-section to be Reynolds number sensitive. The differences can be up to 40% in terms of drag coefficients. On the other hand, Vickery (1982) states that data on sharp

edged shapes suggests that local Reynolds numbers in excess of 1000 will be sufficient to prevent (or considerably diminish) model scale effects in lattice or framed towers.

Yu et al (1993a) developed a three-degree-of-freedom model to comprehensively describe and predict different galloping behaviour observed on a single iced, electrical transmission line, for which vertical, horizontal, and torsional interactions are permitted. Closed-form expressions were derived to check the stability of a transmission line's static profile and to compute the critical wind speed at which galloping is initiated. For the parameter values causing galloping, perturbations were employed in conjunction with a bifurcation theory to deduce the governing equations of motion under the assumption of a weak nonlinearity. These equations made it possible to find explicit steady-state solutions and their stability conditions. A robust criterion was also proposed to assess the reliability of the solutions. In a companion paper (Yu et al., 1993b) the authors noted that the predictions given by the model agreed fairly well with two field observations of galloping. Furthermore, predictions for various wind speeds indicated that the definition of the parameter used to measure the reliability of the time-averaged results was plausible. A comparison of the results arising from models having various degree-of-freedom suggests that it is preferable to employ the three-degrees-of-freedom model to more reliably predict the potential for flashover.

Kobayashi et al. (1994) report on the building of a new type of transmission tower. This has a relatively slim body with trusses having the sides covered in order to harmonise it with the landscape of an urban area. Because there were no data available on wind loads on such bracket, a static force measurement and an aerodynamic test were

carried out. No self-excited oscillation was observed on the bracket model and the tower model.

Finally, we cite the work of Katoh et al (1995) on full-scale measurements on wind-induced vibration of an electrical transmission tower installed on a mountainous area, but at wind speeds of less than 25 *m/s*. They observe that wind direction has a strong influence on wind characteristics; also, that the vibration characteristics of the tower with conductors are strongly influenced by the behaviour of the conductors. The aerodynamic damping is found to play an important role in their total damping.

In summary, it is clear that the behaviour of transmission lines is strongly related to the turbulent wind characteristics and therefore statistical methods are the best approach to describing the wind loading; current wind tunnel tests (sectional models) do not agree well with full-scale measurements; and that aerodynamic damping on these structures is important. It is also known that accidents with transmission lines in strong winds keep happening. And in many instances it is not known why the transmission lines have failed. It has not been proven how these structures really behave in strong winds nor which parameters are of major importance in their response to wind loading, and this includes the consideration of their dynamic properties. The reason for this is that both full-scale measurements during strong winds and aeroelastic wind tunnel tests of meaningful sections of transmission lines are both fraught with significant problems. It is the aim of this thesis to attempt, as far as we know, for the first time, to aeroelastically model a full span transmission line.

1.6 SCOPE OF STUDY

The thesis subject concerns two main topics:

Firstly, to examine the effect of scale of turbulence on the response of a line-like structure (cable model) through wind tunnel tests and to compare experimental results with theoretical predictions. Consistency with theory allows for the development of a new modelling approach to conductor systems using a distorted horizontal (spanwise) length scale to accommodate these systems in the wind tunnel.

Secondly, from a theoretical approach, the design procedure for the establishment of wind loading on transmission towers is reviewed and current procedures compared with the statistical method using influence lines, which is considered more realistic. This latter approach can account for unbalanced loading effects, shear and axial loads and the effects of higher modes of vibration in the calculation of the response factors.

The idea is to examine the behaviour of these systems under very severe turbulent boundary layer winds (V_{10}= *30 m/s* and up).

CHAPTER 2

WIND FORCES ON CABLES

2.1 INTRODUCTION

The forces the wind exerts on cables are (Sachs, 1978):

a) A static drag force, and, on certain types of cables, a static lift force. Drag and lift coefficients may vary with Re.

b) A random gust force, giving rise to random amplitude oscillations.

c) A high-frequency, low amplitude, vortex excitation (also called aeolian vibration).

d) A low-frequency, high amplitude oscillation caused by lift and drag instabilities (galloping excitation).

e) A vertical/horizontal/torsional coupled oscillation of twin conductors.

These forces are interrelated, with the exception of vortex excitation.

The oscillations (c) to (e) can be considered as repetitive or cyclic motions and have their characteristics described in Table 2.1, which is reproduced from EPRI (1979). It must be emphasised that the numerical ranges shown should not be considered as representing extreme limits. They are intended to provide a comparison among the three types of motion. Furthermore, in what refers to galloping, it is not necessary to have the conductor surface covered with an asymmetrical ice deposit, as stated in the table, to have

this type of motion. For some stranded cables yawed to the wind, lift forces can occur, initiating transverse oscillations, as explained below.

Table 2.1 Comparison of Types of Cyclic Conductor Motion (after EPRI, 1979)

	Aeolian Vibration	Conductor Gallop	Wake-Induced Oscillation
Types of Overhead Lines Affected	All	All	Limited to lines with bundled conductors
Approx. Frequency Range (Hz)	3 to 150	0.08 to 3	0.15 to 10
Approx. Range of Vibration Amplitudes (Peak-to-Peak) (Expressed in conductor diameters)	0.01 to 1	5 to 300	Rigid-Body Mode: 0.5 to 80 Subspan Mode: 0.5 to 20
Weather Conditions Favouring Conductor Motion			
Wind Character	Steady	Steady	Steady
Wind Velocity	1 to 7m/s	7 to 18m/s	4 to 18m/s
Conductor Surface	Bare or uniformly iced (i.e. hoarfrost)	Asymmetrical ice deposit on conductor	Bare, dry
Design Conditions Affecting Conductor Motion	Line tension, conductor self- damping, use of dampers, armour rods	Ratio of vertical natural frequency to torsional natural frequency, sag ratio and support conditions	Subconductor separation tilt of bundle, subconductor arrangement, subspan staggering
Damage			
Approx. time required for severe damage to develop	3 mos to 20 + years	1 to 48 hours	1 mo to 8 + years
Direct causes of damage	Metal fatigue due to cyclic bending	High dynamic loads	Conductor clashing, accelerated wear in hardware
Line components most affected by damage	Conductor and shield wire strands	Conductor, all hardware, insulators, structures	Suspension hardware, spacers, dampers, conductor strands

For a plain circular cylinder, the only possible acting static force is the drag, regardless of the angle of yaw. However, the majority of cables do not have a smooth circular surface, but have a helically wound configuration of greater or lesser surface roughness, depending on the wire diameter. This makes the effective roughness different on either side when the cable is yawed to the wind and introduces a lift force on the cable. This is illustrated in Fig. 2.1. A way to prevent such phenomena from happening is to smooth the conductors by wrapping with p.v.c. tape or the like. This has been proved successful by Davis et al (1963).

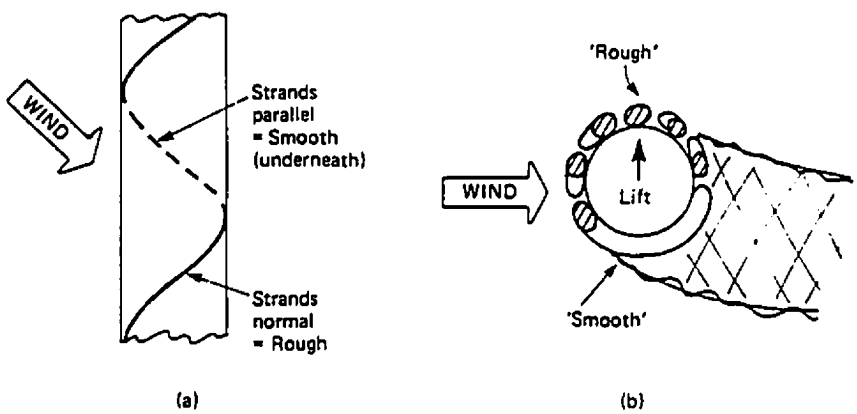

Figure 2.1 Effect of helical strands (after Cook, 1985)

As can be seen in Table 2.1, all cyclic conductor motions occur with velocities under 20m/s, i.e., not very strong winds. Therefore, although very important, they are not addressed in this study and only items a) and b) are approached.

2.2 RELEVANT FACTORS FOR WIND ANALYSIS

2.2.1 Cable Dynamics

Random gust excitations cause oscillations at one or more of the cable's natural modes and frequencies in a vertical (radial), horizontal (pendulum) or torsional manner, singly or combined. The form of oscillation depends on the type of cable, fixing conditions and whether the mode is symmetric or antisymmetric.

The linear theory of free vibrations of a suspended cable (Irvine, 1981) allows for the calculation of the natural frequencies, f_{cj} [Hz], and normalised mode shapes, $\mu_j(x)$, as follows:

a) Out-of-plane (pendulum) mode:

$$f_{cj} = \frac{j}{2L}\sqrt{\frac{T}{m}} \tag{2.1}$$

$$\mu_j(x) = \sin\left(\frac{j\pi x}{L}\right) \tag{2.2}$$

b) In-plane antisymmetric mode:

$$f_{cj} = \frac{j}{L}\sqrt{\frac{T}{m}} \tag{2.3}$$

$$\mu_j(x) = \sin\left(\frac{2j\pi x}{L}\right) \tag{2.4}$$

c) In-plane symmetric mode:

$$f_{cj} = \frac{\varepsilon_j}{2L}\sqrt{\frac{T}{m}} \tag{2.5}$$

$$\mu_j(x) = 1 - \tan\left(\frac{\pi\varepsilon_j}{2}\right)\sin\left(\frac{\pi\varepsilon_j x}{L}\right) - \cos\left(\frac{\pi\varepsilon_j x}{L}\right) \tag{2.6}$$

where j = 1, 2, 3,... signify the first, second, third modes, respectively, and so on. S is the sag, L the horizontal span, l the cable length, T the line tension and m the mass per unit length.

The nondimensional frequency parameter ε_j is found by solving the following transcendental equation:

$$\tan\left(\frac{\pi\varepsilon}{2}\right) = \left(\frac{\pi\varepsilon}{2}\right) - \frac{4}{\lambda^2}\left(\frac{\pi\varepsilon}{2}\right)^3 \tag{2.7}$$

where $\lambda^2 = (mgL/H)^2 L/(Hl/EA)$, being E the modulus of elasticity and A the cable cross-sectional area. The parameter λ^2 compares the relative importance of gravitational and elasticity effects.

Equations regarding the static and dynamic behaviour of suspended cables are given in more detail in Appendix A. Further insight is found in Irvine (1981) and Krishna (1978).

The methodology adopted in this work is the linear theory of vibrations. A review of works dealing with nonlinear vibrations of cables is presented by Sparling (1995). From

there it can be verified that several authors have concluded that nonlinear displacement amplitudes are substantially smaller than predictions based on linear theory. Also, coupling of in-plane and out-of-plane motions can be induced by nonlinear effects.

2.2.2 Cable Aerodynamics

Cable motion is dominated by aerodynamic damping, the structural damping ($\zeta_s \cong$ 0.0005 - Bachmann et al, 1995) being not so important, especially in strong winds. For tower motion, on the other hand, both damping sources may be of equal importance. Aerodynamic damping is a retarding force which is derived from the relative motion between structure and air. It is a linear function of wind speed V and, in the case of a uniform prismatic structure in uniform flow and in drag motion, can be given by the expression (Davenport, 1988; Vickery, 1992):

$$\zeta_{aj} = \left(\frac{C_D}{4\pi}\right)\left(\frac{\rho_a d^2}{m}\right)\left(\frac{V}{f_j d}\right) \tag{2.8}$$

where C_D is the drag coefficient, ρ_a the air density and d the cable diameter. The damping is presented as a fraction of the critical, for the jth mode. As transmission line cables generally have very low mass per unit length values ($m \cong 2$ *kg/m*), the aerodynamic damping can be as high as 60% of the critical for extreme winds. The role of aerodynamic damping in the response of tension structures to turbulent wind is discussed by Davenport (1988).

Regarding the wind velocity variation with height, as long as the sag is not too big, we can assume a constant value of V applied to a certain reference point, generally chosen as the cable's center of inertia, i.e., we assume that the cable is straight and located at the height corresponding to its chosen reference height. This is also due to the fact that, under strong winds, the deflection will be big and the line will be seen by the wind as having a "smaller" sag.

Referring to Fig. 2.2, the drag force on an element dx of the cable can be given by:

$$dF(x,t) = \frac{1}{2} \rho_a V^2(x,t) C_D d \cos^2\beta \, dx \tag{2.9}$$

where β is the wind yaw angle and x relates to cable length.

The velocity $V(x,t)$ is given by:

$$V(x,t) = \overline{V} + v(x,t) \tag{2.10}$$

and

$$V^2(x,t) = \overline{V^2} + 2\overline{V}\, v(x,t) + v^2(x,t) \tag{2.11}$$

where $\overline{V}$ is the mean wind speed and $v(x,t)$ the fluctuating component. The last term can be important in cases where the flow turbulence is very large, which is not likely to be the case for the majority of transmission line locations. Therefore, it is disregarded

(linearization). Errors associated with the linearization of the square law relationship were discussed by Vickery (1995).

The drag coefficient C_D is defined as:

$$C_D = \frac{\overline{F}}{1/2\,\rho_a\,\overline{V}^2 d\,l} \tag{2.12}$$

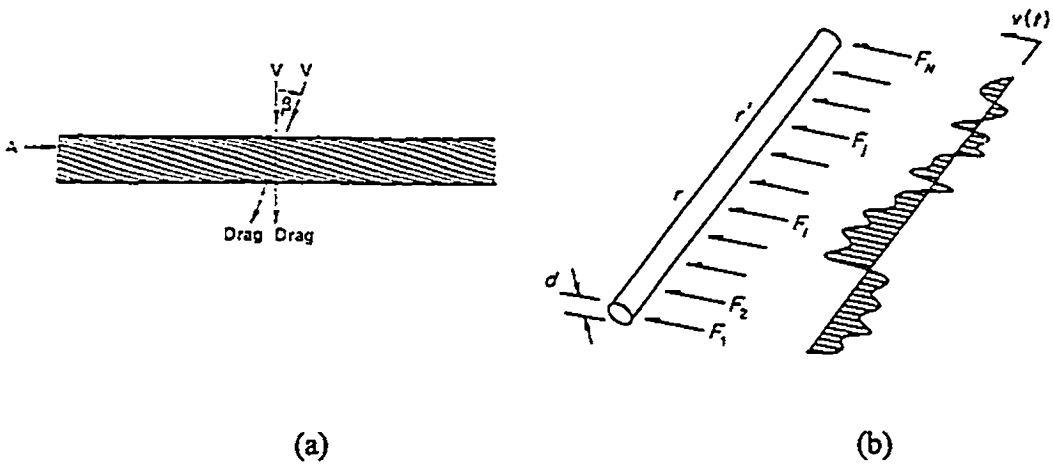

Figure 2.2 (a) Identification of parameters for drag calculation. (b) Fluctuating wind pressures acting on a slender structure.

The drag for a circular cylinder is highly Reynolds number dependent. This is defined as $Re = V\,d\,/\,\nu$, where ν is the kinematic viscosity of the air. Fig. 2.3 shows a typical variation of C_D with Re, in this case for smooth flow and uniform section, while Fig. 2.4 presents some full-scale and wind tunnel measurements of conductor drag coefficients. The drag is also affected by the roughness of the cable section (see Fig. 2.1) and the turbulence of the wind. Figure 2.5 shows the effect of surface roughness and

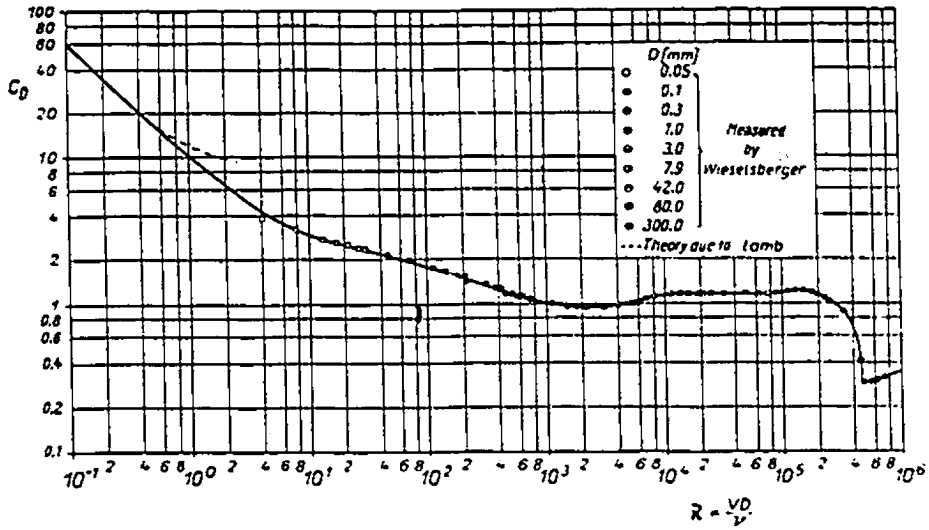

Figure 2.3 Drag coefficient for circular cylinders as a function of Reynolds number (after Schlichting, 1987).

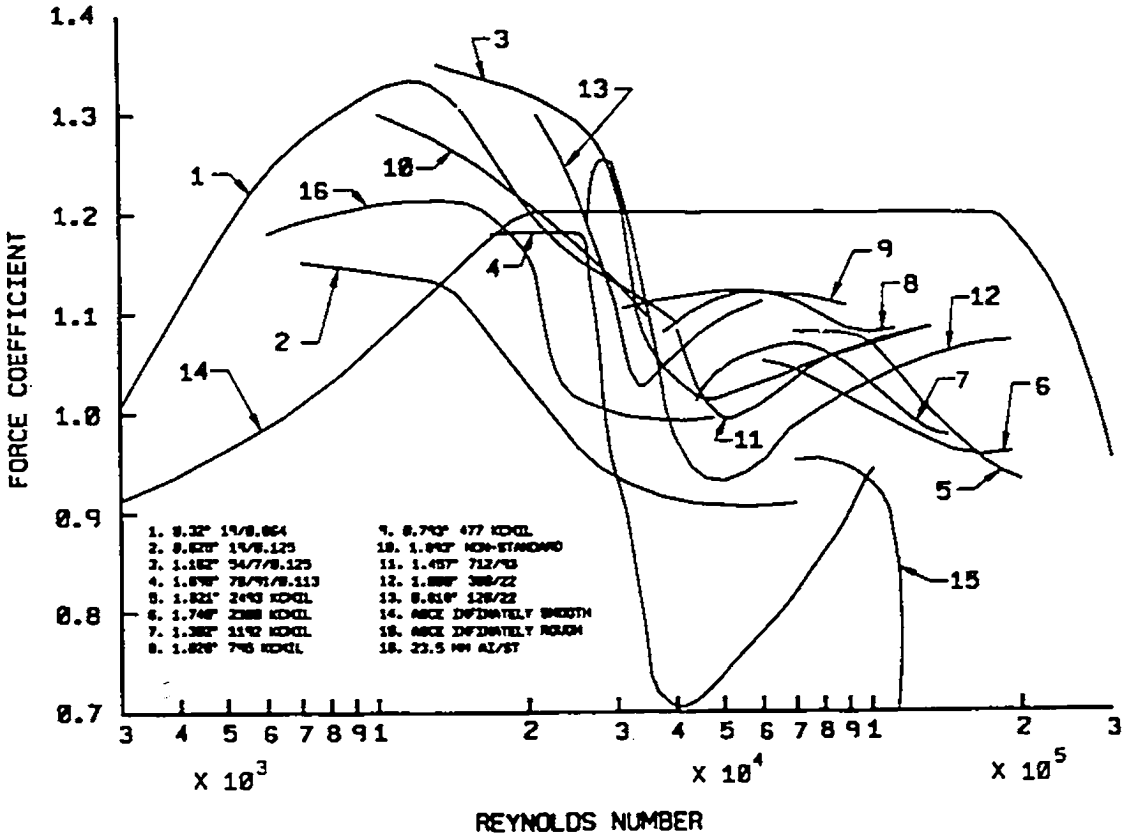

Figure 2.4 Full-scale and wind tunnel conductor drag coefficients (extracted from ASCE, 1991).

Reynolds number on the values of C_D . An increase in the turbulence of the flow has a similar effect as an increase in surface roughness, that is to accelerate the transition in the flow regime over the surface of the cylinder and both can have a substantial influence on the drag variation.

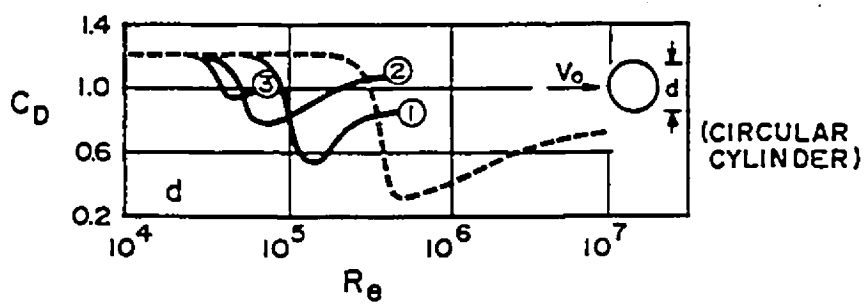

Figure 2.5 Influence of Reynolds number and surface roughness on the values of C_D . - - - - smooth surface; —— sanded surface. (1) $k/d = 0.002$; (2) $k/d = 0.007$; (3) $k/d = 0.020$ (where k is the grain size of sand) (After Scruton, 1971).

2.3 THEORETICAL APPROACH

Adopting Davenport's (1993) approach with the assumptions made above and referring to Chapter 1 for the introduction of the method, we can write the equations for cable response as:

2.3.1 Mean Response

The mean response is given by:

$$\bar{r} = \int_0^l \frac{1}{2}\rho_a \bar{V}^2 C_D\, d\, i(x)\, dx = \frac{1}{2}\rho_a \bar{V}^2 C_D\, d \int_0^l i(x) dx \qquad (2.13)$$

2.3.2 Background Response

The background response is given by:

$$\tilde{r}_B^2 = \int_0^l \int_0^l \rho_a^2 C_D^2 \overline{[\bar{V} v(x,t)\, i(x)][\bar{V} v(x',t)\, i(x')]} d^2\, dx\, dx'$$

$$\tilde{r}_B^2 = \rho_a^2 C_D^2 \bar{V}^2 d^2 \int_0^l \int_0^l \sigma_{v_x} \sigma_{v_{x'}} R(v_x, v_{x'}) i(x)\, i(x')\, dx\, dx' \qquad (2.14)$$

where $R(v_x, v_{x'})$ is the cross-correlation coefficient between v at the two locations and can be expressed by

$$R(v_x, v_{x'}) = \frac{\overline{v(x,t)v(x',t)}}{\sigma_{v_x}\sigma_{v_{x'}}} \cong e^{-(\Delta x/L_v)} \qquad (2.15)$$

where $\Delta x = |x - x'|$

$$r_B^2 = \rho_a^2 C_D^2 \bar{V}^2 d^2 \sigma_v^2 \int_0^l \int_0^l e^{-(\Delta x/L_v)}\, i(x)\, i(x')\, dx\, dx'$$

$$\tilde{r}_B^2 = (2q\, C_D\, d\, I_v)^2 \int_0^l \int_0^l e^{-(\Delta x/L_v)}\, i(x)\, i(x')\, dx\, dx' \qquad (2.16)$$

2.3.3 Resonant Response

For the resonant response, we have the generalized force given by:

$$Q_j(t) = \int_0^l F'(x,t)\mu_j(x)dx$$

$$Q_j(t) = \int_0^l \rho_a \overline{V} v(x,t) C_D \, d \, \mu_j(x) \, dx \tag{2.17}$$

The spectral density of the modal generalized force is:

$$S_{Qj}(f_j) = \rho_a^2 \overline{V}^2 C_D^2 \, d^2 \int_0^l \int_0^l S_v(x,x',f)\mu_j(x)\mu_j(x')dx\,dx' \tag{2.18}$$

where $S_v(x,x',f)$ is the cross spectral density of wind velocity, which is used in the calculation of the correlation of the individual frequency components of wind turbulence, or coherence:

$$\gamma^2(x,x',f) = \frac{\left|S_v(x,x',f)\right|^2}{S_v(f)S_v'(f)} \tag{2.19}$$

The square root of the coherence, when plotted against the reduced frequency, can be approximated by an exponential function of the form:

$$\gamma(\Delta x,f) \equiv e^{-\frac{C|\Delta x|f}{\overline{V}}} \tag{2.20}$$

For a more detailed explanation of coherence refer to 3.3.2.4.

$$S_{Qj}(f) = \rho_a^2 \overline{V}^2 C_D^2 \, d^2 S_v(f) \int_0^l \int_0^l \gamma(x, x', f) \mu_j(x) \mu_j(x') dx \, dx' \tag{2.21}$$

where $S_v(f)$ is the spectral density of horizontal wind velocity at reference height.

$$f_j S_{Qj}(f_j) = (2q \, C_D \, d \, I_v)^2 \frac{f_j \, S_v(f)}{\sigma_v^2} \int_0^l \int_0^l e^{\frac{-C|\Delta x|f}{\overline{V}}} \mu_j(x) \, \mu_j(x') \, dx \, dx' \tag{2.22}$$

The part of equation (2.22) inside (and including) the double integration is called the "Joint Acceptance Function", which can be interpreted as a modal weighting function in the frequency domain which quantifies the contribution of turbulence eddies to the motion in a given mode.

The variance of the generalized modal co-ordinate, y_j, can be given approximately by:

$$\sigma_R^2 (y_j) \approx \frac{\pi}{4(\zeta_{aj} + \zeta_S)} \frac{1}{K_j^2} f_j S_{Qj}(f_j) \tag{2.23}$$

where $K_j = \omega_j^2 M_j$ is the modal stiffness. The modal mass is given by:

$$M_j = \int_0^l m(x) \mu_j^2(x) dx \tag{2.24}$$

The resonant response for local effects (shear, bending moment, etc.) is obtained by multiplying the square root of Eq. (2.23) by the response participation factor:

$$\tilde{r}_{Rj} = \sigma_R(y_j)\int_0^l m(x)\omega_j^2 \mu_j(x) i(x) dx \tag{2.25}$$

and therefore:

$$\tilde{r}_{Rj} = \sqrt{\frac{\pi}{4}\frac{f_j S_{Qj}(f_j)}{(\zeta_{aj}+\zeta_s)}}\frac{\int_0^l m(x)\,\mu_j(x)\,i(x)\,dx}{\int_0^l m(x)\,\mu_j^2(x)\,dx} \tag{2.26}$$

2.3.4 **Joint Acceptance Functions**

The background and resonant responses are given by Eqs. (2.16) and (2.26), respectively. A more convenient way of calculating these responses is by using the analytical expressions of the Joint Acceptance Functions (JAF) corresponding to each specific influence line or mode shape. The ratio between fluctuating and mean response can then be conveniently expressed, facilitating the calculation of the theoretical prediction.

For the background response, the JAF obtained from the double integration part of Eq. (2.16) is:

$$J^2(n) = \frac{2}{n^4}\left(\frac{n^3}{3} - \frac{n^2}{2} + 1 - e^{-n}(n+1)\right) \tag{2.27}$$

where $n = l / L_v$. The influence line used is x / l (reaction at one end of cable). To give the total value of the integration, Eq. (2.27) must be multiplied by l^2. This equation is represented graphically in figure 2.6.

Thus, the ratio between the background and mean responses is:

$$\frac{\bar{r}_B^2}{\bar{r}^2} = I_v^2 \left\{ \frac{32}{n^4} \left[\frac{n^3}{3} - \frac{n^2}{2} + 1 - e^{-n}(n+1) \right] \right\} \tag{2.28}$$

For the resonant response, the JAF obtained from the double integration part of Eq. (2.22) is, for each mode of vibration j, equal to:

$$J_j^2(n) = \frac{n}{n^2 + j^2\pi^2} + 2 \left[\frac{j\pi}{n^2 + j^2\pi^2} \right]^2 (1 - e^{-n} \cos j\pi) \tag{2.29}$$

where now $n = C f \, l / \bar{V}$. The mode shape used was $sin\,(j\,\pi\,x\,/\,l)$. Again, the total value of the integration is given by multiplying Eq. (2.29) by l^2. The JAF are plotted in Fig. 2.7 for six mode shapes.

The ratio between resonant and mean responses for each mode j is then:

$$\frac{\bar{r}_{Rj}^2}{\bar{r}^2} = \frac{16\, I_v^2}{\zeta_{aj}} \frac{f_j S_v(f_j)}{\sigma_v^2} \frac{\cos^2 j\pi}{j^2\pi} \left[\frac{n}{n^2 + j^2\pi^2} + 2 \left[\frac{j\pi}{n^2 + j^2\pi^2} \right]^2 (1 - e^{-n} \cos j\pi) \right] \tag{2.30}$$

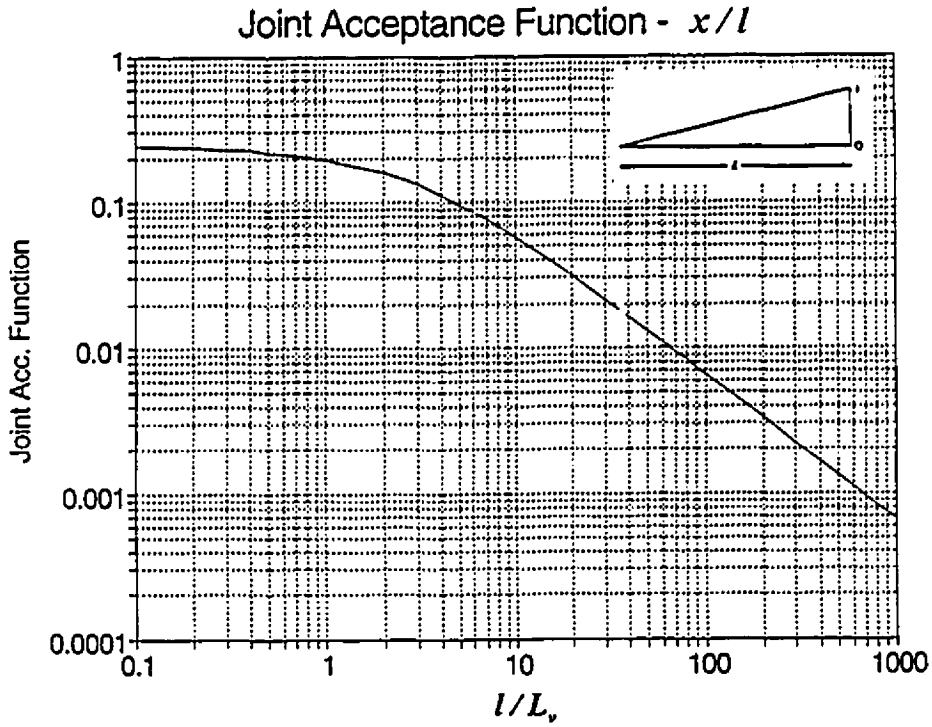

Figure 2.6 Joint Acceptance Function for Background response.

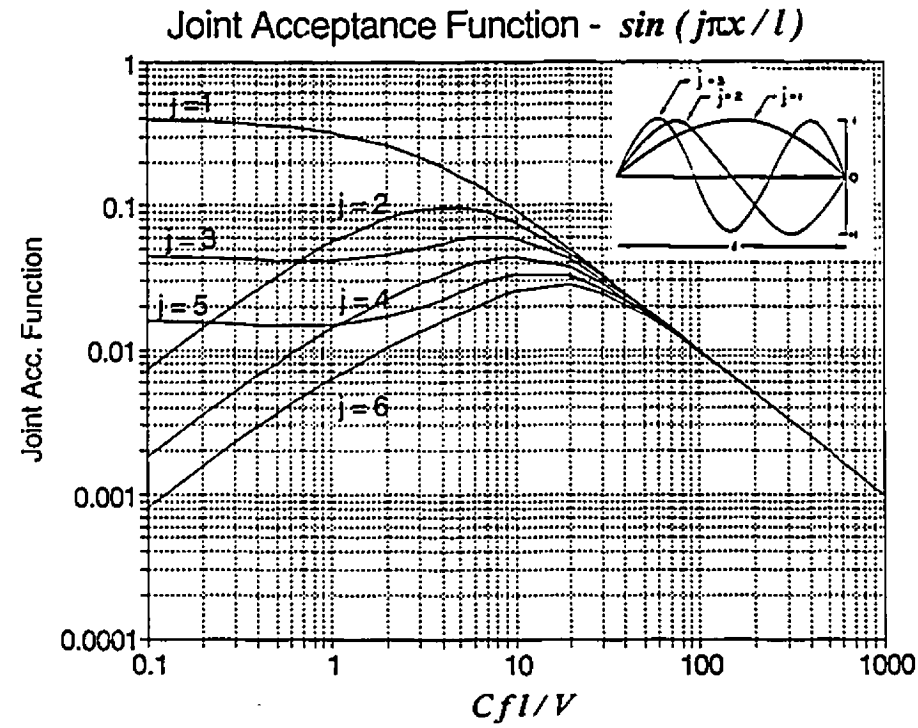

Figure 2.7 Joint Acceptance Functions for Resonant response.

CHAPTER 3

WIND TUNNEL TESTING

3.1 INTRODUCTION

Although sophisticated theoretical models of the aerodynamic behaviour of transmission lines have been developed, and partially adopted in codes, they have been very difficult to verify. Full-scale measurement is a particularly difficult option. Wind tunnel testing is an attractive alternative; however it also poses considerable difficulties.

Currently, there are basically two different types of wind tunnel testing being performed. The first type of testing is referred to as static testing. In this, the mean aerodynamic forces are obtained from short lengths of full-scale conductor or conductor models. These are mounted in force balances and drag and lift coefficients obtained. The other type is called dynamic testing, where again a two-dimensional modelling method is employed. The model is composed of short lengths of rigid conductor having full-scale values of shape and weight. The elastic properties are simulated by a spring suspension system at each end of the rigid conductors.

In spite of a great number of wind loading studies of transmission lines, there is still not a complete understanding of their behaviour in wind nor complete agreement between wind tunnel testing and full-scale measures. Conductor drag forces obtained from full-scale tests have been often found smaller than the corresponding ones obtained in

wind tunnel tests using section models. Furthermore, certain full-span kinds of motions cannot be simulated in these tests.

A more sophisticated approach is to model the full-span aeroelastically. This kind of test is seldom found in the literature. Some work has been done by Wardlaw et al (1975) although it was not the authors' intention that the model be a small scale simulation of a prototype line. The correct modelling of this kind of structure is very difficult for many reasons which are discussed in this chapter. It is the purpose of this work to aeroelastically model the conductors and to introduce a new approach for such modelling.

3.2 AEROELASTIC MODELLING OF THE CABLES

In order to have the aeroelastic behaviour of the cables simulated in the models, the mass, drag forces, reduced frequency and aerodynamic damping should be simulated, together with the properties of the natural wind. ASCE(1987) provides general guidelines on wind tunnel testing of building and structures. Specifically, the following conditions should be met:

3.2.1 Conventional modelling

a) Geometric similarity

The ratio between model and prototype dimensions should be preserved:

$$\frac{L_m}{L_p} = \frac{S_m}{S_p} = \lambda_L \qquad (3.1)$$

where L is the span, S the sag and λ_L the length scale. The subscripts m and p denote model and prototype, respectively.

b) Mass modelling

The requirement for the modelling of the mass of the structure is that the inertia forces of the structure and those of the flow be scaled consistently. Similarity of inertia forces is achieved by maintaining a constant ratio of the bulk density of the cable, ρ, to the density of air, ρ_a :

$$\left(\frac{\rho}{\rho_a}\right)_m = \left(\frac{\rho}{\rho_a}\right)_p$$

Since ρ_a is the same we have the ratio:

$$\lambda_\rho = \frac{\rho_m}{\rho_p} = 1.0$$

The modelling of the generalized mass of particular modes of vibration then becomes:

$$\frac{M_m}{M_p} = \frac{\rho_m L_m^3}{\rho_p L_p^3}$$

or

$$\lambda_M = \lambda_\rho \lambda_L^3$$

When the aeroelastic tests are made through the use of equivalent models, however, what is important is to maintain the mass ratio the same in model and prototype (Tanaka, 1988):

$$\left(\frac{m}{\rho_a L^2}\right)_m = \left(\frac{m}{\rho_a L^2}\right)_p \qquad (3.2)$$

therefore $\lambda_m = \lambda_L^2$, where m is the mass per unit length.

c) Drag force scaling

The drag force, F, in both model and prototype is given by:

$$F = \frac{1}{2}\rho_a V^2 C_D d l$$

where V is the wind speed, C_D the drag coefficient, d the cable diameter and l the cable length. The ratio $\lambda_F = \frac{F_m}{F_p}$ can be written:

$$\lambda_F = \frac{\lambda_M \lambda_L}{\lambda_t^2} = \frac{\lambda_\rho \lambda_L^4}{\lambda_t^2} \quad \text{or} \quad \lambda_F = \frac{\lambda_L^4}{\lambda_t^2} \quad \text{since } \lambda_\rho = 1.0 .$$

Also $\lambda_t = \frac{\lambda_L}{\lambda_V}$, then $\lambda_F = \lambda_L^2 \lambda_V^2 = \frac{V_m^2 C_{Dm} d_m l_m}{V_p^2 C_{Dp} d_p l_p}$

but $\lambda_V = \frac{V_m}{V_p}$, therefore:

$$C_{Dm} d_m = C_{Dp} d_p \lambda_L \qquad (3.3)$$

Due to the dependence of C_D on the Reynolds number it is almost impossible to scale down geometrically the cable diameter, since its drag coefficient would not

correspond to the necessary C_D to give a corrected scaled drag force. For this reason both C_D and d are scaled jointly. The modelling process is explained in 3.3.

d) Reduced frequency

The relationship between length, time and velocity for particular modes of vibration is based on the equality of the reduced frequency in model and in full scale. For the cable the frequency depends a great deal on its sag, which is the important characteristic dimension.

$$\left(\frac{f_c S}{V}\right)_m = \left(\frac{f_c S}{V}\right)_p \tag{3.4}$$

or $\lambda_f = \frac{\lambda_V}{\lambda_L}$, where f_c is the cable natural frequency.

e) Aerodynamic damping

An expression for the aerodynamic damping, ζ_a, can be given by:

$$\zeta_a = \left(\frac{C_D}{4\pi}\right)\left(\frac{V}{fd}\right)\left(\frac{\rho_a d^2}{m}\right)$$

so $(\zeta_a)_m = (\zeta_a)_p$, then:

$$\left(\frac{C_D\, d\, V}{f\, m}\right)_m = \left(\frac{C_D\, d\, V}{f\, m}\right)_p$$

$$\left(\frac{V_m f_p}{V_p f_m}\right)\frac{(C_D d)_m}{(C_D d)_p} = \frac{m_m}{m_p}$$

therefore:

$$\lambda_L \frac{(C_D d)_m}{(C_D d)_p} = \frac{m_m}{m_p} \qquad (3.5)$$

f) Wind / Gravity forces

We must maintain the ratio between wind and gravity forces for both model and prototype:

$$\left(\frac{wind}{gravity}\right)_m = \left(\frac{wind}{gravity}\right)_p$$

$$\left(\frac{\frac{1}{2}\rho_a V^2 C_D l d}{\rho g \frac{\pi d^2}{4} l}\right)_m = \left(\frac{\frac{1}{2}\rho_a V^2 C_D l d}{\rho g \frac{\pi d^2}{4} l}\right)_p$$

but $\rho \frac{\pi d^2}{4} = m$ and $\frac{V_m^2}{V_p^2} = \lambda_V^2$, so:

$$\lambda_V^2 \frac{(C_D d)_m}{(C_D d)_p} = \frac{m_m}{m_p} \qquad (3.6)$$

g) Velocity scaling

For structures where the resistance to deformation is influenced by the action of gravity, it is necessary to maintain Froude number (Fr) similarity, which requires that:

$$\left(\frac{V^2}{gL}\right)_m = \left(\frac{V^2}{gL}\right)_p$$

or

$$\lambda_V^2 = \lambda_L \tag{3.7}$$

This condition makes the aerodynamic damping and wind/gravity forces requirement equations for modelling, to match each other. And they are also equal to the drag force scaling equation, since $m_m/m_p = \lambda_\rho^2$ ($\lambda_\rho = 1.0$).

h) Axial force scaling

To simulate the action of axial forces through the use of equivalent models, the Cauchy number, Ca, must be maintained constant in model and prototype:

$$\left(\frac{EA_c}{\rho_a V^2 L^2}\right)_m = \left(\frac{EA_c}{\rho_a V^2 L^2}\right)_p$$

$(EA_c)_m = (EA_c)_p \lambda_V^2 \lambda_L^2$, but since $A = \frac{\pi d^2}{4}$ and $\lambda_{EA} = \lambda_V^2 \lambda_L^2 = \lambda_L^3$,

$$(Ed^2)_m = (Ed^2)_p \lambda_L^3 \tag{3.8}$$

(It should be remembered that all force scaling is given by $\lambda_F = \lambda_L^3$).

The fulfilment of this requirement is somewhat difficult, especially if we recall that the symmetric in-plane modes also depend on the value of EA and have their own criteria to be satisfied, which does not necessarily match with Eq. (3.8).

3.2.2 Difficulties faced and adopted approach

Just to fix ideas we give a numerical example of a conventional cable modelling. The nominal prototype cable characteristics assumed are L_p= 300 *m*, S_p= 10 *m*, l_p= 300.9 *m*, d_p= 0.04 *m*, m_p= 3 *kg/m* and V_p= 45 *m/s*. From this *Re*≅ 1.2E5 and C_D≅ 1.0, which allows $(C_D d)_p$ = 0.04 *m*. The first fundamental frequency is $(f_{cV})_p$= 0.18 *Hz*. For this example, a geometric scale λ_L= 1/50 is chosen and therefore the velocity scale is $\lambda_V = \sqrt{\lambda_L}$ = 1/7.07. In this case we would have: L_m= 6 *m*, S_m= 0.2 *m*, l_p= 6.02 *m*, m_m= 0.0012 *kg/m* = 1.2 *g/m*, V_m= 6.4 *m/s*, $(C_D d)_m$ = 8E-4 *m* = 0.8 *mm* and $(f_{cV})_m$= 1.24 *Hz*.

In spite of the relatively big geometric scale the mass per unit length has a very low value. This fact makes it difficult to actually build the model. If we compare the full-scale mass per unit length of a suspension bridge cable for example, which has *m* ≅ 5,000 *kg/m*, with the transmission line *m* ≅ 3 *kg/m* or less, and look at the usual model dimensions of a bridge model, we can see the difficulties involved in simulating the transmission line in reduced scale. There is also the problem of simulating *EA* for axial forces and symmetric in-plane mode shapes. And because we are dealing with the line behaviour under design velocities, i.e., high wind speeds, we can be concerned only with the drag forces and avoid the problems related to cross-wind simulation. Furthermore, with a model span as calculated, it is very difficult (in our case impossible) to fit the model in conventional boundary layer wind tunnels that generally do not have such a wide section.

The strategy adopted is to go by parts and try to solve some of the problems and see what are the consequences in the results due to the approaches adopted.

To accommodate such a span or even several spans of these systems in the wind tunnel, a new modelling approach to tower and conductor systems using a distorted scale was developed. Such an approach is based on the idea that distorting horizontally the cable but maintaining the same sag and preserving the properties of the "normal" model (mass, drag, frequency), would not alter significantly its behaviour, since the natural frequencies of the cables are primarily a function of their sags when the cable tension is not too high. That is, the modelling approach would be firstly to go from the full-scale to the "normal" model and from this to the "distorted" model, keeping the model sag the same. The flow conditions in the wind tunnel simulation are also kept the same.

3.2.3 **Distorted modelling**

A reduced span L_m*, obtained from the distortion of the original model span L_m by an amount γ, is utilised, so that $L_m^* = \gamma L_m$. The new length scale is then:

$$\lambda_L^* = \frac{L_m^*}{L_p} = \frac{\gamma L_m}{L_p} = \gamma \lambda_L \tag{3.9}$$

where the symbol * refers to a quantity used in the distorted model.

In order to have the same behaviour in both models the mass, drag forces, aerodynamic damping and reduced frequency must be kept the same:

a) Mass

$$M_m = M_m^*$$

$$m_m L_m = m_m^* L_m^*$$

$$m_m L_m = m_m^* \gamma L_m$$

$$m_m^* = \frac{m_m}{\gamma} \tag{3.10}$$

Eq. (3.10) implies that the original mass per unit length, m_m, has to increase by $1/\gamma$ if the total mass, M_m, is to be maintained.

b) Drag Force

$$\left(\tfrac{1}{2}\,\rho_a\, V^2 C_D\, d\, L\right)_m = \left(\tfrac{1}{2}\,\rho_a\, V^2\, C_D\, d\, L\right)_m^*$$

but $V_m = V_m^*$ so,

$$(C_D d)_m L_m = (C_D d)_m^* \gamma L_m$$

therefore,

$$(C_D d)_m^* = \frac{(C_D d)_m}{\gamma} \tag{3.11}$$

Distorting the mass per unit length and $C_D d$ by the same amount γ guarantees that the ratio between wind and gravity forces, Eq. (3.6), is also preserved.

At this point it should be pointed out that the correct length dimension to be used in the calculation of the "new" mass per unit length and drag force per unit length is l (the actual cable length) and therefore a $\gamma' = l^*/l$ should be used for distortion. However this γ' has practically no difference from the $\gamma = L^*/L$ in the models studied here and the ratio between the spans L will be kept for convenience.

c) Aerodynamic damping

$$\left(\frac{C_D V \rho_a d^2}{4\pi f d \; m}\right)_m = \left(\frac{C_D V \rho_a d^2}{4\pi f d \; m}\right)_m^*$$

$$\left(\frac{C_D d}{f m}\right)_m = \left(\frac{C_D d}{f m}\right)_m^*$$

$$\frac{(C_D d)_m}{f_m m_m} = \frac{(C_D d)_m}{\gamma} \frac{\gamma}{m_m} \frac{1}{f_m^*}$$

therefore,

$$f_m = f_m^* \tag{3.12}$$

That is, to maintain the same aerodynamic damping the two models must have the same natural frequency.

d) Reduced frequency

$$\left(\frac{fS}{V}\right)_m = \left(\frac{fS}{V}\right)^*_m$$

Since $S_m = S_m^*$ and $V_m = V_m^*$, then $f_m = f_m^*$. Again, the same requirement as for the aerodynamic damping: the distorted model must have the same frequency as the normal model. This condition is closely satisfied since the natural frequencies of suspended cables are primariiy a function of their sags when the cable tension is not extremely high.

c) Axial Force

$$\left(\frac{EA_c}{\rho_a V^2 L^2}\right)_m = \left(\frac{EA_c}{\rho_a V^2 L^2}\right)^*_m$$

$$\left(\frac{Ed^2}{L^2}\right)_m = \left(\frac{E^* d^{*2}}{\gamma^2 L^2}\right)_m$$

therefore,

$$E^* d^{*2} = \gamma E d^2 \qquad (3.13)$$

Strictly speaking, we should diminish Ed^2 by γ, although this would not make the strain of both models be the same (the reason being the difference in cable tension of the two models). However, due to the already mentioned difficulties in EA simulation, this condition will not be strictly followed. This gives more flexibility in the choice of the cable diameters for the design and construction of the models. The consequences of this assumption will be verified in the results.

As usual in aeroelastic studies, it is very difficult to satisfy all the requirements and some compromise has to be made. For the case of transverse wind loads transmitted by the cables to their supports, the conductor tension was found by Armitt et al (1975) to have a negligible influence on the transverse loadings.

3.3 TESTING DISTORTION THEORY

3.3.1 Design of models 1 & 2

To initiate the study, two cable models corresponding to the same prototype were tested. One was a "normal" model and the other a "distorted" one. The general characteristics are indicated in table 3.1 together with the estimated first natural frequencies for a "no wind " condition. The predicted natural frequencies for other modes of vibration are shown in tables B.1a and B.1b in Appendix B for both, tension due to its own weight (or a "no wind" condition) and resultant tension due to the combination of its

own weight and the mean wind speed based on the velocities considered. The values of EA adopted are considered as well.

The models were built by employing a technique broadly used in wind tunnel modelling of bridge cables and also used by Vickery (1981) in a simulation of elevator cables. It consists in using a basic cable of very small diameter to simulate, if desired, the axial stiffness and flexibility, over which are attached lumped pieces (cylinders or spheres) of a certain material to give, together with the basic cable, the required average mass per unit length and the required average $C_D d$ per unit length.

Both models were built using as basic cable a steel piano wire with diameter ϕ=2.29E-4 m over which lumped foam cylinders (3mm diameter, 10mm length) were attached. Some views of the models are shown in Figs. 3.1, 3.2 and 3.5. It was decided to keep the mass as low as possible in the first models for two reasons: (a) to test if it was possible to make a model work in a lower extreme case (corresponding smaller values are not expected to be found in full-scale), and (b) to keep the influence of the mass and related properties a minimum.

Table 3.1 General characteristics of first models tested (target).

	L [m]	S [m]	l [m]	m [kg/m]	V [m/s]	$C_D d$ [m]	f_1 [Hz]
Prototype (nominal)	150.0	7.50	151.00	1.0000	45.0	0.0300	0.20
Normal Model	3.0	0.15	3.02	0.0004	6.4	0.0006	1.44
Distorted Model (γ=0.5)	1.5	0.15	1.54	0.0008	6.4	0.0012	1.48

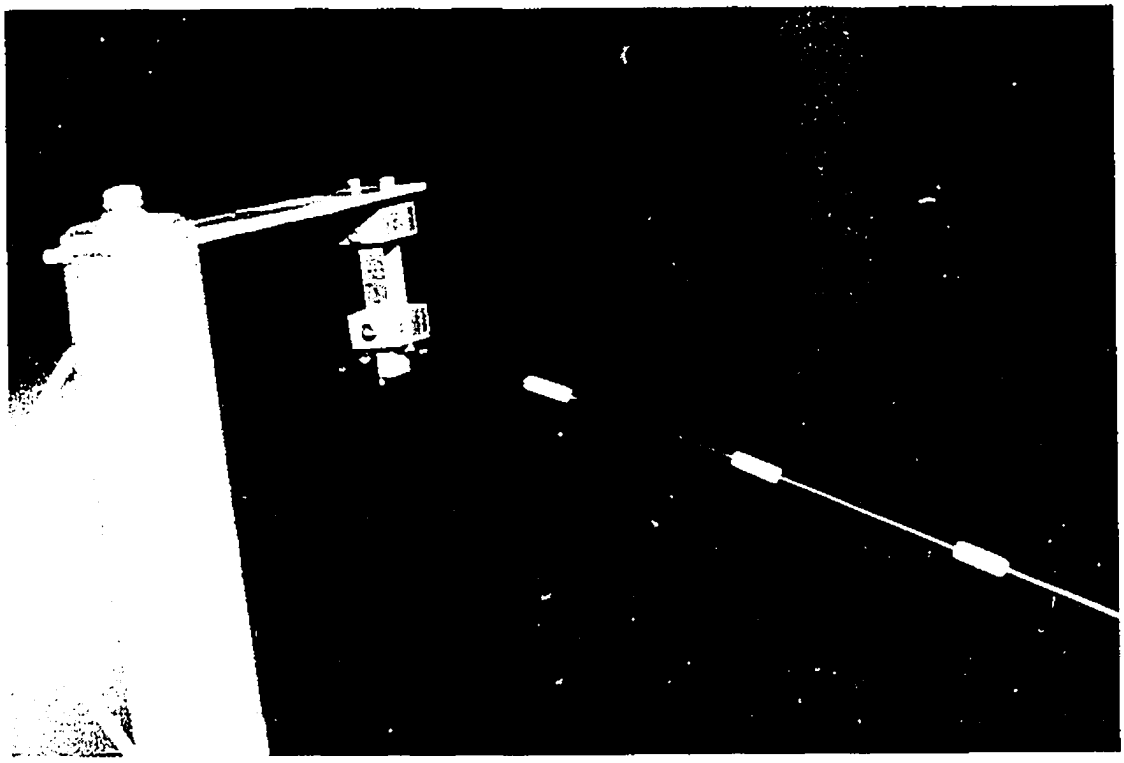

Figure 3.1 Detail of cable configuration and load cell.

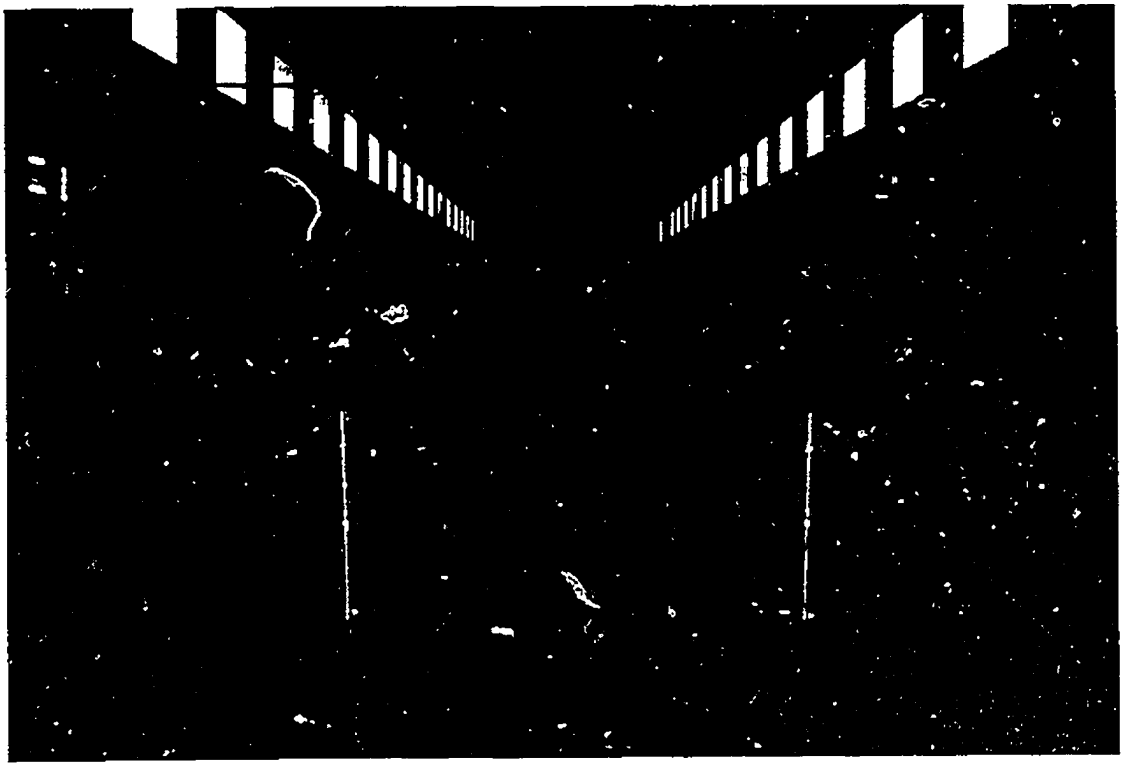

Figure 3.2 View of model 2 (distorted) in the wind tunnel.

The natural frequencies of the distorted and the normal models are very close and can be assumed to be the same. The actual values obtained for the total mass of the cable models were M_1=1.3g and M_2=1.1g, which gives $m_1 \cong 0.43 g/m$ and $m_2 \cong 0.71 g/m$. The value of $C_D d$ is chosen from a smooth flow regime and therefore the correctness of the model design will be checked using the results from exposure 3 - smooth flow.

3.3.2 **Wind Simulation**

The tests were done in the low-speed section of the BLWT II, in which the length of the working section upstream of the model is about 43m. Three different exposures were used in the study. The method employed for simulating the natural wind in boundary layer wind tunnels is very well known and has been described by Davenport and Isyumov (1967). The adopted exposures are shown in figures 3.3 to 3.5. One of the reasons to use the low speed section is its large width (4.88m) and its lower wind velocities (Froude number requirement), making it the best option to test the transmission lines.

3.3.2.1 **Wind Profiles**

Pitot-Prandtl tube and hot-wire measurements of the mean wind speed and intensity of turbulence were made at several points along a horizontal line corresponding to the width of the wind tunnel (Fig. 3.6), and vertically, in the midspan portion of the

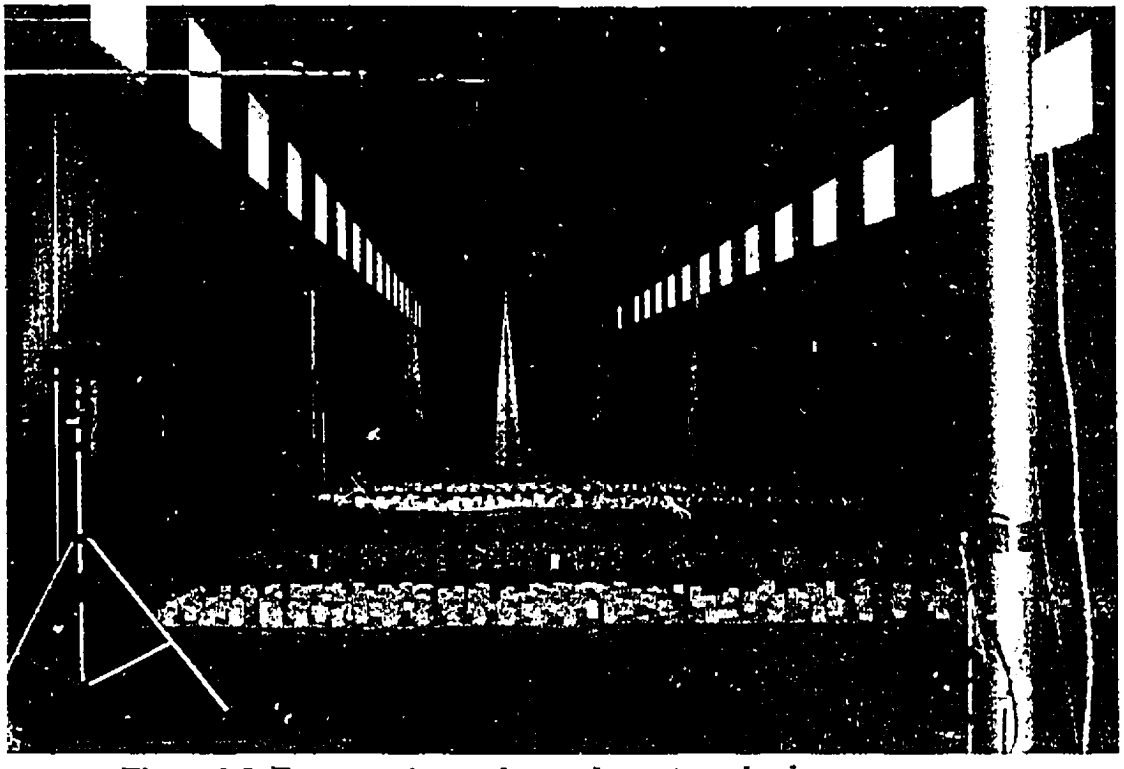

Figure 3.3 Exposure 1: roughness elements and spires.

Figure 3.4 Exposure 2: spires only.

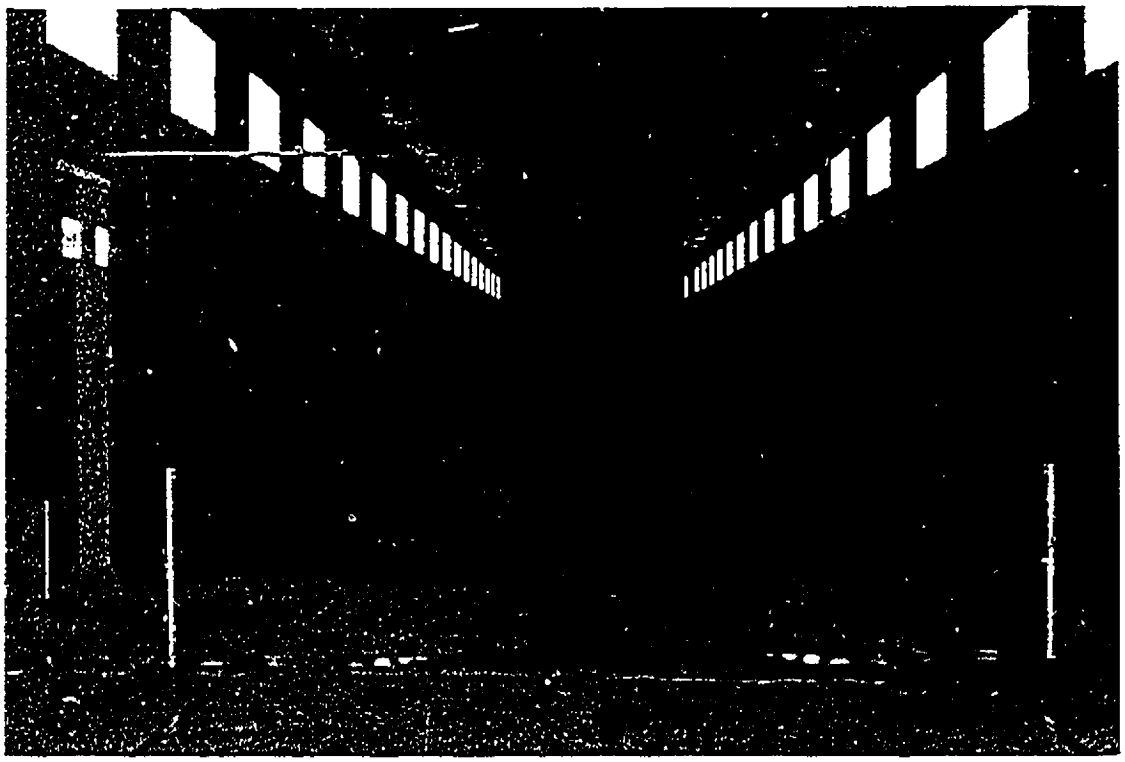

Figure 3.5 Exposure 3: bare floor.

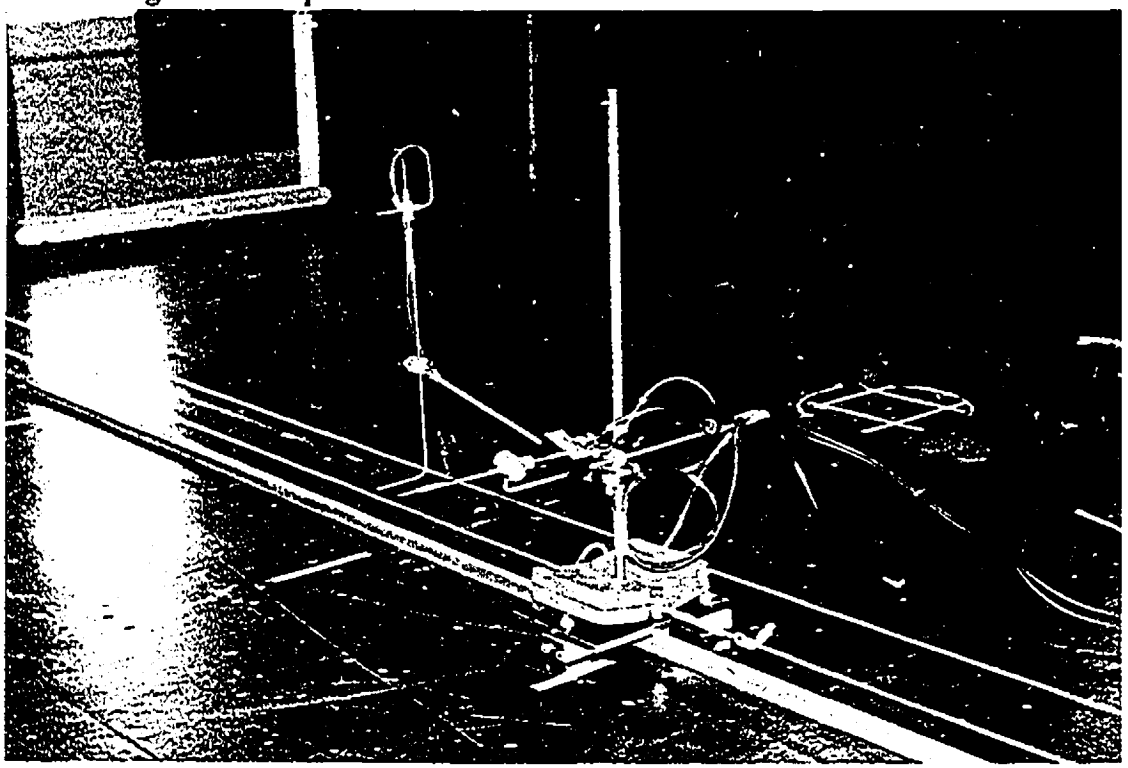

Figure 3.6 Device used to carry Pitot-Prandtl tube and hot-wire anemometer along wind tunnel cross-section.

lines. The vertical velocity profiles for the exposures tested are shown in Figs. 3.7 to 3.9 normalised by the largest reading. These are plotted together with the local intensity of turbulence $\sigma(z)/V_z$, which are $I_v = 0.14$ for exposure 1 and $I_v = 0.11$ for exposure 2.

From the horizontal profiles it was verified that the boundary layer of the walls was less than 1 *m*, therefore leaving a "useful" 3 *m* wide test section.

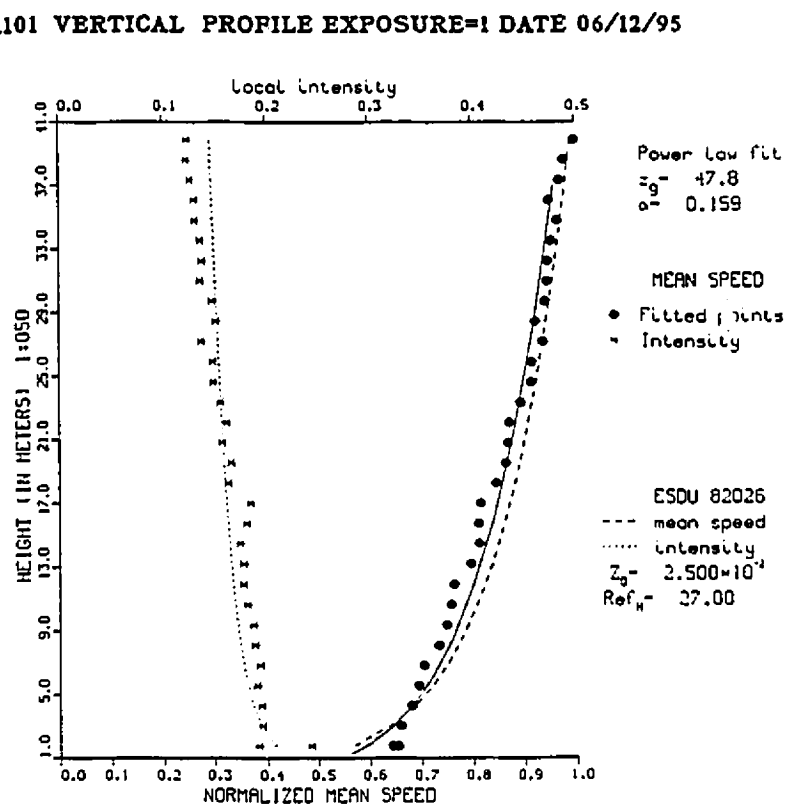

Figure 3.7 Vertical wind profile for exposure 1.

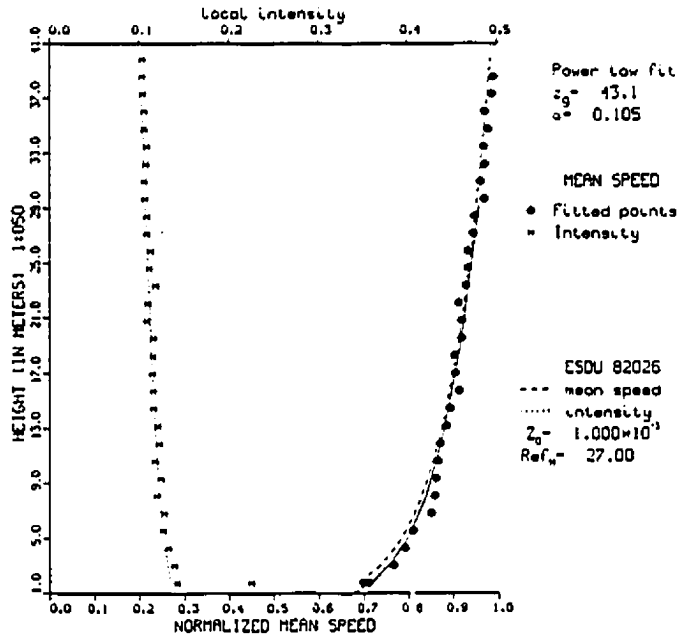

Figure 3.8 Vertical wind profile for exposure 2.

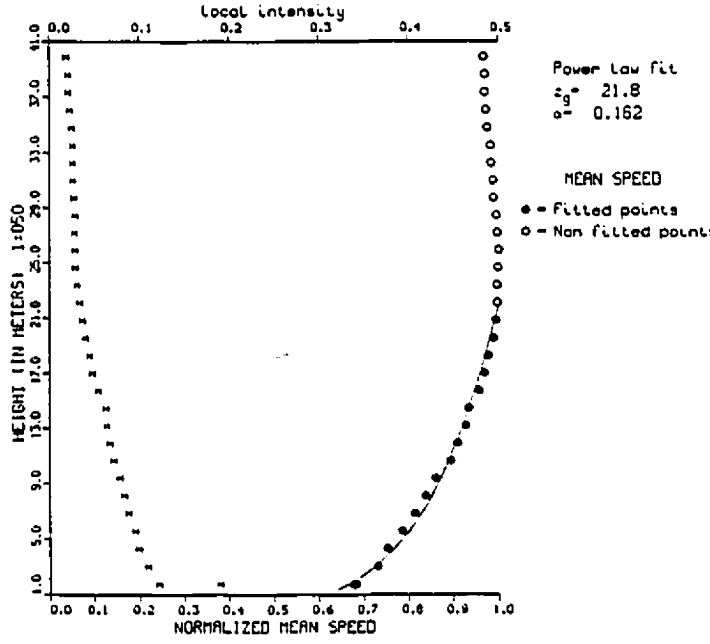

Figure 3.9 Vertical wind profile for exposure 3.

3.3.2.2 Span-wise Cross-correlation of the Wind

A spatial covariance (or cross-covariance, or cross-correlation) function is formed by multiplying together pairs of values of velocity components measured simultaneously at two separated points and taking the time-averaged value. The cross-covariance functions are usually normalised by dividing by the standard deviations of the constituent components to obtain a cross-correlation coefficient defined as:

$$R_{xx'}(v_x, v_{x'}) = \frac{\overline{v(x,t)v(x',t)}}{\sigma_{v_x}\sigma_{v_{x'}}} \tag{3.14}$$

where:

$v(x,t)$, $v(x',t)$ = fluctuating components of wind speeds at points x and x'.

$\sigma_{v_x}, \sigma_{v_{x'}}$ = standard deviations of wind speeds at points x and x'.

The variation of the cross-correlation coefficient $R_{xx'}$ with span-wise separation and exposures for the longitudinal fluctuating velocity component is given in Fig. 3.10. It is interesting to note that the cross-correlation coefficients for exposure 1 are a bit smaller than those for exposure 2, even though exposure 1 has more turbulence intensity at the same height. This suggests that the turbulence length scale for exposure 2 is bigger than exposure 1. The turbulence was generated by small roughness elements 65*mm* high placed 16*m* upstream of the model (only for exposure 1) and by 2.5*m* high spires, used in both exposures.

Figures 3.11 and 3.12 show the cross-correlation coefficients for both exposures and the exponential function $e^{-(\Delta x/L)}$ used to approximate the cross-correlation function. In this case $L_1 \cong 310mm$ (or $15.5m$ full-scale) and $L_2 \cong 340mm$ (or $17m$ full-scale). The measurements were made close to the center of the wind tunnel cross-section, at the cables height, as shown in Fig. 3.19. The fixed probe was located $150mm$ from the center line and the moving probe crossed the center line.

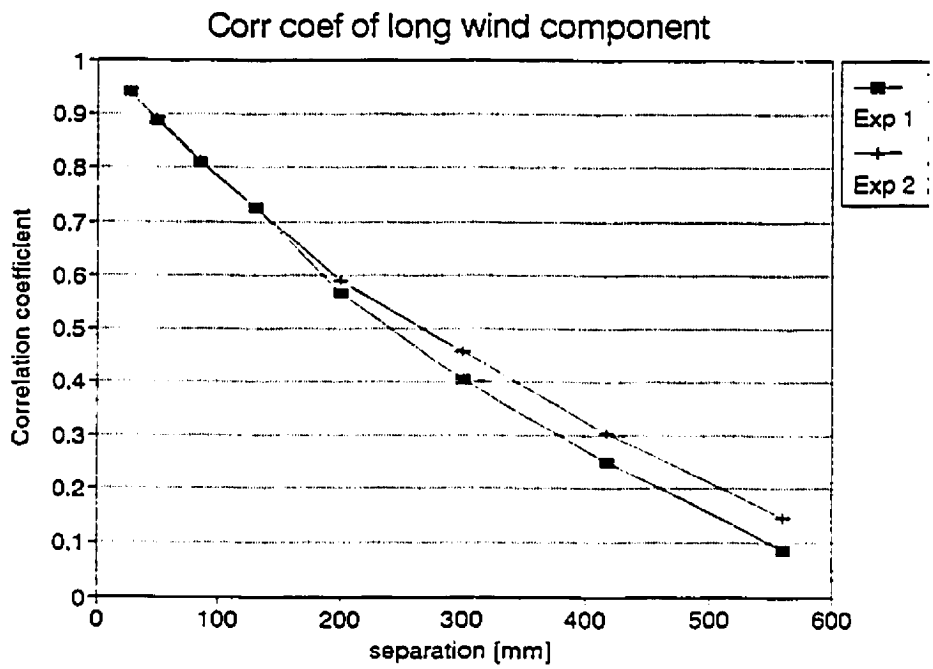

Figure 3.10 Variation of the cross-correlation coefficient with span-wise separation and exposures for the longitudinal fluctuating velocity component.

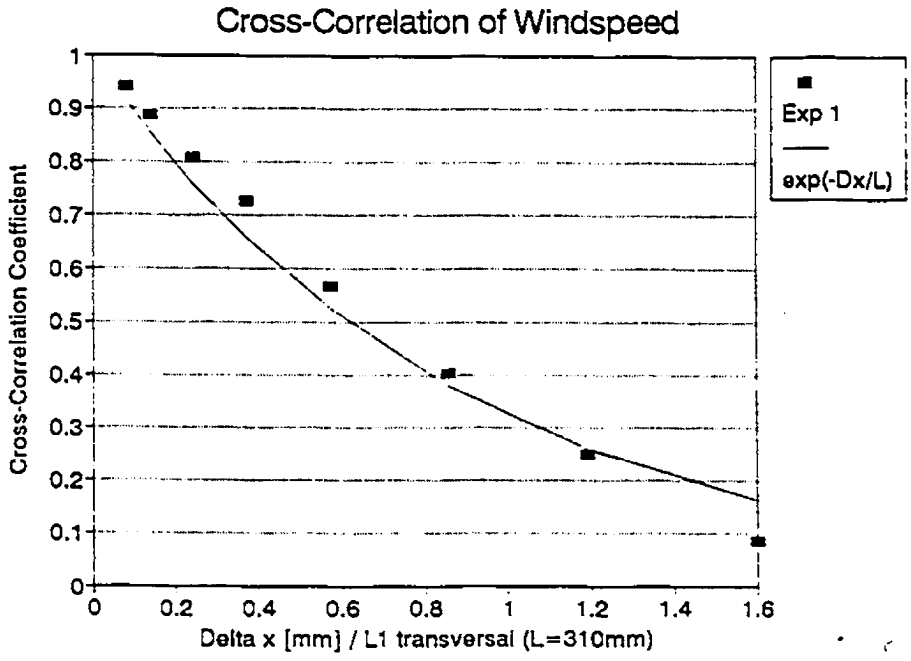

Figure 3.11 Cross-correlation of wind speed for exposure 1 and fit by exponential function.

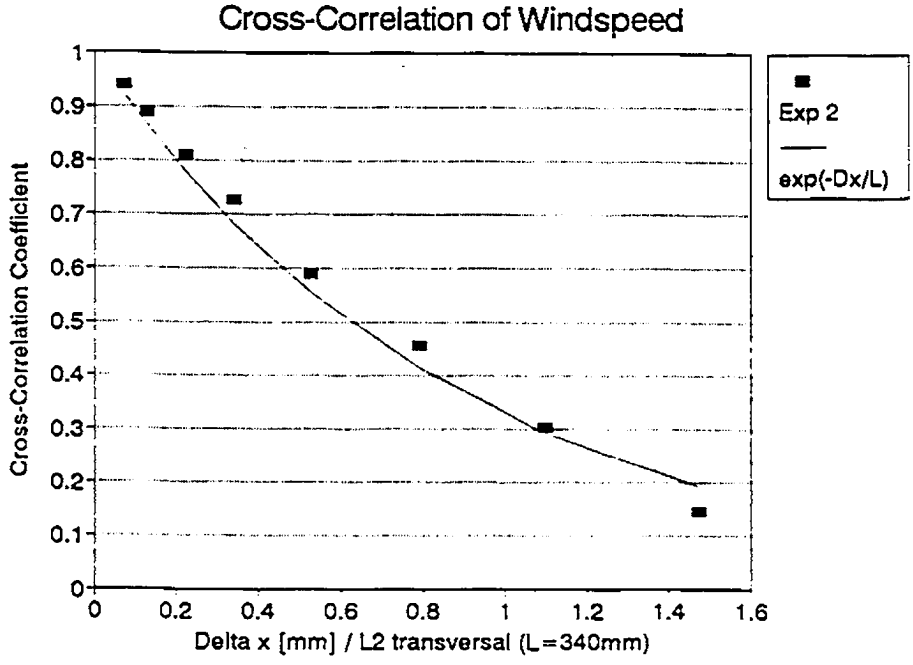

Figure 3.12 Cross-correlation of wind speed for exposure 2 and fit by exponential function.

3.3.2.3 Wind Spectra

It is often more convenient to work in the frequency domain rather than in the time domain. In this context spectral functions of atmospheric turbulence are appropriate because they provide information on the frequency distribution of the kinetic energy of the fluctuating velocity components (ESDU 74030).

Wind energy as a function of frequency is commonly expressed in terms of the "spectral density" function $S(f)$. The spectral density in the longitudinal (along-wind) direction is denoted $S_v(f)$ and in the vertical direction $S_w(f)$. The measured data, $fS(f)$, can be plotted normalised by σ^2, the total variance or area under the spectrum, or by $\overline{V}^2$ which effectively presents a simultaneous comparison of the distribution of spectral content and overall turbulence intensity. The expression used to fit the data is from ESDU(1974) and is of the form:

$$\frac{fS_v(f)}{\sigma_v^2} = \frac{4\,n_v}{(1+70.8\,n_v^2)^{5/6}} \tag{3.15}$$

$$\frac{fS_w(f)}{\sigma_w{}^2} = \frac{4\,n_w(1+755.2\,n_w^2)}{(1+283.2\,n_w^2)^{11/6}} \tag{3.16}$$

where $n_v = L_v f / \overline{V}$ and $n_w = L_w f / \overline{V}$.

The spectra normalised by $\overline{V}^2$ are obtained multiplying those expressions by the corresponding turbulence intensity squared:

$$\frac{fS_v(f)}{\overline{V}^2} = \frac{fS_v(f)}{\sigma_v^2} I_v^2 \tag{3.17}$$

$$\frac{f S_w(f)}{\overline{V}^2} = \frac{f S_w(f)}{\sigma_w^2} I_w^2 \qquad (3.18)$$

where $I_v = \sigma_v / \overline{V}$ and $I_w = \sigma_w / \overline{V}$.

ESDU gives expressions for turbulence length scales in the along wind direction:

$$^{y}L_v = 25\, z^{0.35} / z_o^{0.063} \qquad (3.19)$$

$$^{y}L_w = 0.35\, z \qquad (3.20)$$

where z is the height, in meters, and z_o the roughness length, also in meters.

The power spectra of the longitudinal and vertical components of the turbulence were measured at a few points along the line. Figs. 3.13 to 3.16 show the spectra for the center of the line at half the sag length. The (on-line) power spectra were obtained using the Fast Fourier Transform method, with 512 points, 50 blocks (or degrees of freedom) and a sampling rate of 400 Hz. The sampling frequency was chosen to be at least two times the maximum desired frequency, to avoid aliasing (Randall, 1987).

The values of the turbulence length scales obtained from the ESDU 74031 equations (3.19) and (3.20), using values from the wind profiles fitting, are given in Table 3.2 for z=27m full-scale. The value of $z_0 \cong 0.025\ m$ for Exp 1 and $z_0 \cong 0.001\ m$ for Exp 2. Exposure 3 gives a smooth flow at the reference height and therefore does not simulate a natural wind. It will be used just for comparison among the cables measured forces.

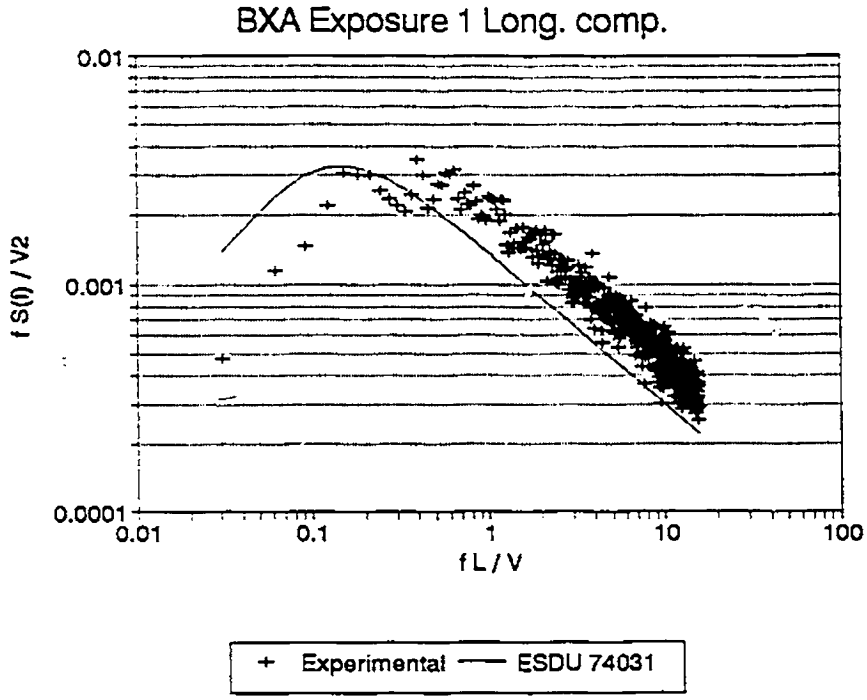

Figure 3.13 Power spectrum of the longitudinal component of wind turbulence for exposure 1.

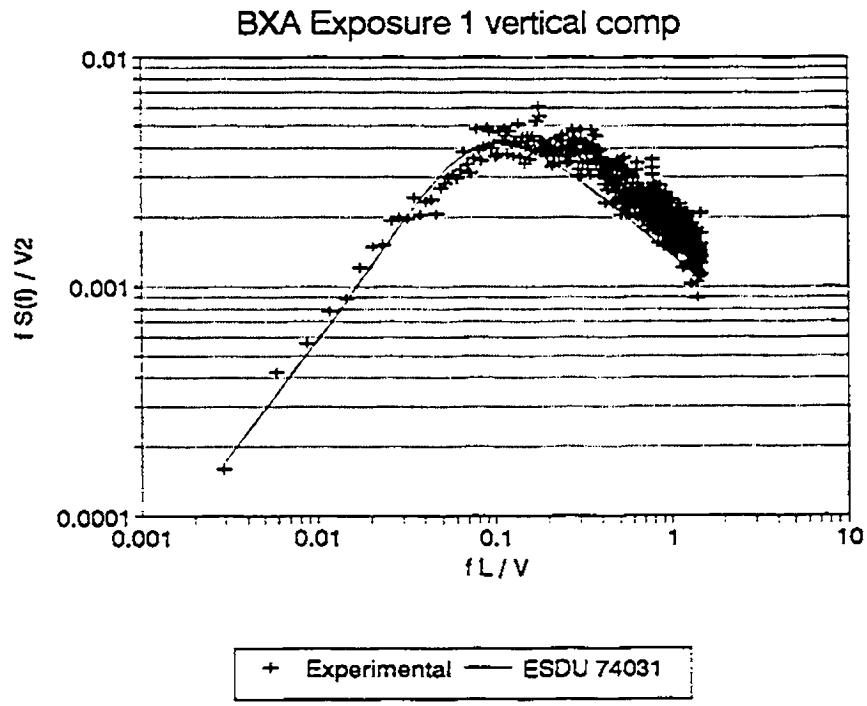

Figure 3.14 Power spectrum of the vertical component of wind turbulence for exposure 1.

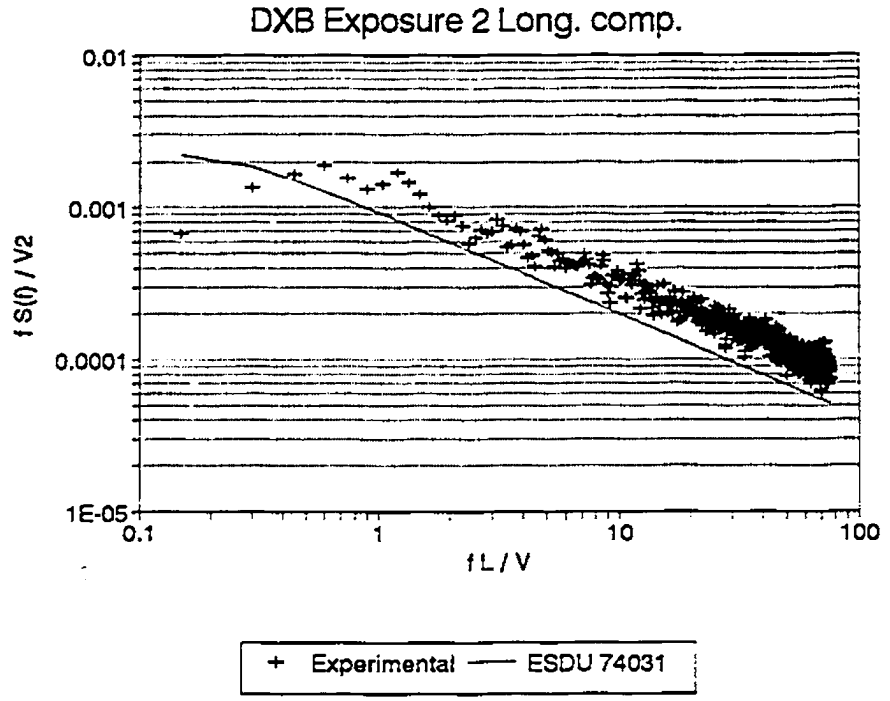

Figure 3.15 Power spectrum of the longitudinal component of wind turbulence for exposure 2.

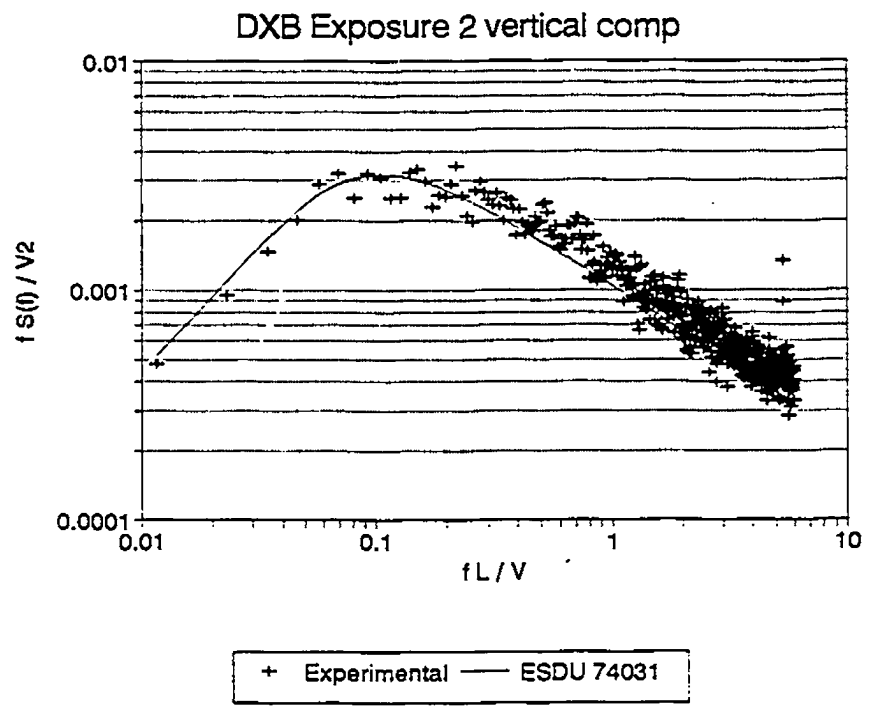

Figure 3.16 Power spectrum of the vertical component of wind turbulence for exposure 2.

Table 3.2 Turbulence length scales obtained from Eqs. (3.19), (3.20) and (3.21).

	Length [m]		
Turbulence component	Exposure	Eq. (3.21)	Eqs. (3.19),(3.20)
${}^{x}L_{v}$	1	3.00	2.00
${}^{x}L_{v}$	2	3.90	2.45
${}^{x}L_{w}$	1 , 2	0.30	0.19

It is also possible to estimate the length scales of turbulence (or macroscales) from the wave number corresponding to the peak of the spectra through the relationship:

$$L_{v,w} = \frac{1}{2\pi} \frac{U}{f_{peak}} \tag{3.21}$$

evaluated at the peak of the normalised spectrum of the given component.

${}^{x}L_{v}$ gives an estimate of the longitudinal component in the along wind direction; the transverse scale is roughly between one third to one half this measure. Several expressions to obtain the turbulence length scales are found in the literature and the variability among them may not be small in many instances. A comparative study of those was made by Blessmann (1995).

3.3.2.4 **Coherence**

Of particular interest when examining dynamic response of structures is the correlation of individual frequency components of wind turbulence, or "narrow-band

correlation". This examines the relation of wind properties at two different points separated by a distance Δx at a narrow band of frequencies around any given frequency f.

The cross-spectrum between any two points has both in-phase (real) and out-of-phase (imaginary) components:

$$S_{12}(f) = Co_{12}(f) + i\, Qu_{12}(f) \tag{3.22}$$

where

$S_{12}(f)$ = Cross-spectrum between points x_1 and x_2
$Co_{12}(f)$ = Co-spectrum (in phase)
$Qu_{12}(f)$= Quadrature spectrum (out-of-phase)

A "Coherence Function" can be defined as:

$$Coherence\ (f) = \frac{Co_{12}^2(f) + Qu_{12}^2(f)}{S_{11}(f)\, S_{22}(f)} \tag{3.23}$$

where $S_{11}(f)$, $S_{22}(f)$ = spectra at points x_1 and x_2.

A narrow-band correlation function is then defined as (and related to the coherence function by):

$$\sqrt{Coherence(f)} = \gamma_{12}(\Delta x, f) = e^{-\frac{C|\Delta x|f}{V}} \tag{3.24}$$

A fundamental assumption in the theory of predicting the dynamic response of structures to turbulent wind is that the span-wise coherence of the fluctuating aerodynamic forces is the same as the span-wise coherence of the fluctuations of the velocity components. The Joint Acceptance Function (see Chapter 2) is estimated by making use of this "strip assumption" and it is common practice in wind engineering to accept it as valid. However, this may not be what really happens in some structures. Larose (1992) observed that, in performing wind tunnel tests and full-scale measurements on the West Gate Bridge, Melbourne (1982) has found the span-wise coherence of the pressure fluctuations at the leading edge of the deck to be larger, by a significant amount, than the span-wise coherence of the longitudinal velocity fluctuations. Similar conclusions have been reached by Jancauskas and Sankaran (1992). In the present work, due to the enormous difficulties involved in actually measuring the pressures along the model span, both span-wise coherences (wind velocity fluctuations and fluctuating aerodynamic forces) are assumed to be the same. For transmission line cables however, this seems to be a reasonable assumption since the cable cross-section has much smaller dimensions (width and depth) than a bridge deck cross-section.

Figures 3.17 and 3.18 show the classical representation of the span-wise coherence of the wind velocity fluctuations for the longitudinal component, while Fig. 3.19 shows the two hot-wire probes used to measure them. The plots show the square root of the coherence versus the reduced frequency $f\,\Delta x / V$ (which is the ratio of the separation to the wave length λ of the fluctuations) and the curves are expected to collapse. The points are fitted by the empirical expression $exp(-C\,\Delta x\, f / V)$. However, this

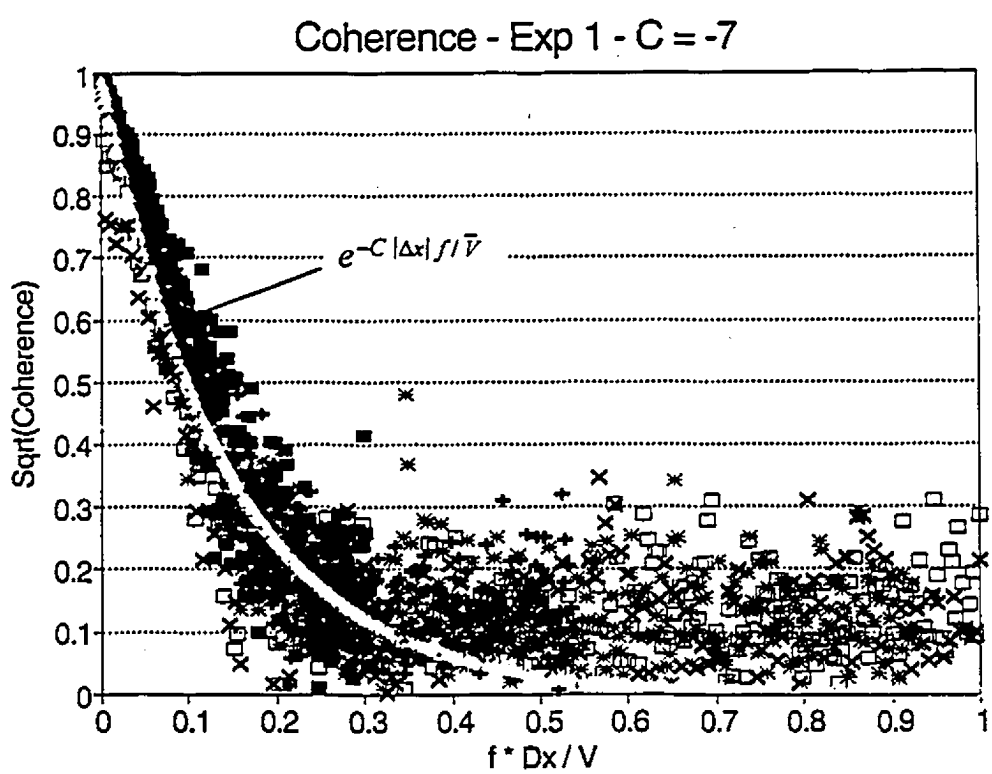

Figure 3.17 Square-root of wind speed coherence for exposure 1.

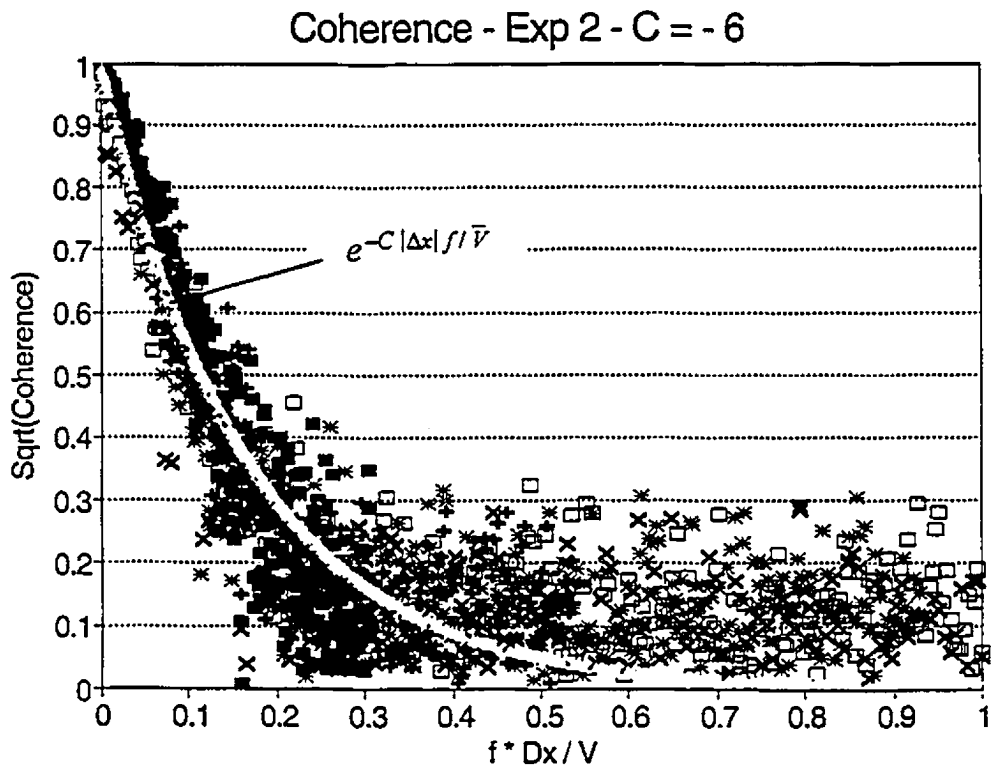

Figure 3.18 Square-root of wind speed coherence for exposure 2.

is most valid for separations Δx somewhat smaller than the scale of the turbulence and collapse for larger separations Δx at lower values of reduced frequency are generally not satisfactory. Larose (1992) compares this method with the work by Roberts and Surry (1973), which suggests that the von Kármán parameter is a more appropriate choice for collapsing the coherence data than the separation to wave length ratio. A similar procedure is adopted by Jancauskas and Sankaran (1992). Due to its applicability in the theoretical approach, however, the former parameter is used in this work, and the values of the constant are C=7 for exposure 1 and C=6 for exposure 2.

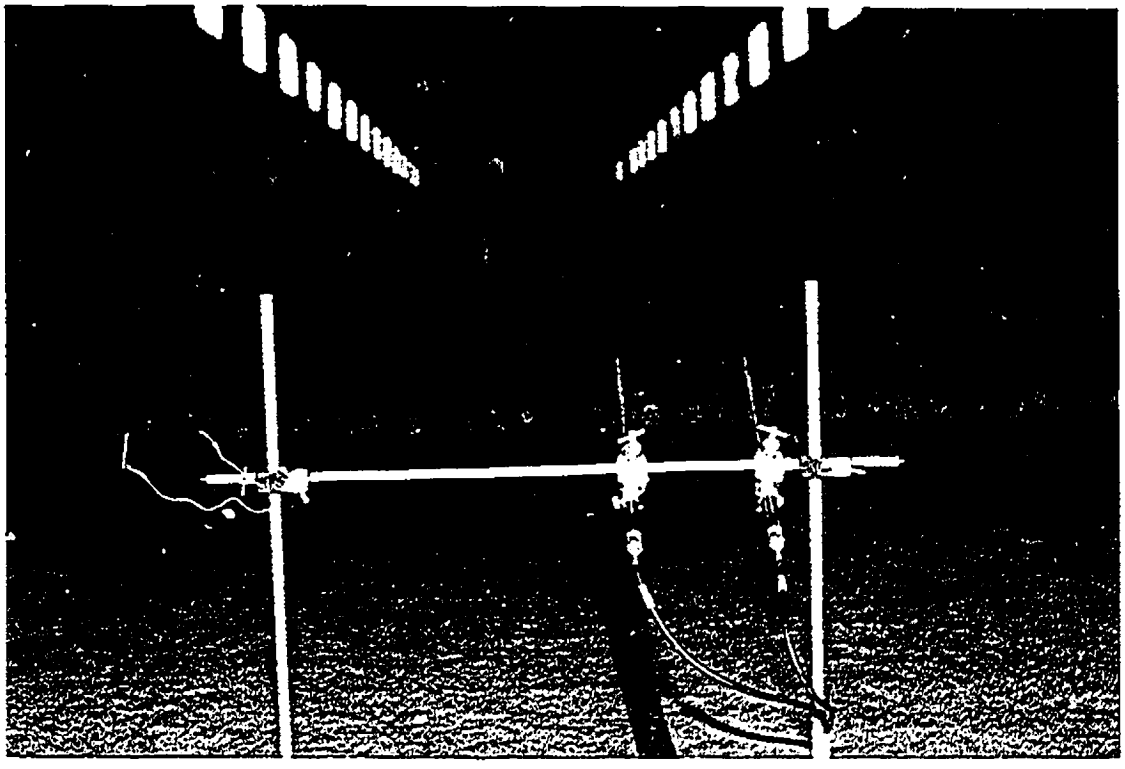

Figure 3.19 Hot-wire probes and set-up for coherence and cross-correlation measurements.

3.3.3 Instrumentation

Force balances were used to measure the drag forces at the cables extremes. These load cells, already shown in Fig. 3.1, were developed by Omega Engineering Inc. and used by Mounla (1995) in his Doctoral Thesis. The load cell is connected to a Vishay power supply and signal amplifier. The signal output is amplified 2100 times, with an excitation voltage of 6 *V* dc. Before the bridge is excited, the amplifier is balanced to correct for the resistance in the cable and connections. The Vishay output is connected to a low-pass signal filter set at 55 *Hz*. The filter output is then connected to the Data Acquisition System and the signal sampled at 160 *Hz* to avoid aliasing.

The load cells were calibrated by applying a (known) load and recording the output voltage. The applied loads varied from 1 to 20 *g*. A plot of the output voltage vs. applied load yielded the calibration curve for each load cell, as shown in Fig. 3.20 for one load cell.

From the estimated loading of the cables it was verified that the maximum corresponding voltage generated would be less than 0.4 *V*. To increase the reliability of the measurements and to diminish the influence of noise it was decided to amplify the signal by 10 times (20 *dB* in the filter). This would serve the intended purpose by increasing the signal to around 4 *V* maximum and still be under the + or - 5 *V* limit of the aquisition system.

For the case of the spectrum of the force fluctuation, there is another resource to apply even if the original signal is above 0.5 *V*. That is to connect a high-pass filter to the

Vishay before passing through the low-pass filter. The high-pass is set at 0.1 *Hz* and eliminates the D.C. component (mean), leaving "room" for amplification of the fluctuating part and diminishing noise influence.

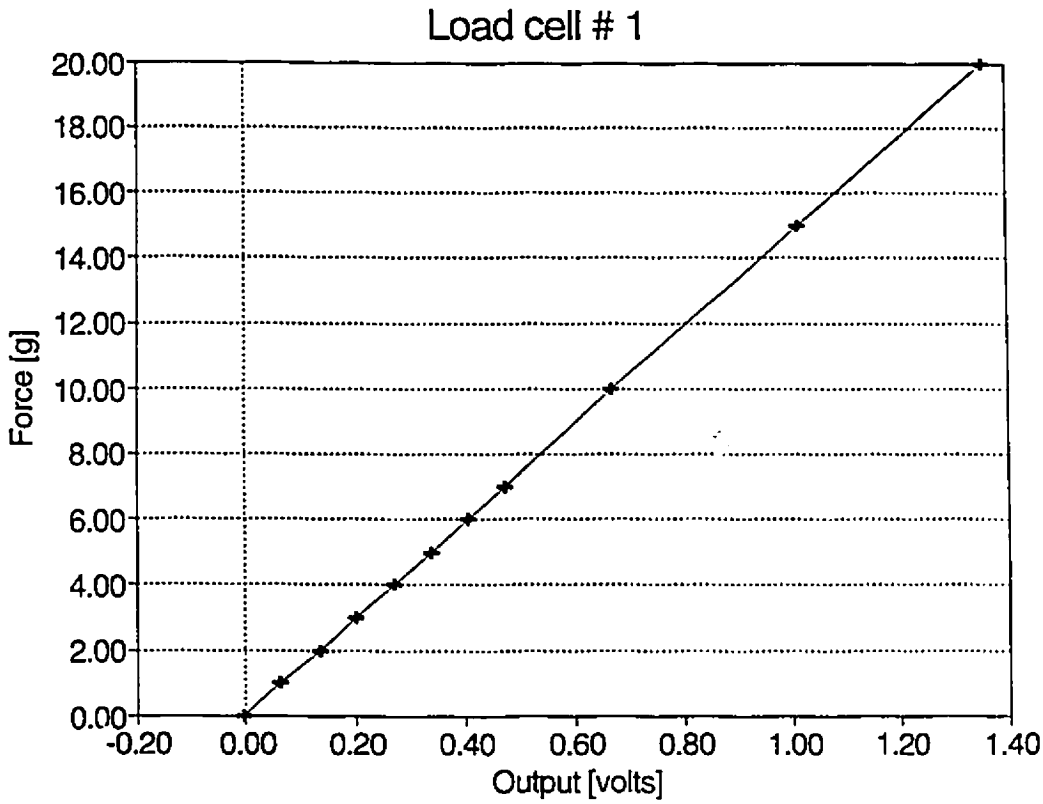

Figure 3.20 Force balance calibration, showing the linear behaviour between strain and force.

3.3.4 Experimental results for models 1 & 2 (Normal/Distorted)

The testing of the cable model included measurements of the time history of the drag force over a period of time (500 seconds) corresponding to approximately 60 minutes in full-scale for the desired wind speed. From these, the mean, root-mean-square

(rms), maximum and minimum values of the response as well as the force spectra were obtained. The spectra were also measured independently, through specific software, and have compared very well with those obtained from the time series.

Two angles of incidence were tested: 0° incidence (transverse wind) and 45° incidence (oblique wind). The models were also tested for a slightly higher velocity and a slightly smaller velocity in the case of the time series, plus 3 extra lower velocities in the measurements of the force spectra. Although the model was not designed for those wind speeds, they serve the purpose of qualitative information.

The values obtained are shown in tables 3.3 and 3.4.

Table 3.3 Cable models drag forces at one extreme for transverse wind incidence (0°).

Model	Exposure	Velocity [*m/s*]	Max [*gf*]	Min [*gf*]	Mean [*gf*]	RMS [*gf*]	Variance [$(gf)^2$]
normal	1	5.8	2.92	1.21	1.99	0.213	0.04517
		6.4	3.73	1.44	2.43	0.254	0.06457
		6.6	3.97	1.58	2.65	0.279	0.07790
distorted	1	5.8	3.37	0.88	2.01	0.318	0.10098
		6.4	4.27	1.48	2.74	0.369	0.13653
		6.6	4.47	1.28	2.65	0.400	0.15987
normal	2	5.9	2.92	1.34	2.14	0.180	0.03223
		6.4	3.74	2.04	2.82	0.208	0.04317
		6.7	4.12	2.25	3.11	0.233	0.05437
distorted	2	5.9	3.41	1.34	2.33	0.269	0.07225
		6.4	3.98	1.61	2.63	0.291	0.08469
		6.7	4.46	1.70	2.88	0.318	0.10133

Table 3.4 Cable models drag forces at one extreme for oblique wind incidence (45°).

Model	Exposure	Velocity [*m/s*]	Max [*gf*]	Min [*gf*]	Mean [*gf*]	RMS [*gf*]	Variance [$(gf)^2$]
normal	1	5.8	1.69	0.47	1.06	0.170	0.029
		6.4	2.19	0.63	1.34	0.202	0.041
		6.6	2.36	0.73	1.54	0.221	0.049
distorted	1	5.8	2.10	0.41	1.13	0.219	0.048
		6.4	2.53	0.55	1.48	0.263	0.069
		6.6	3.16	0.64	1.65	0.295	0.087
normal	2	5.9	1.73	0.71	1.17	0.141	0.020
		6.4	2.09	0.86	1.41	0.170	0.029
		6.7	2.37	0.96	1.59	0.187	0.035
distorted	2	5.9	2.00	0.49	1.15	0.192	0.037
		6.4	2.44	0.77	1.48	0.224	0.050
		6.7	2.79	0.93	1.72	0.243	0.059

From the analyses of tables 3.3 and 3.4 it can be observed that:

-- The mean values measured from the normal model have, in general, a fairly good agreement with the mean values obtained from the distorted values. This is illustrated in Figure 3.21.

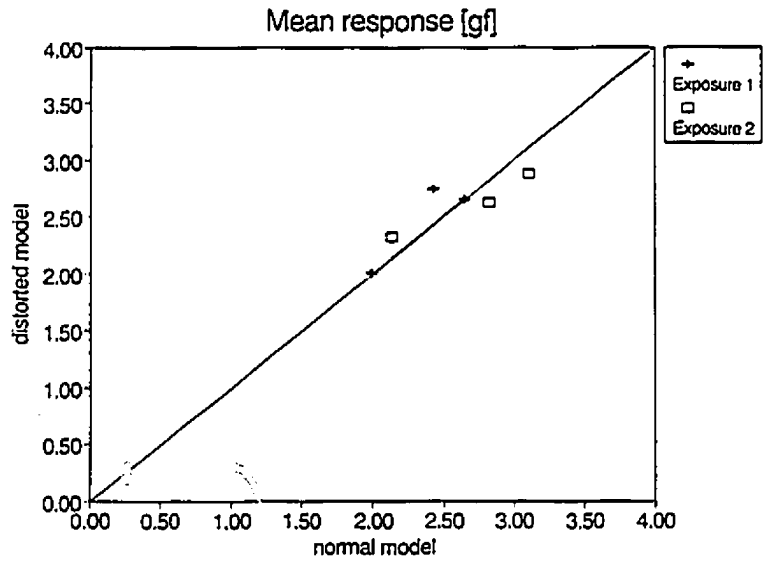

Figure 3.21 Comparison of mean responses given by normal and distorted models.

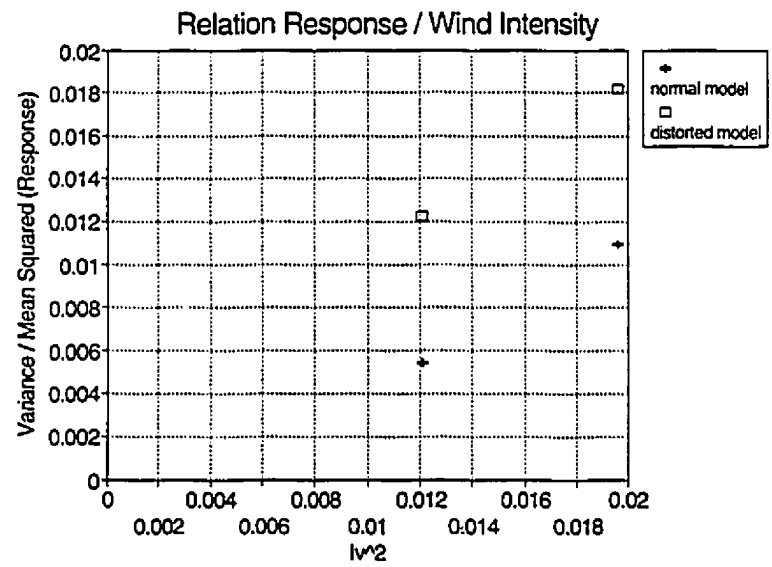

Figure 3.22 Relation between intensity of turbulence (squared) and ratio Variance/Mean response squared, for exposures 1 and 2, and V=6.4*m/s*.

-- The values of the variance were in general very small and, in the case of the normal cable values, roughly half their corresponding values from the distorted model. This leaves the rms values for the distorted model overestimated by roughly between 1.4 and 1.5 times the normal value for transverse wind (0°), and roughly between 1.3 to 1.4 for the oblique incidence (45°). The reason for this may due to the fact that, because the wind characteristics remain unchanged, the turbulence is "seen" as having a larger correlation in the case of the distorted model and, therefore, the variance is bigger. To illustrate the influence of turbulence in the dynamic response of the cable, figure 3.22 shows the variation of the ratio between the variance and the mean response squared, with intensity of turbulence squared, for exposures 1 and 2, and V =6.4 *m/s* (the other cases follow the same trend).

These results are very important since they demonstrate the effect of turbulence in the dynamic response. Theory says that the variance is directly proportional to the ratio between turbulence length scale and the structure's span, and that is exactly what is demonstrated in these experiments by changing the structure and leaving the wind flow characteristics unchanged.

-- The maximum values followed the same trend and therefore were bigger for the distorted model. The minimum values, however, were almost all smaller for the distorted model.

The values from exposure 3 were used to calculate the model values of $C_D d$ and check if the design was correct. Table 3.5 shows the values obtained from dividing the total force (sum of the two extremes) by the product of the dynamic pressure q and the cable length l.

Table 3.5 Values of $C_D d$ obtained from smooth-flow tests.

model	mean velocity [m/s]	total mean force [N]	cable length l [m]	$C_D d$ [m]	ratio normal/distorted
normal	6.1	0.04238	3.02	0.00063	0.496
	6.4	0.04827	3.02	0.00065	0.512
	7.1	0.05866	3.02	0.00064	0.498
distorted	6.1	0.04356	1.54	0.00127	
	6.4	0.04807	1.54	0.00127	
	7.1	0.06004	1.54	0.00129	

From table 3.5 it can be observed that the expected design values of $C_D d$ = 0.0006, for the normal model, and $C_D d$ = 0.0012, for the distorted one, were closely matched, although slightly bigger values were obtained. The ratio between normal and distorted $C_D d$ values, however, was practically the same (≅0.50). These results were considered satisfactory.

The force spectra for the drag in one extreme of the cable are shown in Figs. 3.23 to 3.32. In those, Cable 1 corresponds to normal model and Cable 2 to distorted model. The frequencies may be normalised by multiplying them by the ratio between the cable's sag and the mean wind speed.

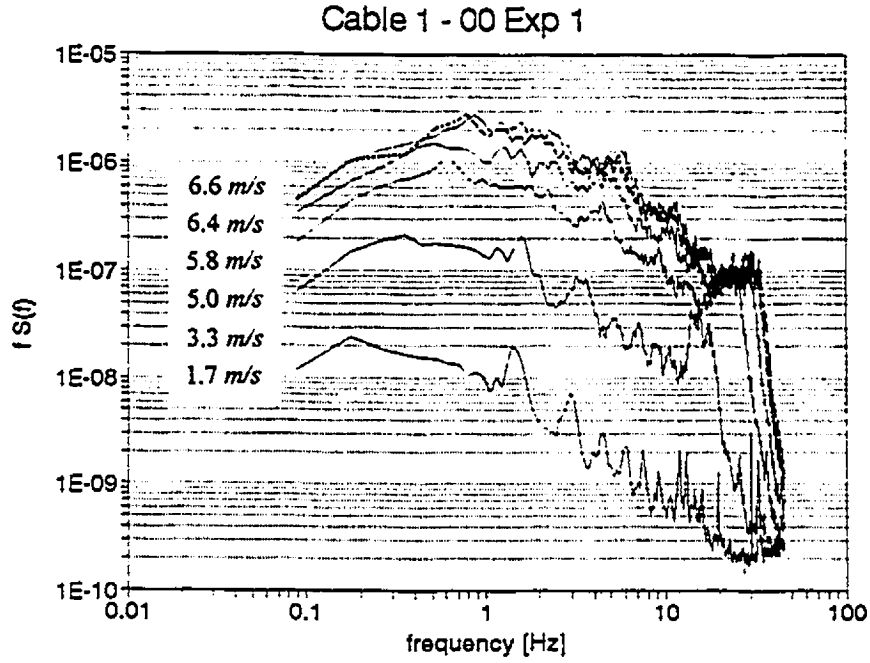

Figure 3.23 Spectra of drag force [N] at one end of cable 1 for exposure 1 and transverse wind (0°) for several wind speeds.

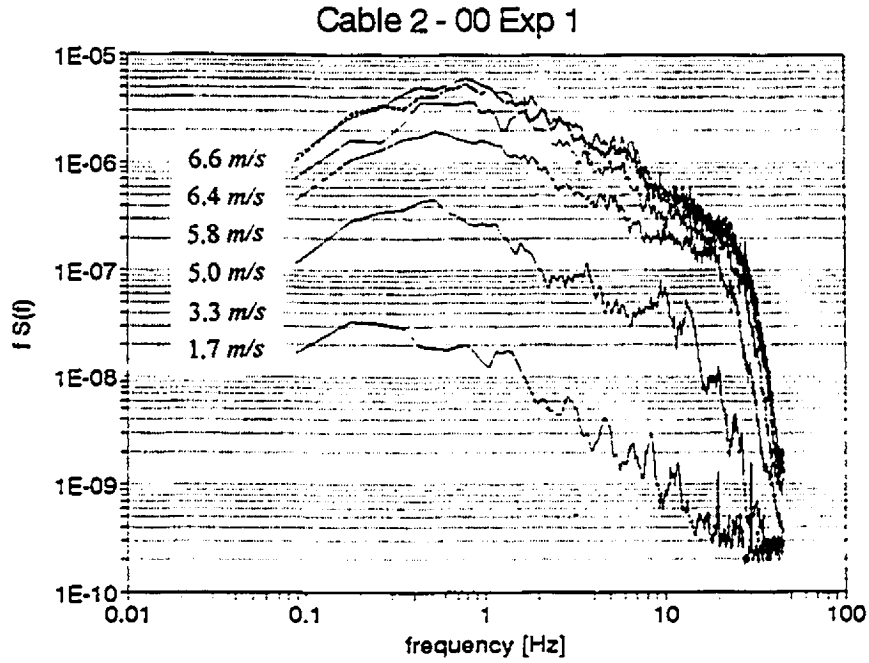

Figure 3.24 Spectra of drag force [N] at one end of cable 2 for exposure 1 and transverse wind (0°) for several wind speeds.

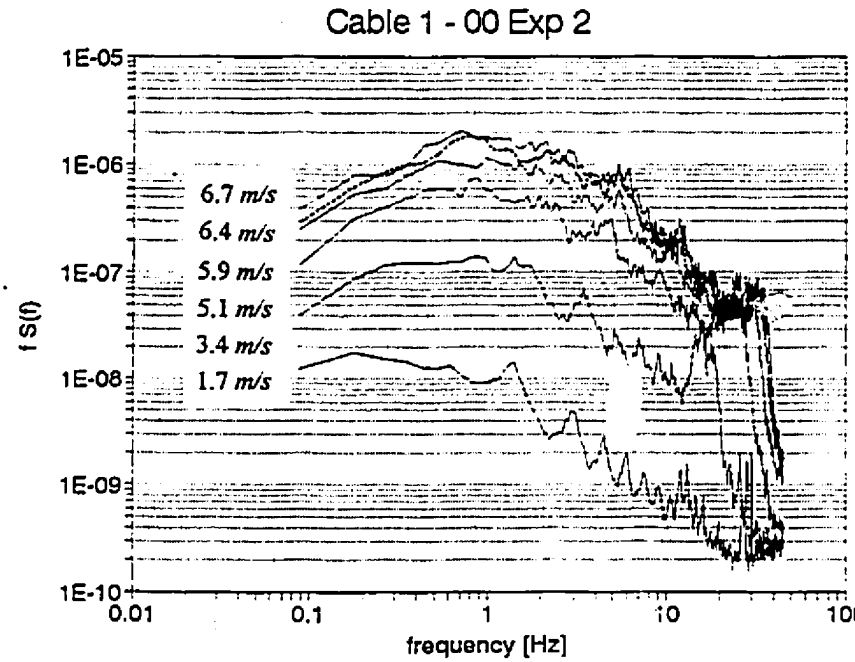

Figure 3.25 Spectra of drag force [N] at one end of cable 1 for exposure 2 and transverse wind (0°) for several wind speeds.

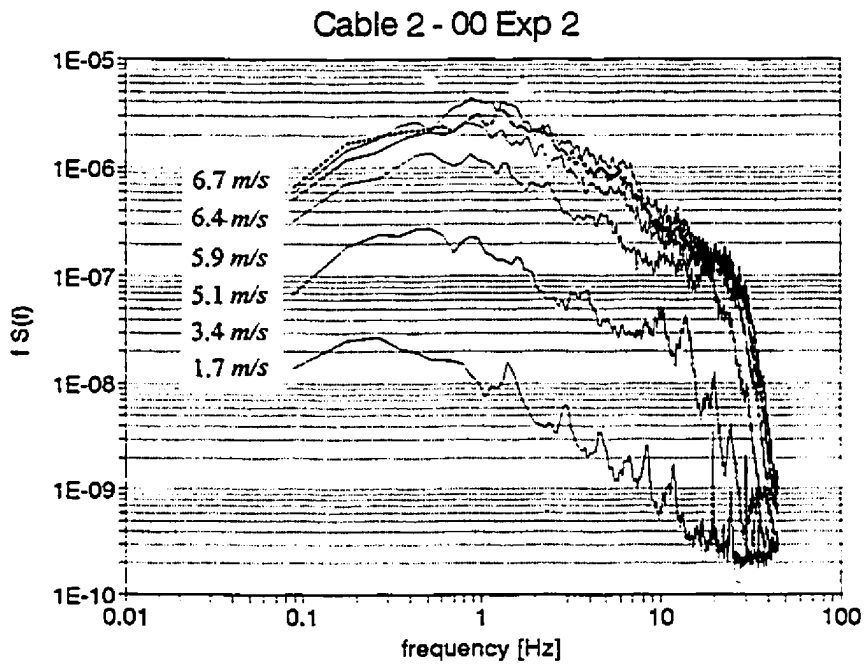

Figure 3.26 Spectra of drag force [N] at one end of cable 2 for exposure 2 and transverse wind (0°) for several wind speeds.

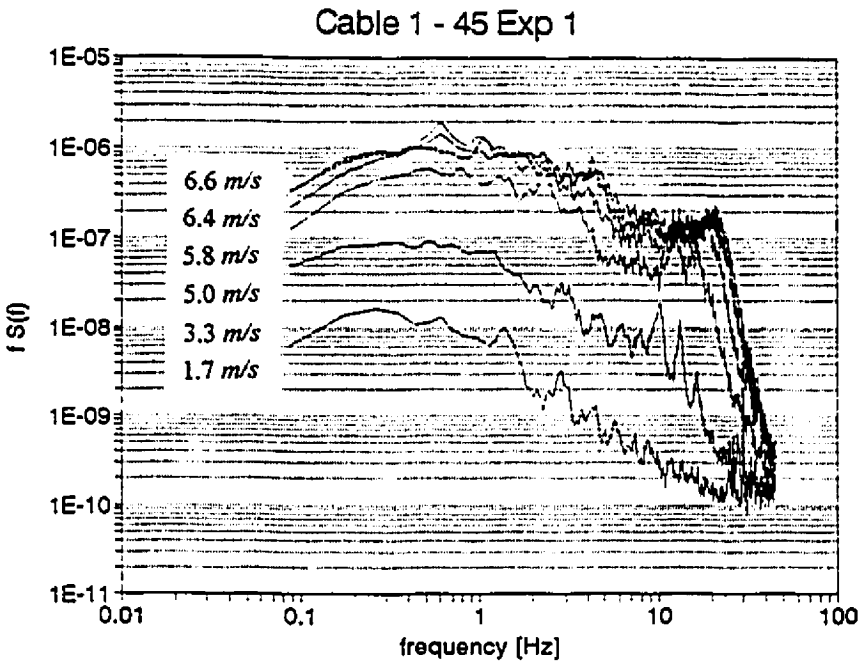

Figure 3.27 Spectra of drag force [N] at one end of cable 1 for exposure 1 and oblique wind (45°) for several wind speeds.

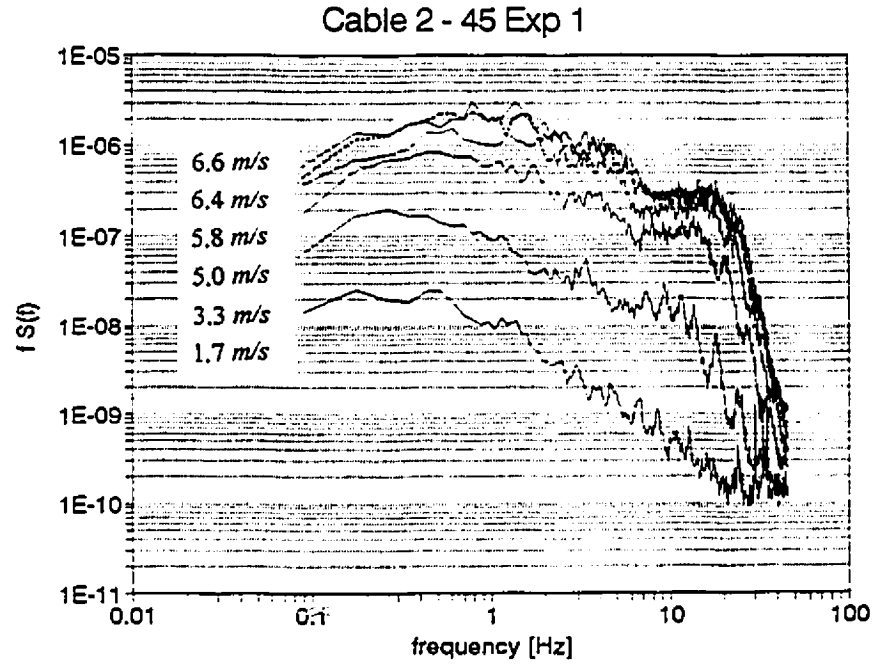

Figure 3.28 Spectra of drag force [N] at one end of cable 2 for exposure 1 and oblique wind (45°) for several wind speeds.

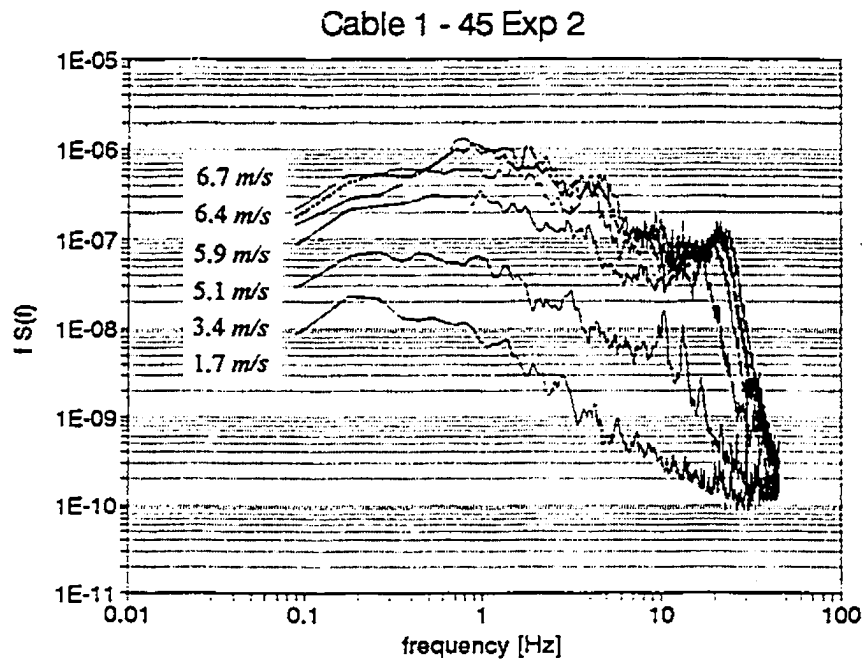

Figure 3.29 Spectra of drag force [N] at one end of cable 1 for exposure 2 and oblique wind (45°) for several wind speeds.

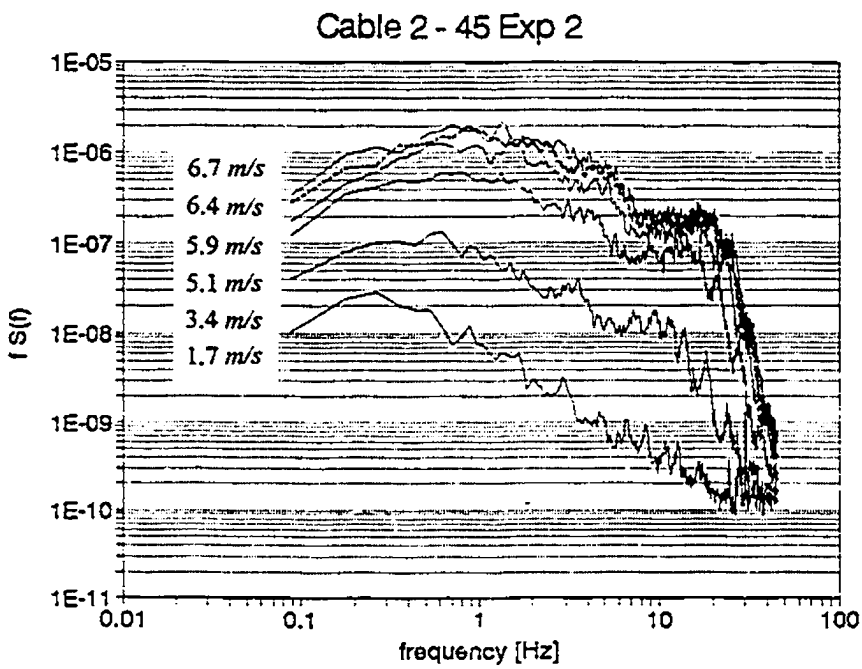

Figure 3.30 Spectra of drag force [N] at one end of cable 2 for exposure 2 and oblique wind (45°) for several wind speeds.

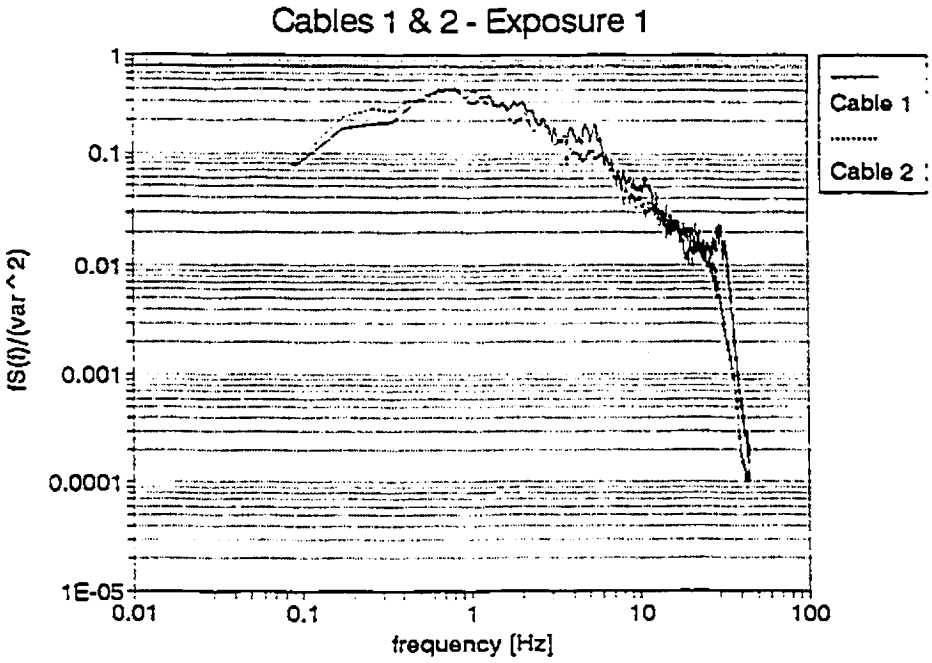

Figure 3.31 Normalised spectrum of drag force [N] at one end of cables 1 & 2 for exposure 1 and transverse wind (0°) V=6.4 *m/s*.

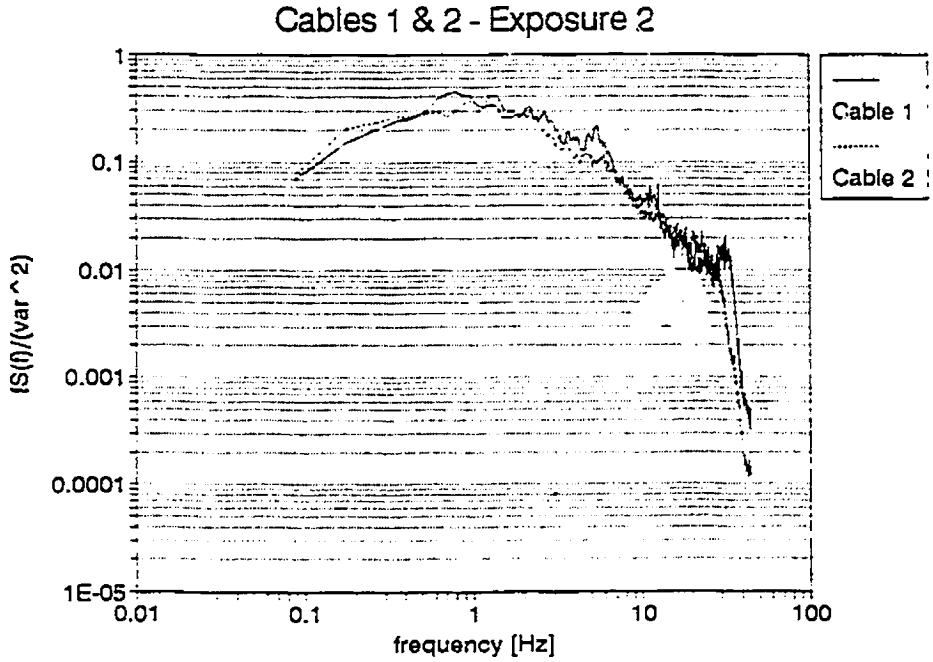

Figure 3.32 Normalised spectrum of drag force [N] at one end of cables 1 & 2 for exposure 2 and transverse wind (0°) V=6.4 *m/s*.

From the analyses of Figs. 3.23 to 3.30 spectra we can observe that cable 2 (distorted model) had bigger values of $fS(f)$, which agrees with the time series values for the force variance, and, repeating the observation, may be due to the bigger correlation of the gusts for the distorted model in relation to the normal one. The difference is larger for exposure 1 (more turbulent), although not too much. Another observation is that the normal cable had the peaks in the spectra a little bit more distinct than the distorted. This can be due to the smaller aerodynamic damping of cable 1. At the model design velocities it was almost impossible to see any distinct peaks in the spectra, those becoming more distinct as the velocity decreases. This could be attributed to the aerodynamic damping which is directly proportional to the wind velocity and inversely proportional to the mass per unit length. From the smaller velocity spectra we can infer the natural frequencies of the cable, which are in the range of the expected theoretical predictions.

Figures 3.31 and 3.32 show the spectra of the drag forces normalised by their variances and present the normal and distorted models in the same plot. Although $fS(f)$ and the variance are bigger for the distorted model, the normalised spectra of both models have a pretty good match.

The normalised force spectra were plotted together with the normalised wind spectra as shown in Figs. 3.33 to 3.36. For exposure 1, transfer functions were obtained by dividing the force spectrum by the wind spectrum and are plotted together in Figs. 3.33 and 3.34.

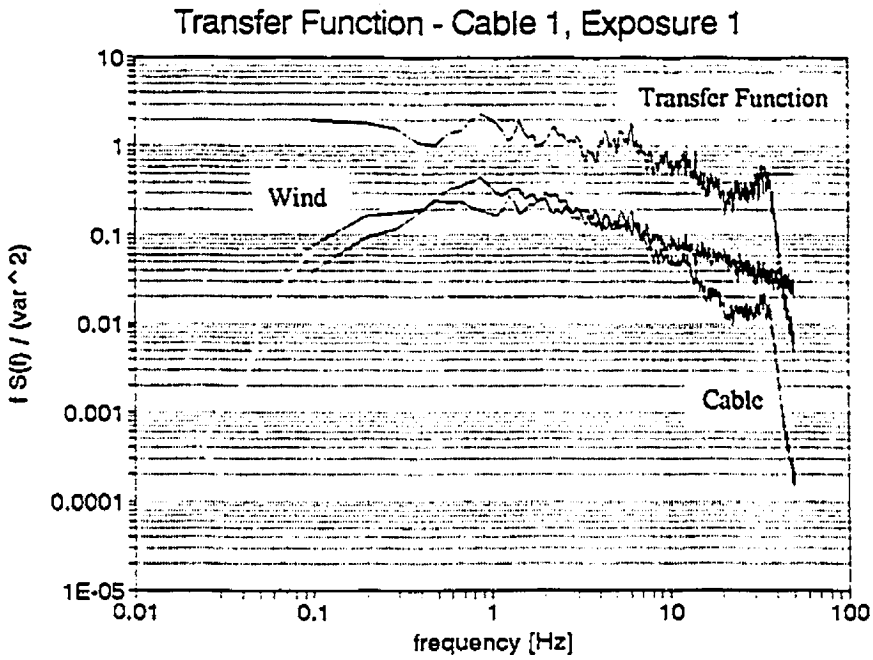

Figure 3.33 Force and wind spectra and transfer function for cable 1, exposure 1.

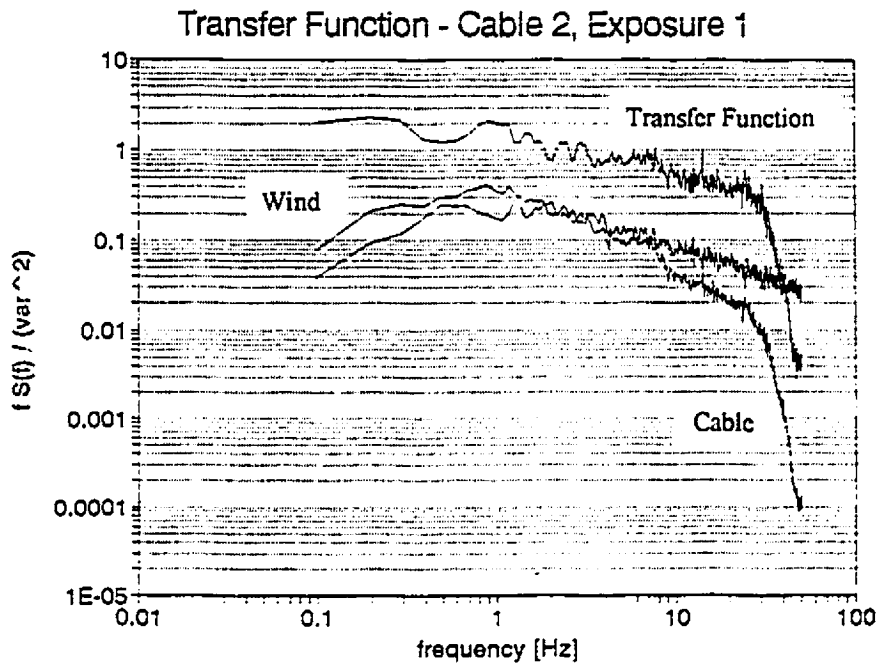

Figure 3.34 Force and wind spectra and transfer function for cable 2, exposure 1.

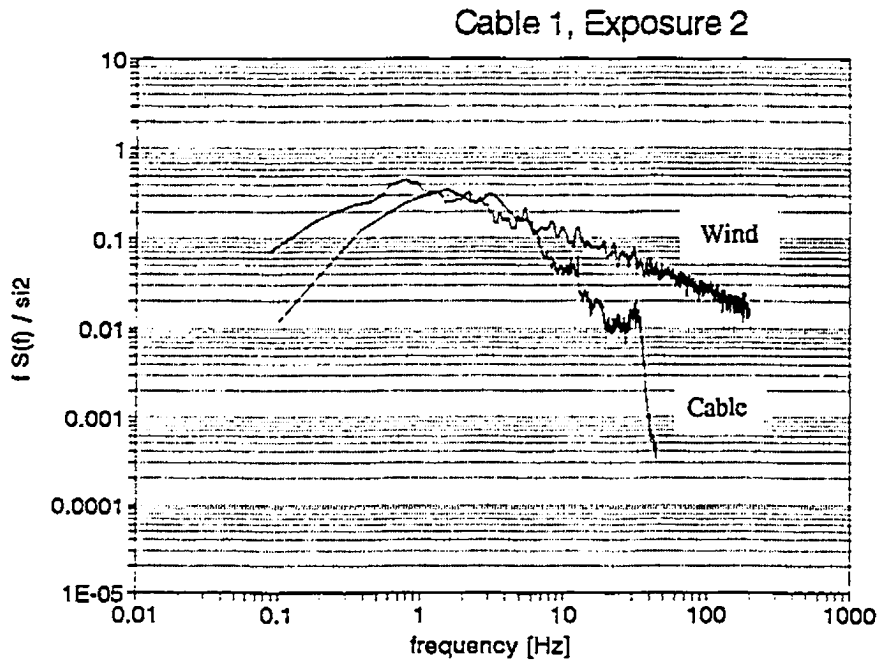

Figure 3.35 Force and wind spectra for cable 1, exposure 2.

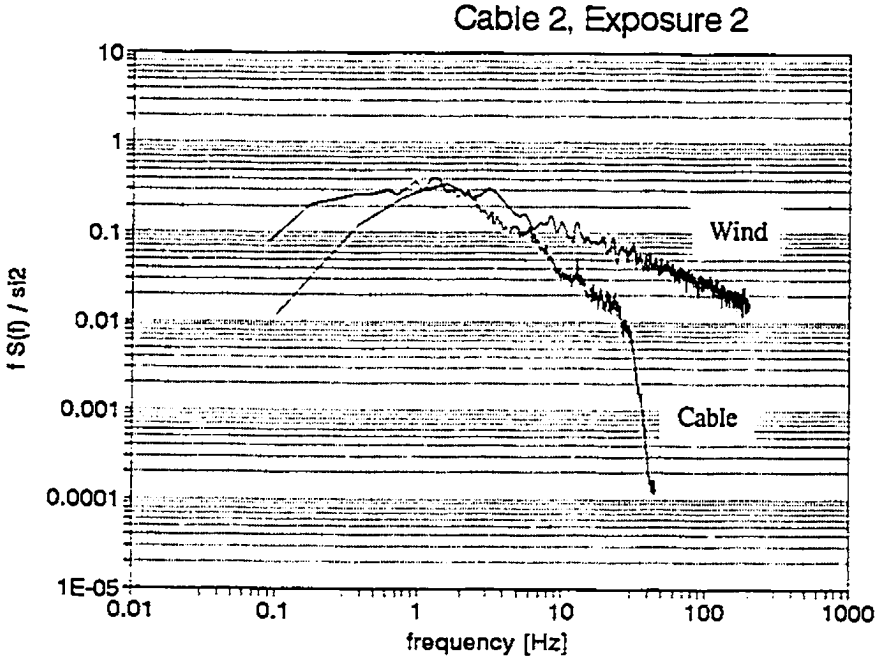

Figure 3.36 Force and wind spectra for cable 2, exposure 2.

The angular displacement of the cables under those severe wind conditions were expectedly high. Figures 3.37 and 3.38 show the behaviour of the models under the simulated strong winds. These extreme angular displacements have been found in real lines under extreme winds, as proven in Fig. 3.39.

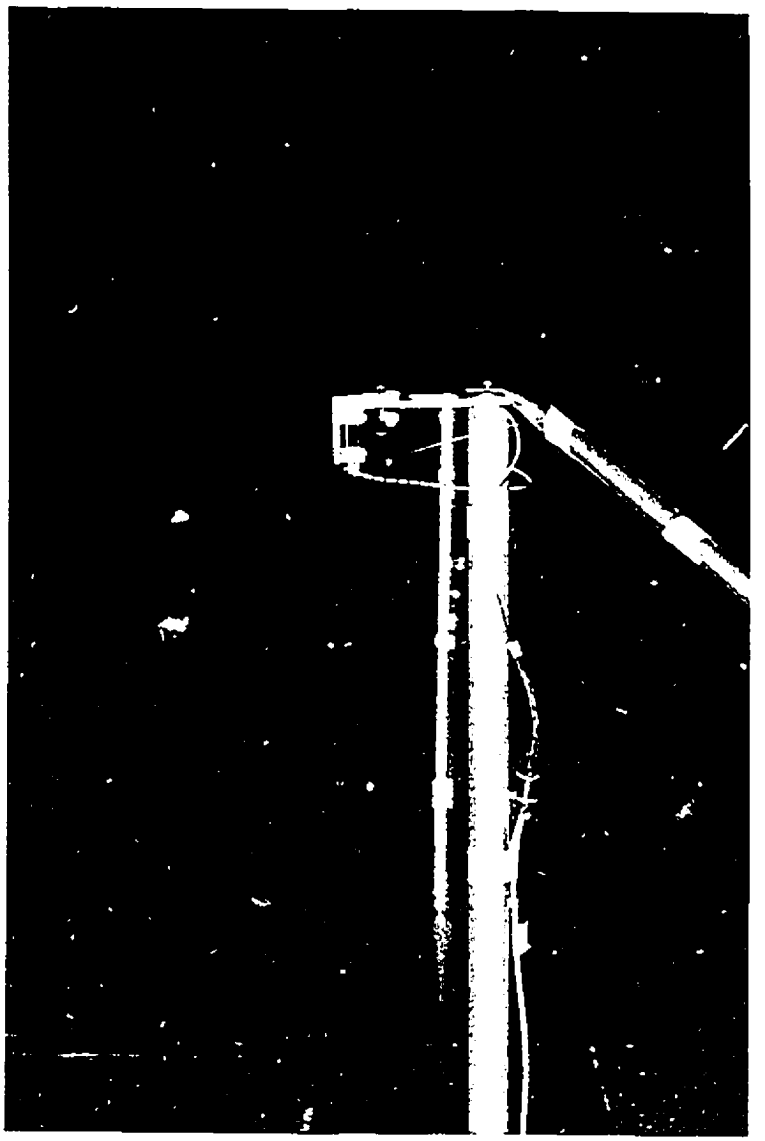

Figure 3.37 Angular displacement of model cable under high wind.

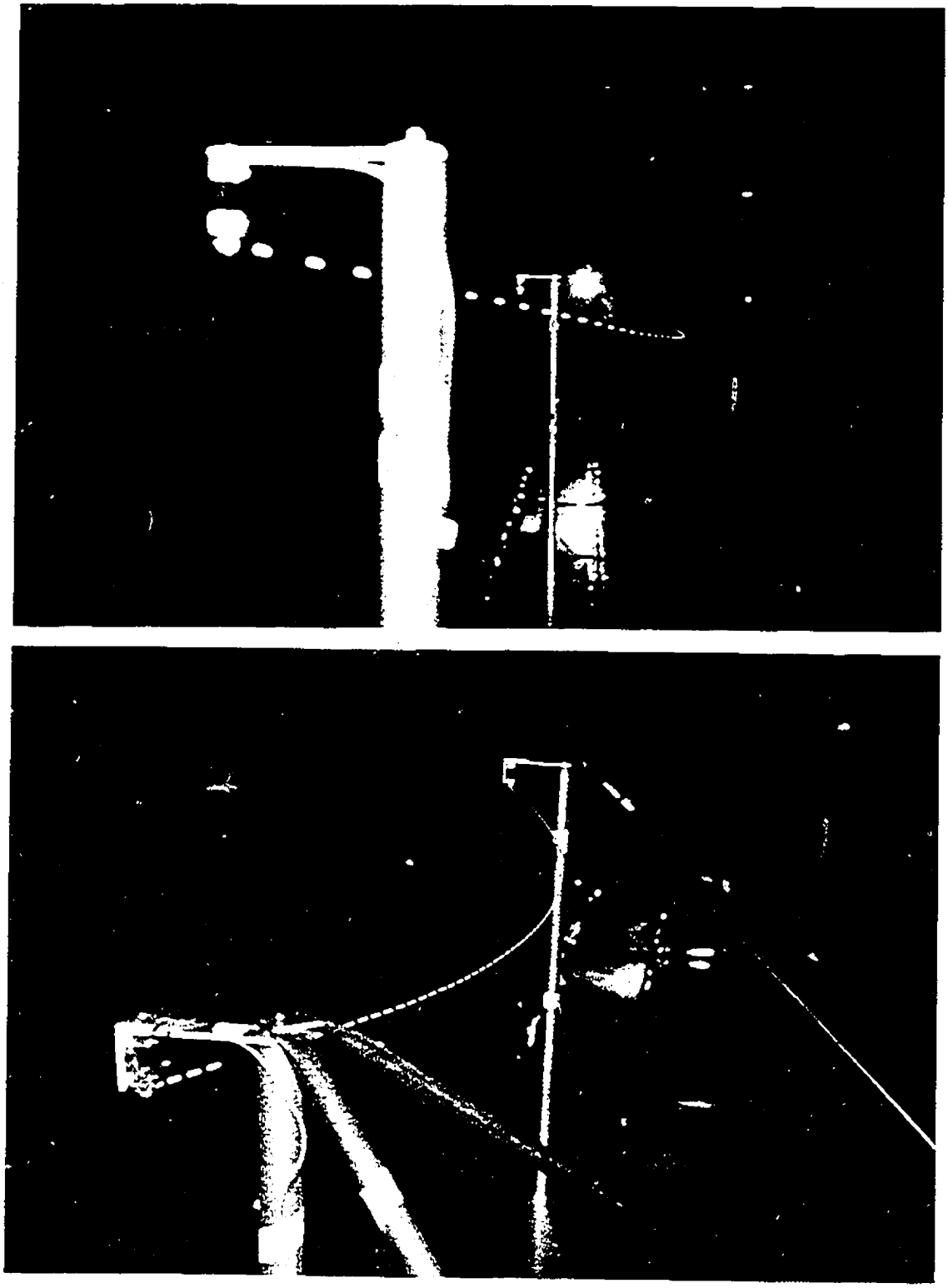

Figure 3.38 Behaviour of cables under strong winds.

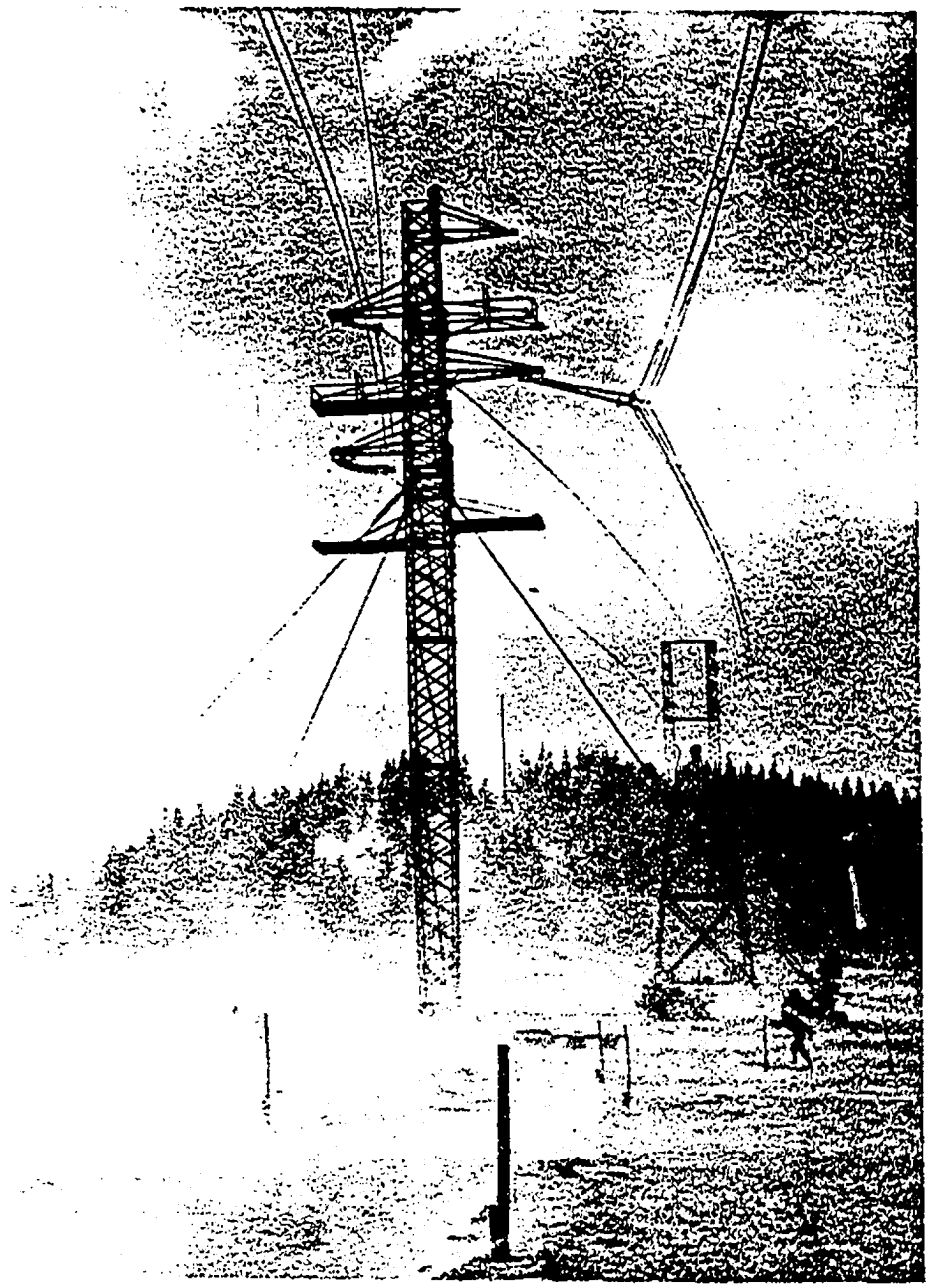

Bild 231 / 8 Extreme Ausschwingwinkel bei Oststurm (Aufwind)

Figure 3.39 Behaviour of real transmission lines under extreme wind speeds (after Leibfried and Mors, 1964).

3.3.5 Theoretical prediction

The statistical method using influence lines described in Chapter 2 is employed for the theoretical prediction of the cable responses and comparison with experimental values. Model 1 and exposure 1 are chosen for the detailed calculation (below) and Eqs. (2.28) and (2.30) are used for the other cases.

Cable data: Span length, L = 3*m*; sag, S = 0.15*m*; cable length, l = 3.02*m*; mass per unit length, m = 0.43E-03 *kg/m*; fundamental frequency (pendulum), f_1=1.44*Hz*; fundamental mode shape, $\mu_1(x)=sin(\pi x / l)$.

Wind data: Mean wind speed, V = 6.4*m/s* at reference height, z =0.54*m* (at the sag's center); air density, ρ_a= 1.2 *kg/m*^{3}; the reference velocity pressure is, therefore, q = 24.6 *Pa*; longitudinal turbulence intensity, I_v = 0.14; transverse scale of the longitudinal component of turbulence, ${}^xL_v \cong$ 0.31*m* ; exponential decay factor for "narrow band" correlation, C = 7.

Aerodynamic data: Drag coefficient times cable diameter: $C_D d$ = 0.00065*m*.

The response, r, which will be considered is the drag force on the cable support, for which the influence line is $i(x) = x / l$.

a) Mean response:

Using equation (2.13) we find:

$$\bar{r} \cong 0.02412\ N \cong 2.46\ gf$$

b) Background response:

Equation (2.16) allows:

$$(2\,q\,C_D\,d\,I_v)^2 \cong 2\text{E-}05\ N^2/m^2$$

$$\int_0^l \int_0^l e^{-\left(|x-x'|/L_v\right)} \frac{x}{l}\,\frac{x'}{l}\,dx\,dx' = 0.53\ m^2$$

and therefore

$$\tilde{r}_B \cong 0.0032\ N \cong 0.326\ gf$$

c) Resonant response:

The procedure is shown in detail for the first mode of vibration. The value of $f_1 S_{Q1}(f_1)$ is calculated from equation (2.22), by using:

$$(2\,q\,C_D\,d\,I_v)^2 \cong 2\text{E-}05\ N^2/m^2$$

$$\frac{f_1\,S_v(f_1)}{\sigma_v^2} \cong 0.07 \quad \text{(from Figure 3.13)}$$

$$\int_0^l \int_0^l e^{\frac{-7|x-x'|}{6.4}^{1.44}} \sin\left(\frac{\pi x}{l}\right)\sin\left(\frac{\pi x'}{l}\right)dx\,dx' \cong 1.51\ m^2$$

which allows $f_1 S_{Q1}(f_1) \cong 2.11\text{E-}6\ N^2$

The aerodynamic damping is obtained from (2.8):

$$\zeta_{a1} = \left(\frac{1}{4\pi}\right)\left(\frac{1.2 \times 0.00065}{0.43E-03}\right)\left(\frac{6.4}{1.44}\right) \cong 64\%$$

The participation factor is: $m\int_0^l \sin\left(\frac{\pi x}{l}\right)\frac{x}{l}\,dx = m\ 0.96\ kg$

The modal mass is: $m\int_0^l \sin^2\left(\frac{\pi x}{l}\right)dx = m\ 1.51\ kg$

The resonant response is then obtained from (2.26):

$$\tilde{r}_{R1} = \sqrt{\frac{\pi}{4}\frac{2.11E-6}{0.64}}\left(\frac{0.96}{1.51}\right) = 0.0010\,N \cong 0.104\,gf$$

The total rms response is then:

$$\tilde{r} = 0.0034\,N \cong 0.342\,gf$$

Table 3.6 presents RMS values of the drag force at one extreme of the cable obtained from the measurements and calculated from theory using the estimated values of the transverse length scale of turbulence. Theory predicts well the mean responses and overestimates a little bit the experimental findings for the fluctuating part of the response. The value of the background response alone is enough to predict the latter. There are, however, uncertainties in the determination of ${}^{x}L_{v}$. The value used was from the fit of the

correlation curve by an exponential function and the area under the real curve seems to be actually lower than the area given by the fitting curve. A lower value of ${}^{x}L_{v}$ in the calculation would mean a background response coinciding with the measurements. The resonant response does not seem to be important in this case, which can also be seen from the spectra.

Table 3.6 Comparison between measured and calculated RMS values of drag (L_v=0.31m for exp. 1 and L_v=0.34m for exp. 2).

Model	Exposure	Velocity [m/s]	Intensity of turbulence	RMS [gf] calculated	RMS [gf] measured	RMS Ratio Calc./Meas.
normal	1	5.8	0.14	0.273	0.213	1.28
		6.4		0.332	0.254	1.31
		6.6		0.353	0.279	1.26
distorted	1	5.8	0.14	0.359	0.318	1.13
		6.4		0.437	0.369	1.18
		6.6		0.465	0.400	1.16
normal	2	5.9	0.11	0.222	0.180	1.23
		6.4		0.271	0.208	1.30
		6.7		0.288	0.233	1.24
distorted	2	5.9	0.11	0.291	0.269	1.08
		6.4		0.354	0.291	1.22
		6.7		0.376	0.318	1.18

From the time series and normalised spectra results of the line studied it can be seen that the distortion works relatively well and can constitute a valid technique. It is necessary, however, that a correction be made to the values of the variance measured in the distorted model. In agreement with theoretical expectations, the variance from the

distorted model should be multiplied by γ, the horizontal geometric distortion of the cable, which in this case is 0.5.

3.4 **Behaviour of two parallel cables**

It is of practical importance to know the behaviour of the cables in each arm of the towers as a whole. The assumption that the loads on each cable act simultaneously on the towers is common practice; this suggests the necessity to investigate to what degree this assumption is valid. A mechanism possible to occur and affect the tower loading (coupling cables and tower motion) is related to the "convection" of gusts of wind across the tower's arm length by the mean wind. If the mean velocity of the wind is V and the tower's arm length is B, gusts striking the upwind cable will strike the downwind cable a time interval B/V later. If this time interval is roughly one cycle of drag vibration later the drag forces in the two cables will reinforce one another. If the time lag is half a cycle of torsional vibration later it will excite the torsional mode of vibration of the tower's arm. This could influence the torsional stability of the tower's arm (Davenport, 1994).

3.4.1 **Design of models 3 & 4** (Double cables , distorted)

With the aim of studying the behaviour and determining the existing correlation between the cable forces, wind tunnel tests were made of two cables with two different separation lengths. Adopting the distorted model approach, the cables tested had the

general characteristics as shown in table 3.7. Two different sets of pairs of cables, each pair with a different diameter, were built and tested with the purpose of verifying if the axial stiffness would make a difference in the results. The basic piano wire cables had diameters of ϕ =1.27E-4 m (cable 3) and ϕ =2.29E-4 m (cable 4). Both models had small lumped wood cylinders (4mm diameter, 20mm length) attached to the steel piano wire (62 for cable 3 and 60 for cable 4). Contrary to models 1 & 2, in this case it was decided to test a model with a mass per unit length value corresponding to an upper extreme case and to check the effect of such a choice.

Table 3.7 General characteristics of cables 3 & 4 tested.

	L [m]	S [m]	l [m]	m [kg/m]	V [m/s]	$C_D d$ [m]	f_{cl} [Hz]
Protot. (nominal)	300	10	300.9	~4.3	40	0.0400	0.18
Normal	6	0.2	6.02	0.0017	5.7	0.0008	1.24
Distorted $\gamma = 0.5$	3	0.2	3.04	0.0034	5.7	0.0016	1.26

Cable 3 had $EA_3 \cong 2534$ N and cable 4 $EA_4 \cong 8237$ N. The theoretical frequencies are given in tables B2 and B3 in Appendix B. Model 3 was also tested with a sag S=0.3m.

The separation lengths were chosen to represent full-scale distances of 8m and 16m which at a model scale of 1/50 corresponds to 0.16m and 0.32m, respectively. The wind tunnel set-up and models are shown in Figures 3.40 and 3.41. The simulated wind had the same characteristics as the first test.

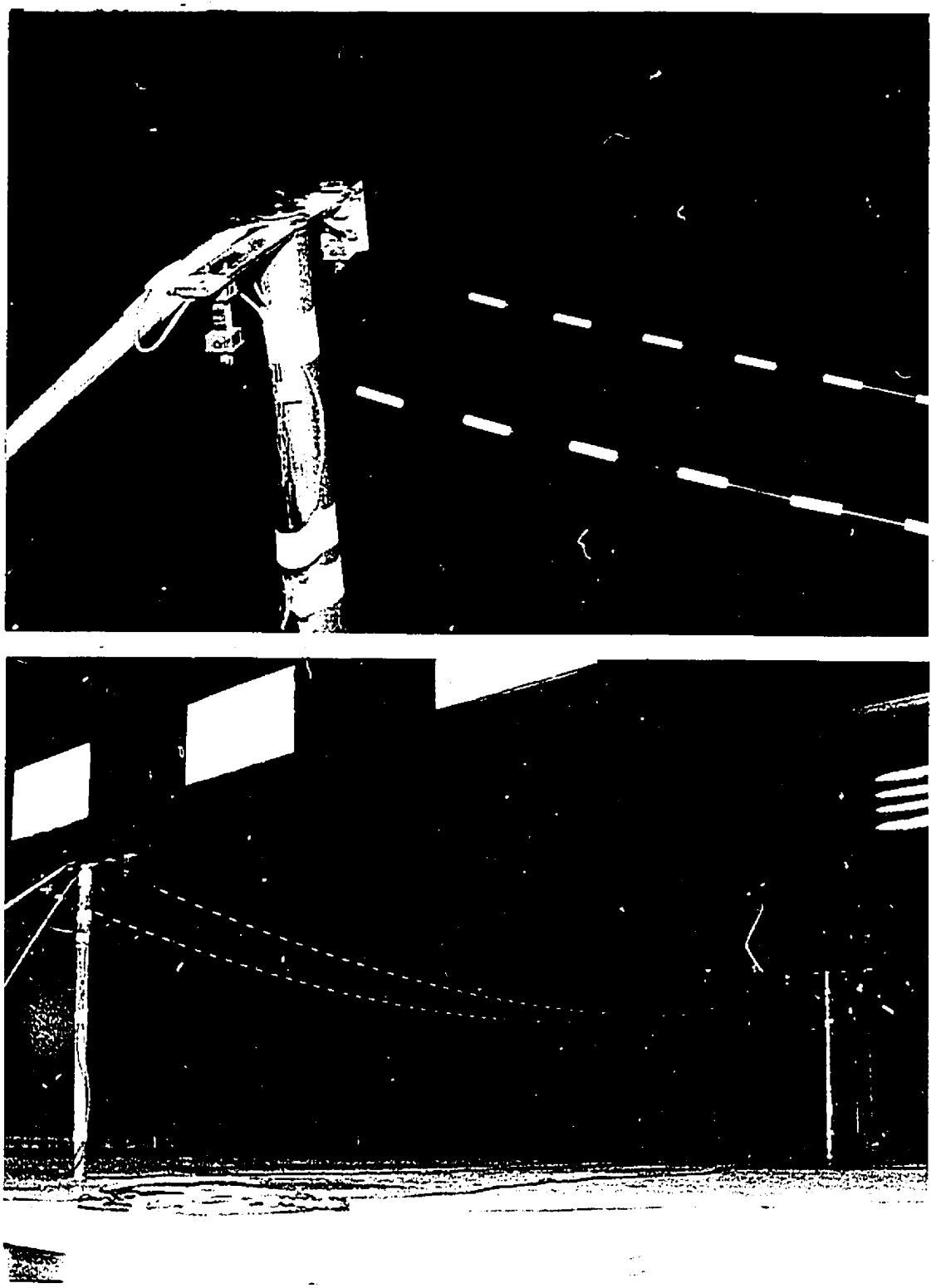

Figure 3.40 Details of model, load cells and support system for cable #3.

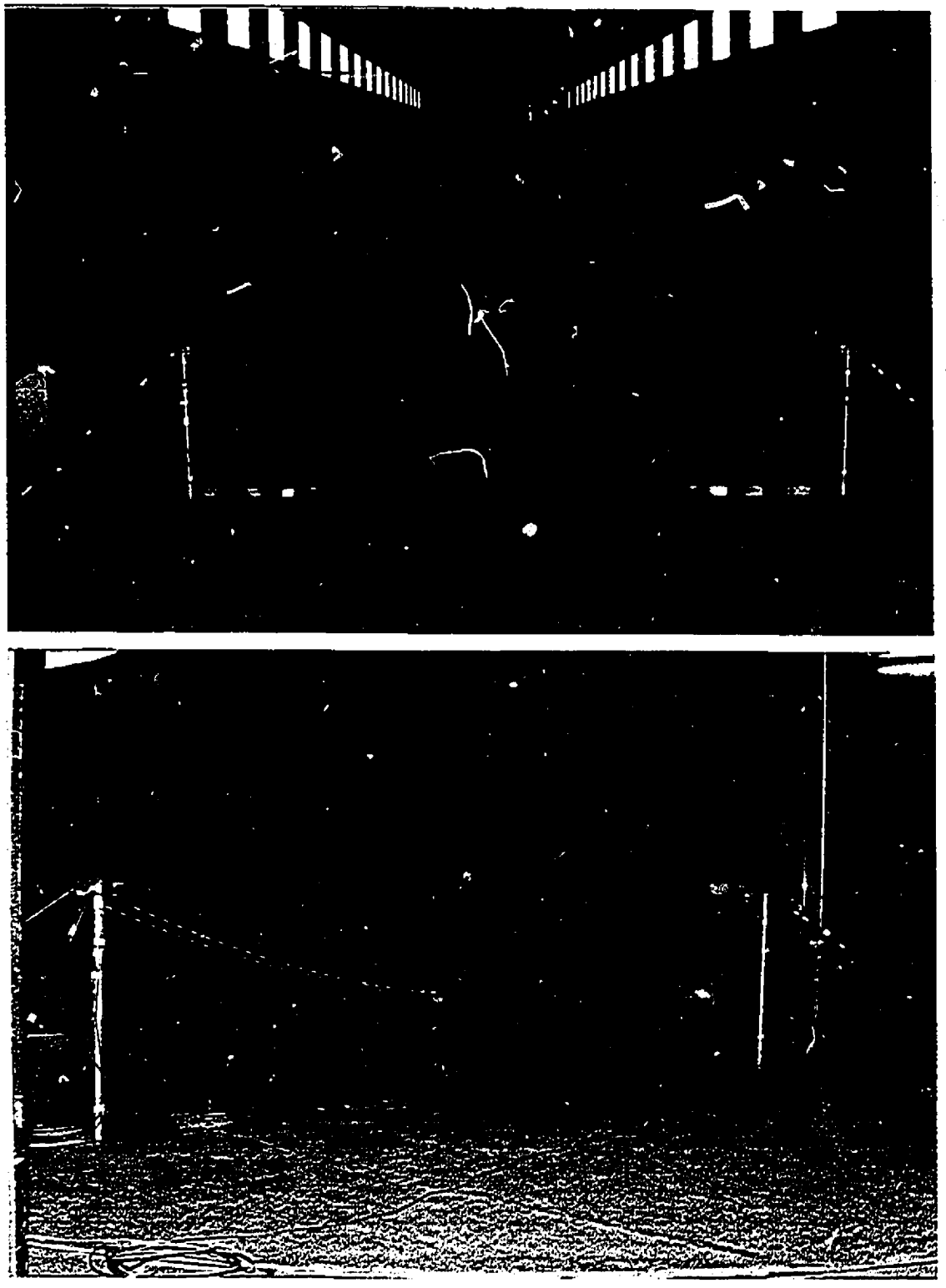

Figure 3.41 Views of wind tunnel and model set-up for cables #3. Upper figure: S=0.2*m*; Lower figure: S=0.3*m*.

3.4.2 Experimental results for models 3 & 4

Again, the testing of the cable models included measurements of the time history of the drag force over a period of time of 500 seconds, from which the mean, root-mean-square (rms), maximum and minimum values of the response as well as the force spectra were obtained. The direction of the wind was perpendicular to the lines, which were tested with 4 velocities, although the model was designed for V=5.7m/s.

The measured values are given in table 3.8 for the windward cable and in table 3.9 for the leeward cable, both for sag S=0.20m. Table 3.10 shows the values for cable 3 with sag S=0.30m, which was measured for V=5.7m/s and exposure 1 only.

Table 3.8 Measured values for windward cable #3 (S=0.2m).

Spacing [m]	Exposure	Velocity [m/s]	Max [(gf)]	Min [(gf)]	Mean [(gf)]	RMS [(gf)]	Variance [$(gf)^2$]
0.16	1	6.2	8.84	2.58	5.74	0.835	0.697
		5.7	8.06	2.28	4.90	0.713	0.509
		5.0	6.05	1.62	3.71	0.557	0.310
		3.3	2.71	0.64	1.60	0.274	0.075
	2	6.3	8.84	3.75	6.44	0.709	0.503
		5.7	8.69	3.09	5.31	0.603	0.364
		5.0	6.56	2.37	4.15	0.493	0.243
		3.4	2.87	0.97	1.85	0.251	0.063
0.32	1	6.2	8.80	2.20	5.40	0.786	0.618
		5.7	7.67	2.02	4.61	0.673	0.453
		5.0	5.49	1.42	3.45	0.521	0.271
		3.3	2.69	0.28	1.52	0.277	0.077
	2	6.3	8.84	3.26	5.98	0.681	0.464
		5.7	7.48	2.92	5.03	0.565	0.319
		5.0	5.70	2.31	3.94	0.445	0.198
		3.4	2.82	0.92	1.78	0.245	0.062

Table 3.9 Measured values for leeward cable #3 (S=0.2m).

Spacing [m]	Exposure	Velocity [m/s]	Max [(gf)]	Min [(gf)]	Mean [(gf)]	RMS [(gf)]	Variance [$(gf)^2$]
0.16	1	6.2	8.26	2.54	5.46	0.750	0.562
		5.7	7.41	2.20	4.61	0.643	0.414
		5.0	5.91	1.72	3.59	0.507	0.257
		3.3	2.53	0.53	1.44	0.265	0.070
	2	6.3	8.26	3.91	6.11	0.643	0.413
		5.7	7.86	3.23	5.17	0.550	0.303
		5.0	6.06	2.45	4.03	0.451	0.203
		3.4	2.67	0.76	1.68	0.253	0.064
0.32	1	6.2	7.85	2.26	5.15	0.707	0.500
		5.7	6.99	2.16	4.51	0.615	0.378
		5.0	5.45	1.46	3.32	0.491	0.241
		3.3	2.28	0.27	1.25	0.268	0.072
	2	6.3	8.26	3.15	5.68	0.609	0.371
		5.7	7.23	2.97	4.84	0.518	0.268
		5.0	5.51	2.29	3.82	0.422	0.178
		3.4	2.43	0.61	1.49	0.247	0.061

Table 3.10 Time series results from cable 3 with S=0.3m for exposure 1.

Spacing [m]	Cable position	Velocity [m/s]	Max [(gf)]	Min [(gf)]	Mean [(gf)]	RMS [(gf)]	Variance [$(gf)^2$]
0.16	windward	5.7	7.56	2.29	4.72	0.681	0.464
	leeward	5.7	7.01	2.19	4.40	0.614	0.377
0.32	windward	5.7	6.93	1.75	4.22	0.644	0.415
	leeward	5.7	6.65	1.54	3.89	0.609	0.371

The force spectra for the drag force at one support are shown in Figs. 3.42 to 3.47.

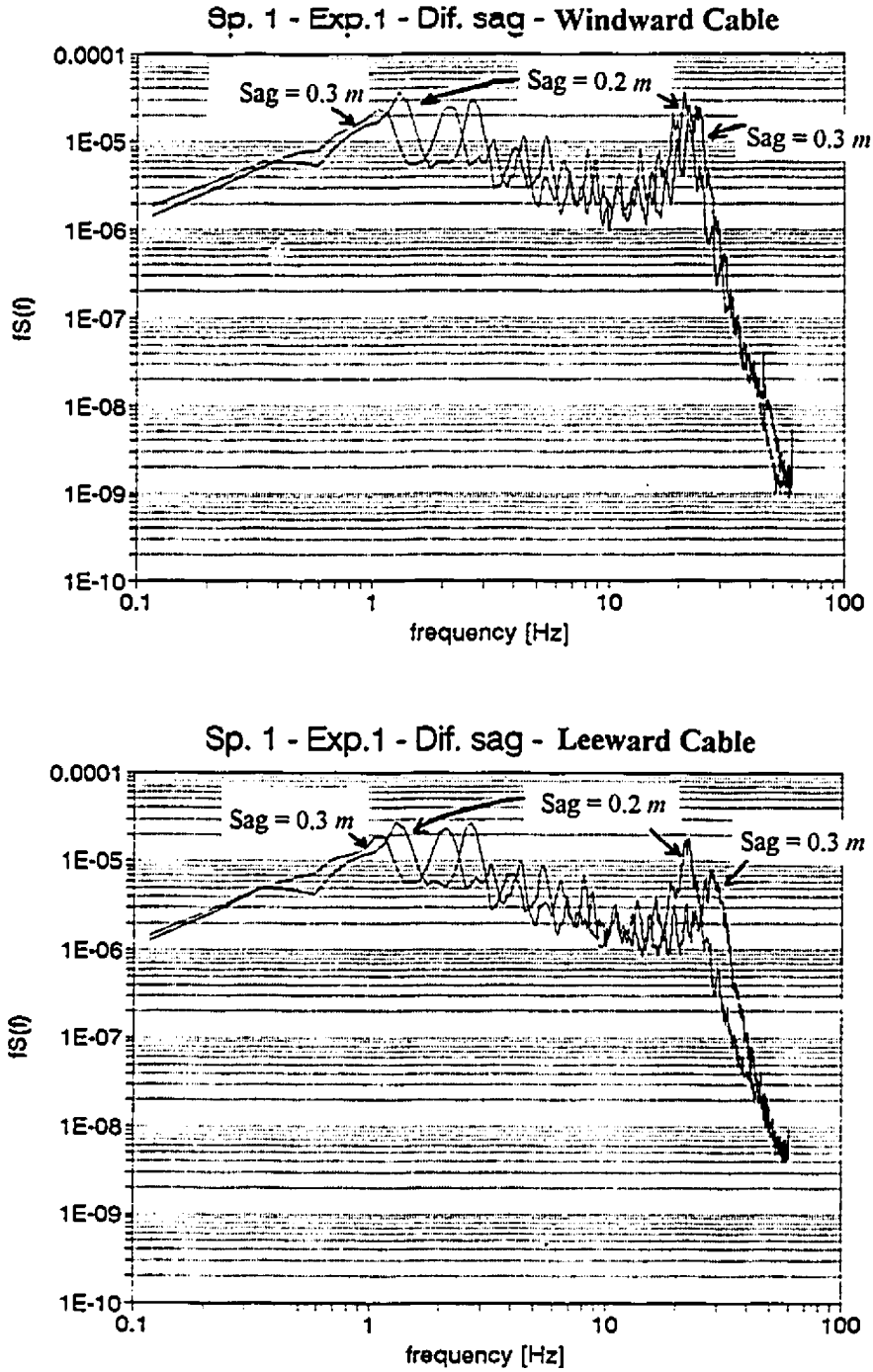

Figure 3.42 Drag Force [N] spectra for the two cable sags tested for spacing 1 and exposure 1. Upper figure: windward cable; Lower figure: leeward cable.

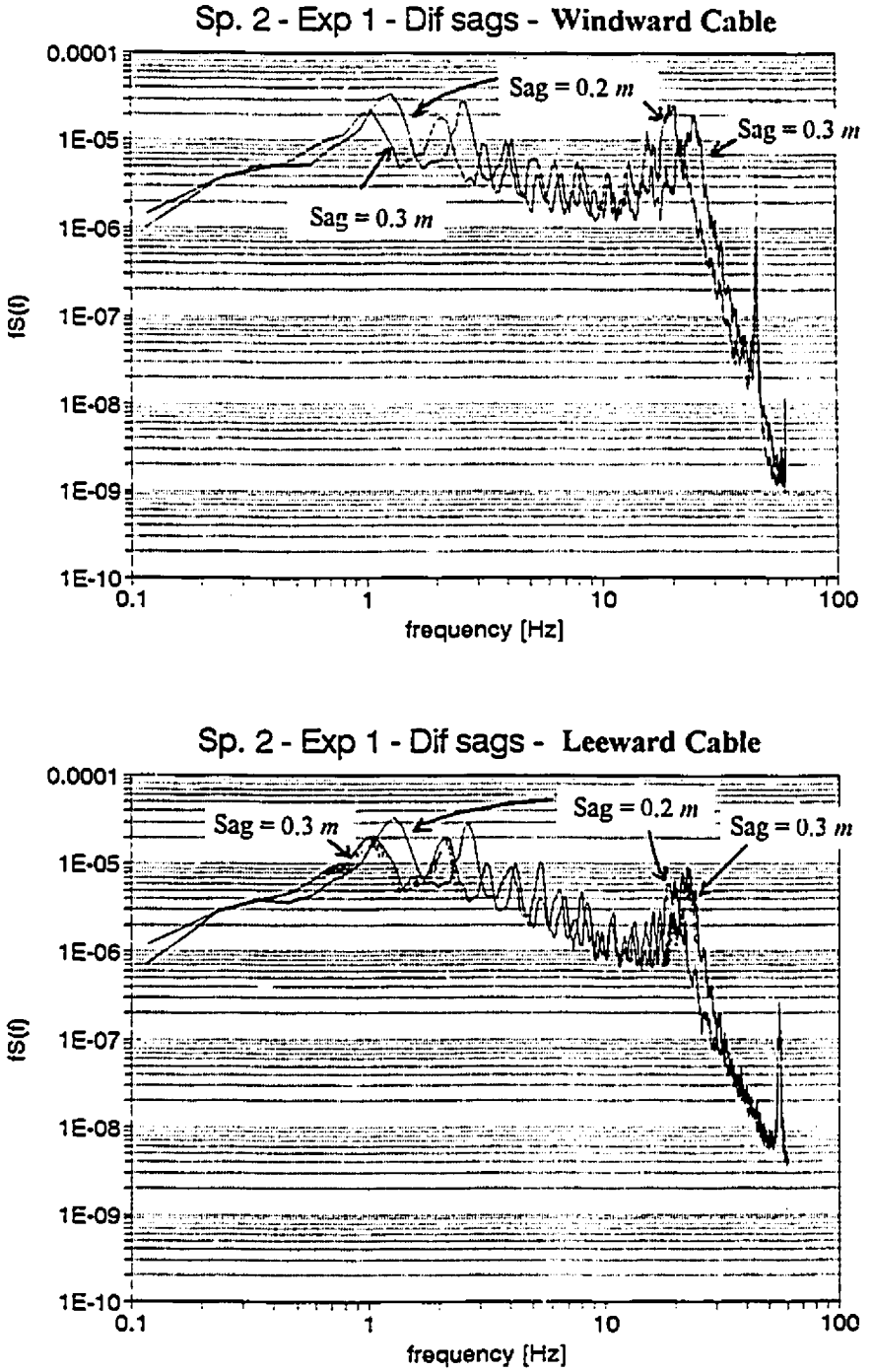

Figure 3.43 Drag Force [N] spectra for the two cable sags tested for spacing 2 and exposure 1. Upper figure: windward cable; Lower figure: leeward cable.

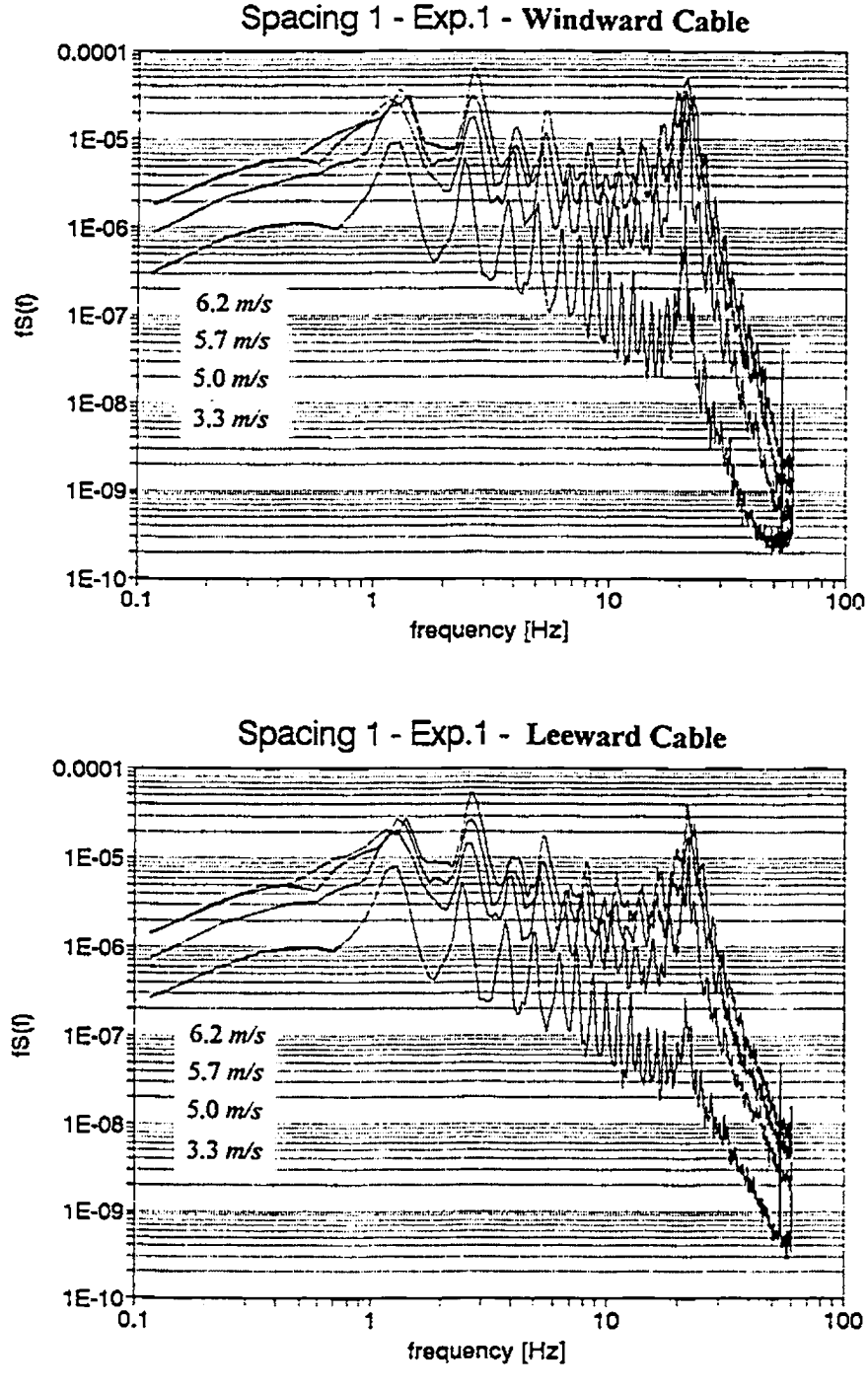

Figure 3.44 Drag Force [N] spectra for the different velocities tested for spacing 1 and exposure 1 (S=0.2m). Upper figure: windward cable; Lower figure: leeward cable.

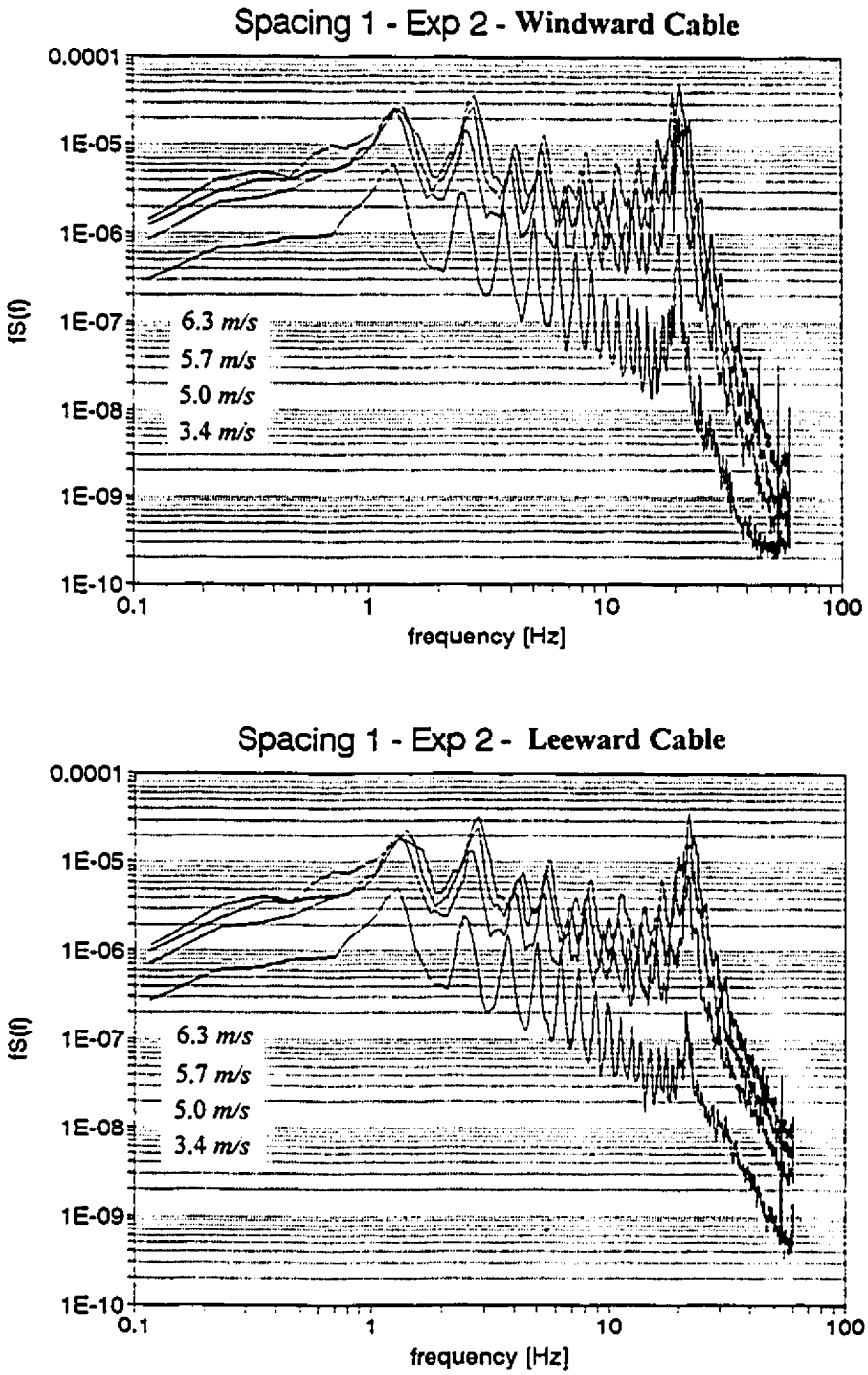

Figure 3.45 Drag Force [N] spectra for the different velocities tested for spacing 1 and exposure 2 (S=0.2m). Upper figure: windward cable; Lower figure: leeward cable.

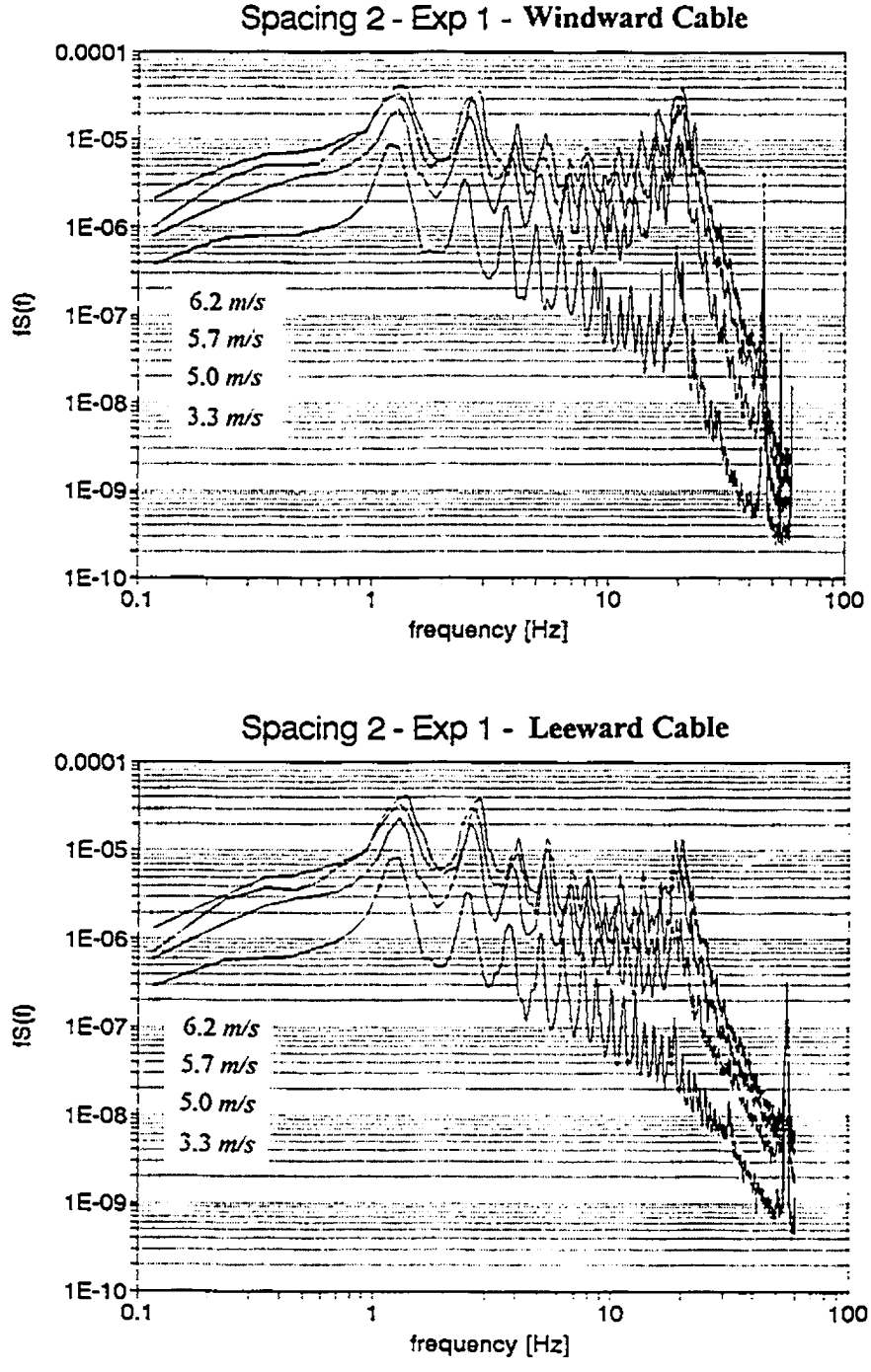

Figure 3.46 Drag Force [N] spectra for the different velocities tested for spacing 2 and exposure 1 (S=0.2m). Upper figure: windward cable; Lower figure: leeward cable.

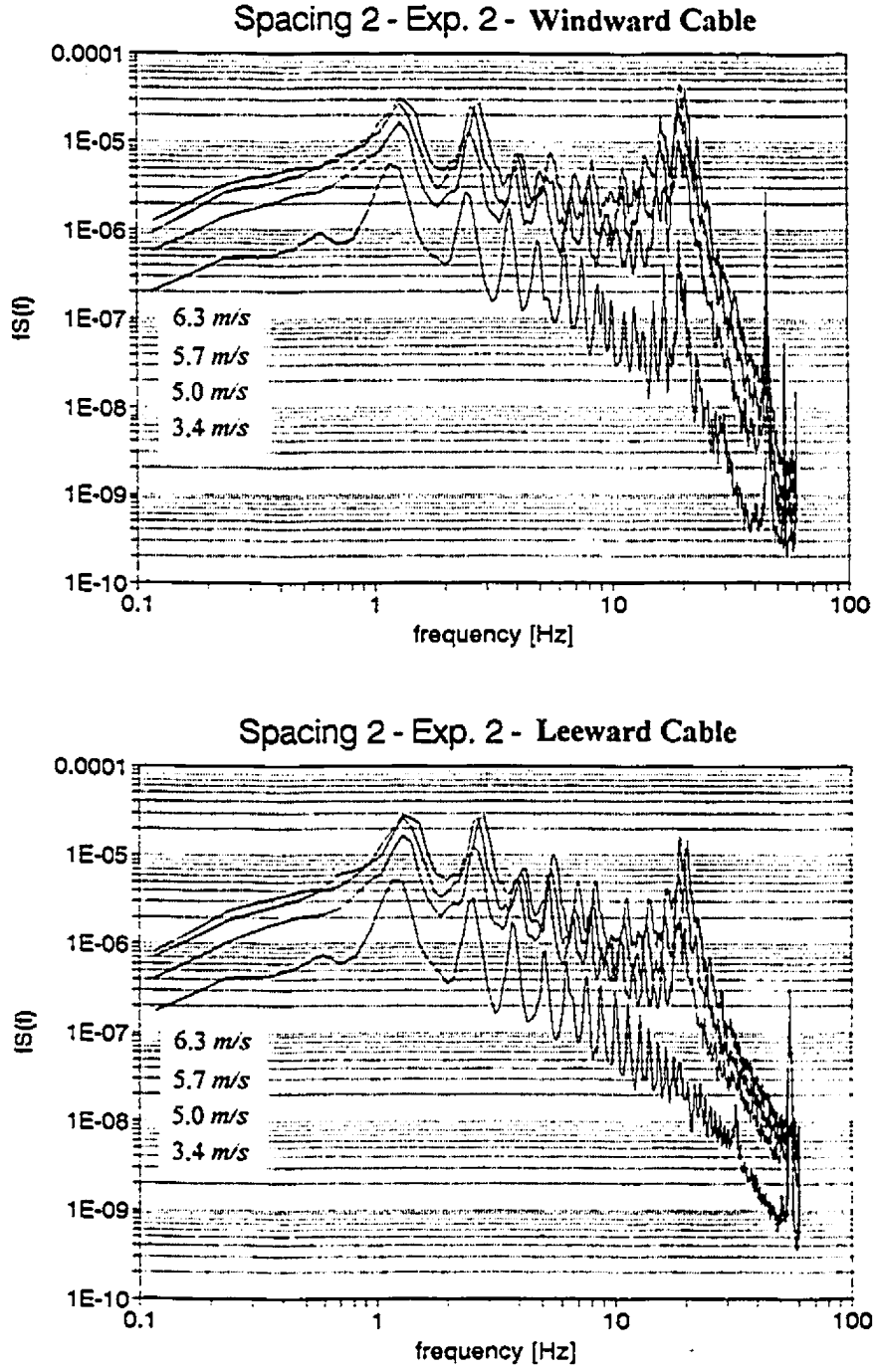

Figure 3.47 Drag Force [N] spectra for the different velocities tested for spacing 2 and exposure 2 (S=0.2m). Upper figure: windward cable; Lower figure: leeward cable.

The mean values were a bit smaller for exposure 1 (more turbulent flow) and the variance was bigger for the same exposure. The mean values of the leeward cables were slightly smaller than the front cable mean values, but at this relative magnitude they can be considered, in engineering terms, as being the same. The effect of the wake of the windward cable on the behaviour of the leeward cable was not studied here, but it should be investigated for closer separations between cables.

A comparison of the force spectra for the two cable sags tested, with V=5.7m/s, is presented in figures 3.42 and 3.43. Contrary to cables 1 & 2, the spectra of cables 3 & 4 presented distinguishable peaks at the expected natural frequencies of the cables, although as the frequency increases they start to overlap and a proper identification becomes more difficult. The possible reason why the peaks are more distinct is that the velocity is a bit smaller and the mass per unit length is bigger, therefore bringing the aerodynamic damping to a lower value in relation to the first models. At the range of frequencies between 20Hz and 30Hz a more pronounced peak appears, although the spectral density value at these frequencies ($S(f)$ only) is not so big.

Figures 3.44 to 3.47 show the force spectra for the different velocities tested for cable sag S=0.20m. As in cables 1 & 2 the lower velocity has the peaks more clearly defined. The big peak $fS(f)$ is centered around 20Hz. They were always less pronounced for the leeward cable. When the cable spacing increases, these peaks maintain roughly the same intensity for the windward cables, but are smaller for the leeward cable, diminishing with increasing spacing. The turbulence intensity level differences did not seem to cause significant effects. A possible explanation for the high peak energy at higher frequencies

could be attributed to coupling of cable frequencies from out-of-plane and symmetrical and antisymmetrical in-plane modes, where the frequencies of these modes all converge.

The spectra for cables 3 & 4 were effectively the same. Although they had different EA values, the resultant λ^2 allowed the same symmetrical in-plane natural frequencies. For that reason, cable 3 results only are presented.

3.4.3 **Theoretical prediction**

Again, the statistical method using influence lines described in Chapter 2 is employed for the theoretical prediction of the cable responses and comparison with experimental values. Model 3 and exposure 1 are chosen for the detailed calculation (below) and Eqs. (2.28) and (2.30) are used for the other cases.

Cable data: Span length, $L = 3m$; sag, $S = 0.20m$; cable length, $l = 3.04m$; mass per unit length, $m = 0.0034$ kg/m; fundamental frequency (pendulum), $f_1 = 1.26Hz$; fundamental mode shape, $\mu_1(x) = \sin(\pi x / l)$.

Wind data: Mean wind speed, $V = 5.7m/s$ at reference height, $z = 0.54m$; air density, $\rho_a = 1.2$ kg/m^3; the reference velocity pressure is, therefore, $q = 19.5$ Pa; longitudinal turbulence intensity, $I_v = 0.14$; transversal scale of the longitudinal component of turbulence, ${}^xL_v \cong 0.31m$; exponential decay factor for "narrow band" correlation, $C = 7$.

Aerodynamic data: Drag coefficient times cable diameter: $C_D d = 0.0016m$.

The response, r, which will be considered is the drag force on the cable support, for which the influence line is $i(x) = x / l$.

a) Mean response:

Using equation (2.13) we find:

$$\bar{r} \cong 0.0474\ N \cong 4.83\ gf$$

b) Background response:

Equation (2.16) allows:

$$(2\,q\,C_D\,d\,I_v)^2 \cong 7.63\text{E-}05\ N^2/m^2$$

$$\int_0^l \int_0^l e^{-\left(|x-x'|/L_v\right)} \frac{x}{l}\frac{x'}{l}\,dx\,dx' = \quad 0.53\ m^2$$

and therefore

$$\bar{r}_B \cong 0.0064\ N \cong 0.648\ gf$$

c) Resonant response:

The procedure is shown in detail for the first mode of vibration. The value of $f_1 S_{Q1}(f_1)$ is calculated from equation (2.22), by using:

$$(2\,q\,C_D\,d\,I_v)^2 \cong 7.63\text{E-}05\ N^2/m^2$$

$$\frac{f_1\,S_v(f_1)}{\sigma_v^2} \cong 0.06 \quad \text{(from Fig. 3.13)}$$

$$\int_0^l \int_0^l e^{\frac{-7|x-x'|1.26}{3.7}} \sin\left(\frac{\pi x}{l}\right) \sin\left(\frac{\pi x'}{l}\right) dx\, dx' \cong 1.54\ m^2$$

which gives $f_1 S_{Q1}(f_1) \cong 7.05\text{E-}6\ N^2$

The aerodynamic damping is obtained from (2.8):

$$\zeta_{a1} = \left(\frac{1}{4\pi}\right)\left(\frac{1.2 \times 0.0016}{0.0034}\right)\left(\frac{5.7}{1.26}\right) \cong 20\%$$

The participation factor is: $m \int_0^l \sin\left(\frac{\pi x}{l}\right) \frac{x}{l}\, dx = m\ 0.97\ kg$

The modal mass is: $m \int_0^l \sin^2\left(\frac{\pi x}{l}\right) dx = m\ 1.52\ kg$

The resonant response is then obtained from (2.26):

$$\tilde{r}_{R1} = \sqrt{\frac{\pi}{4} \frac{7.05E-6}{0.2}} \left(\frac{0.97}{1.52}\right) = 0.0034\ N \cong 0.342\ gf$$

The total rms response is then:

$$\tilde{r} = 0.0072\ N \cong 0.739\ gf$$

Table 3.11 presents RMS values of the drag force at one extreme of the cable obtained from the measurements (total) and calculated (background) from theory using the estimated values of the transverse length scale of turbulence. Theory predicts well the

mean responses and now, in contrast to what was found for cables 1 & 2, the background response alone is not enough to predict the total RMS response measured. The resonant response for the first mode was then included in the total (calculated) RMS response and this was then enough to predict the experimental findings. But remembering that there are uncertainties in the determination of ${}^{x}L_{v}$ and that the value used was from the fit of the correlation curve by an exponential function and the area under the real curve seems to be actually lower than the area given by the fitting curve, it is possible that the inclusion of more components of the resonant response may be necessary if lower values of ${}^{x}L_{v}$ are used in the theoretical prediction. These findings agree with the spectra of cable 3, which show distinct peaks at the natural frequencies, in contrast to cables 1 & 2, for the velocities studied.

Table 3.11 Comparison between measured (total) and calculated (background) RMS values of drag (L_v=0.31m for exp. 1 and L_v=0.34m for exp. 2).

Model	Exposure	Velocity [m/s]	Intensity of turbulence	RMS [gf] calculated	RMS [gf] measured	RMS Ratio Calc./Meas.
		6.2		0.770	0.835	0.92
cable 3	1	5.7	0.14	0.651	0.713	0.91
$S = 0.2m$		5.0		0.501	0.557	0.90
		3.3		0.218	0.274	0.80
		6.3		0.649	0.709	0.91
cable 3	2	5.7	0.11	0.531	0.603	0.88
$S = 0.2m$		5.0		0.409	0.493	0.83
		3.4		0.189	0.251	0.75

3.4.4 Correlation between cable forces

The correlation between the windward cable and the leeward cable forces at one extreme of the cable was calculated for each spacing, velocity and exposure studied. A Correlation Coefficient $R_{12}(F_1', F_2')$ was determined, as shown in table 3.12, by normalising the correlation by its standard deviation:

$$R_{12}(F_1', F_2') = \frac{\overline{F(1,t)F(2,t)}}{\sigma_{F1}\sigma_{F2}} \tag{3.25}$$

where:

$F(1,t)$, $F(2,t)$ = fluctuating components of drag force at cable supports: 1-windward, 2-leeward.

σ_{F1} , σ_{F2} = standard deviations (or rms) of drag force at points 1 and 2.

The correlation coefficients are practically invariant with wind speed, for each spacing and exposure. They are bigger for the smaller separation, around 0.7 to 0.8 for exposures 1 and 2, and around 0.6 for the bigger cable separation, for the same exposures. It is expected that for smaller cable separations the value of the coefficient will rise.

For highly turbulent winds, as those inside cities for instance, it is expected that the correlation will diminish and cables may move independently from each other. If the cables' spacing is short, there is a possibility that clashing between them will occur.

This was tested qualitatively during the experiments by submitting the cables to the wake generated by a person's body, i.e., a person stayed in front of the cables (at midspan) and his body's wake made the cables lose correlation and move in different directions. If they were closely separated they would clash. In a wind tunnel test where

quantitative results are necessary, an understanding of the effects of other bodies' wakes on the cable models is imperative. Theoretical expressions for the prediction of this cable behaviour are being developed and are expected to be published in the near future.

Table 3.12 Correlation coefficients of the drag forces at one extreme of the cables.

Sag [*m*]	spacing [*m*]	Exposure	Velocity [*m/s*]	Correlation Coefficient
0.20	0.16	1	6.2	0.667
			5.7	0.717
			5.0	0.786
			3.3	0.720
		2	6.3	0.711
			5.7	0.746
			5.0	0.792
			3.4	0.772
	0.32	1	6.2	0.603
			5.7	0.620
			5.0	0.645
			3.3	0.516
		2	6.3	0.634
			5.7	0.629
			5.0	0.634
			3.4	0.450
0.30	0.16	1	5.7	0.745
	0.32	1	5.7	0.653

Figure 3.48 shows the simultaneous time series for the cables with spacing 1, exposure 1 and V=5.7*m/s*.

Figure 3.49 shows the cable model displacement under the simulated wind.

The coherence between these forces were also calculated and one case is shown in figure 3.50 for Exposure 1 and velocities 5.7*m/s* and 3.3*m/s*. Equation (3.23) was used for the calculation, where points 1 and 2 now correspond to the drag forces at one extreme of each cable. From the figures (only two are shown) the following observations can be made:

-- the flow turbulence made only a small difference in the coherence of cable forces, these being slightly less coherent for the more turbulent flow.

-- the coherence between the forces at the two supports is smaller for the larger separation, for the same kind of flow, and decreases with wind velocity. The difference in coherence between the two separations is also smaller for lower velocities.

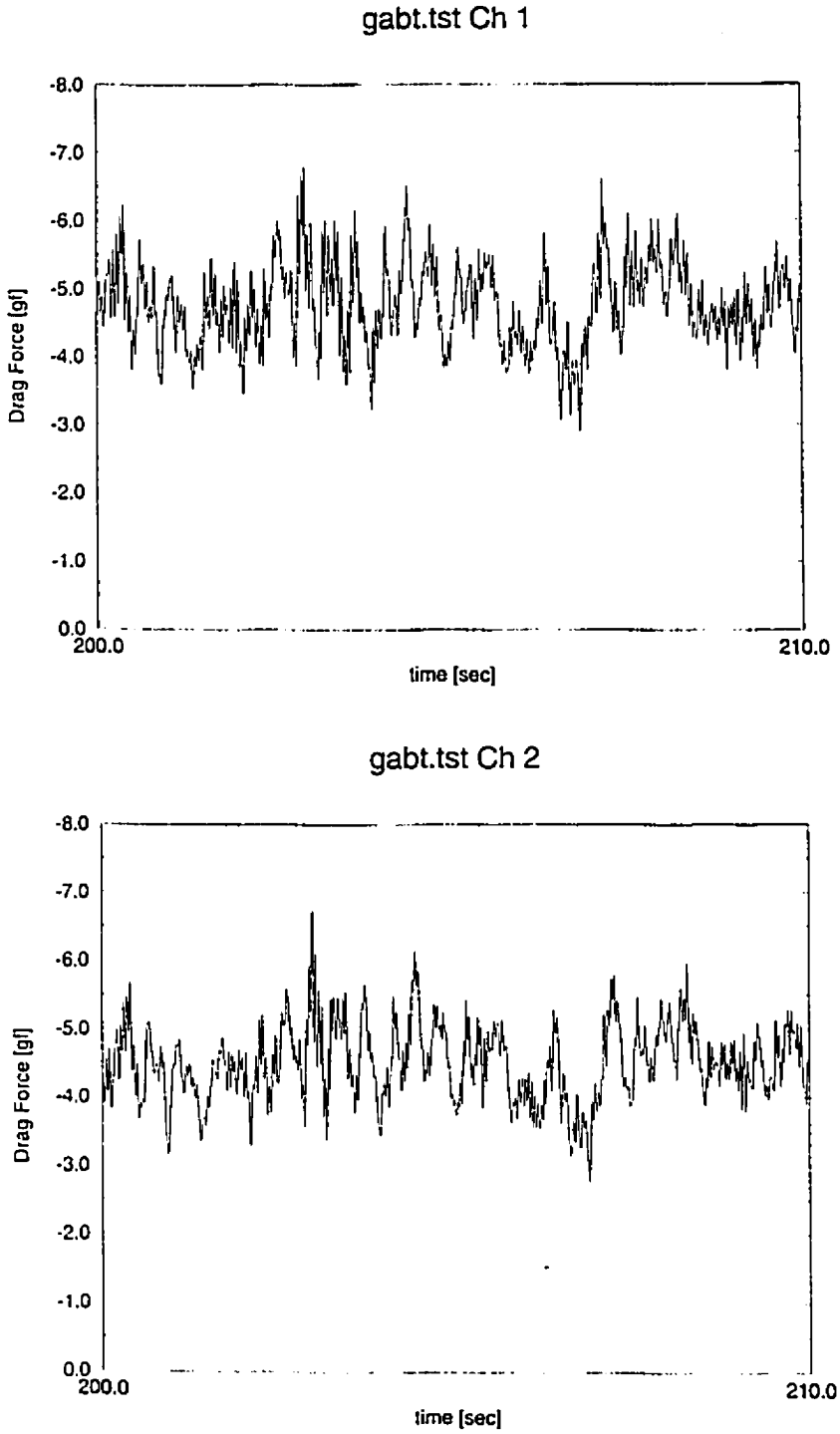

Figure 3.48 Simultaneous time series for the cables with spacing 0.16*m*, exposure 1 and *V*=5.7*m/s*.

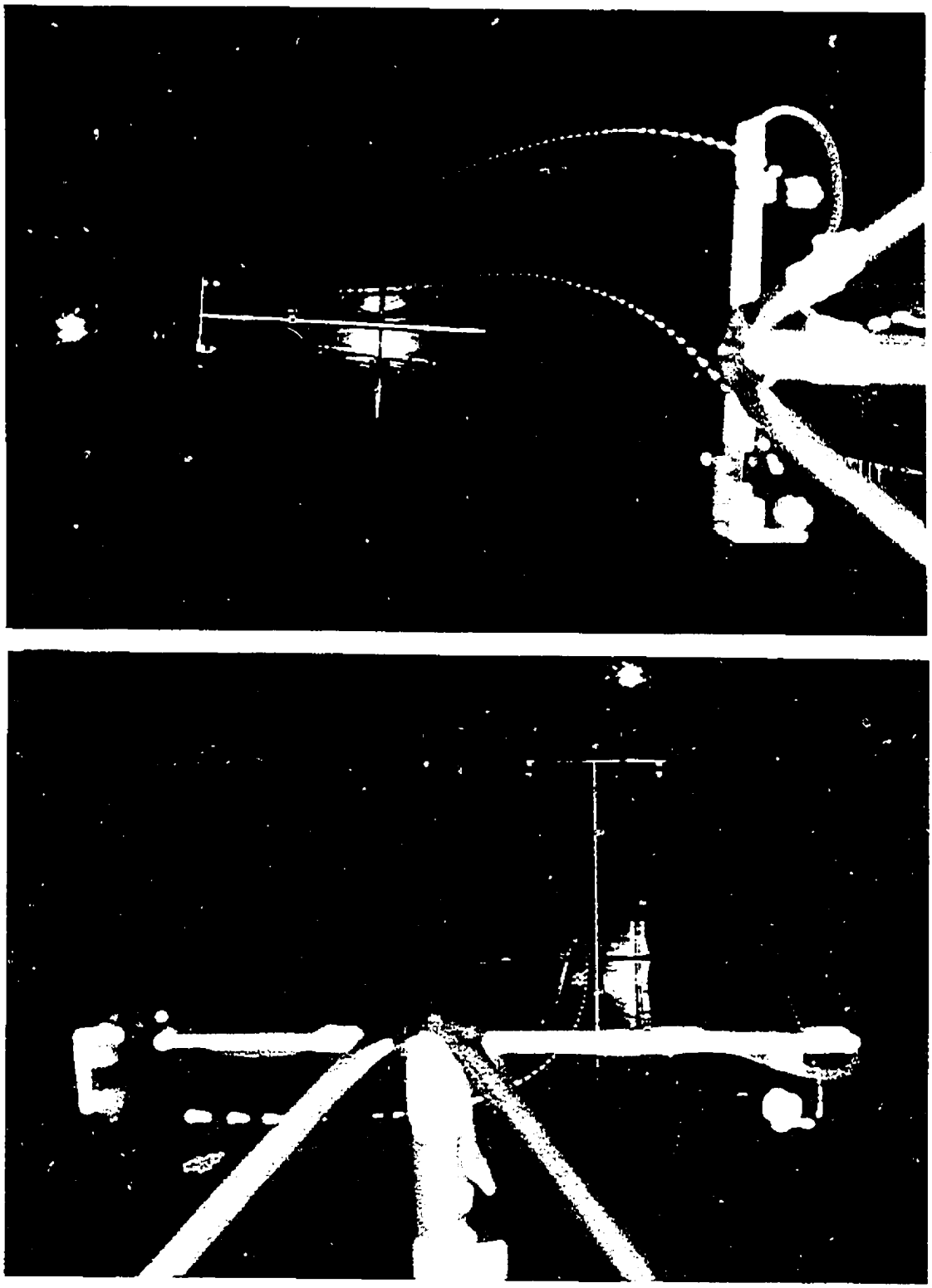

Figure 3.49 Cable model displacement under simulated wind.

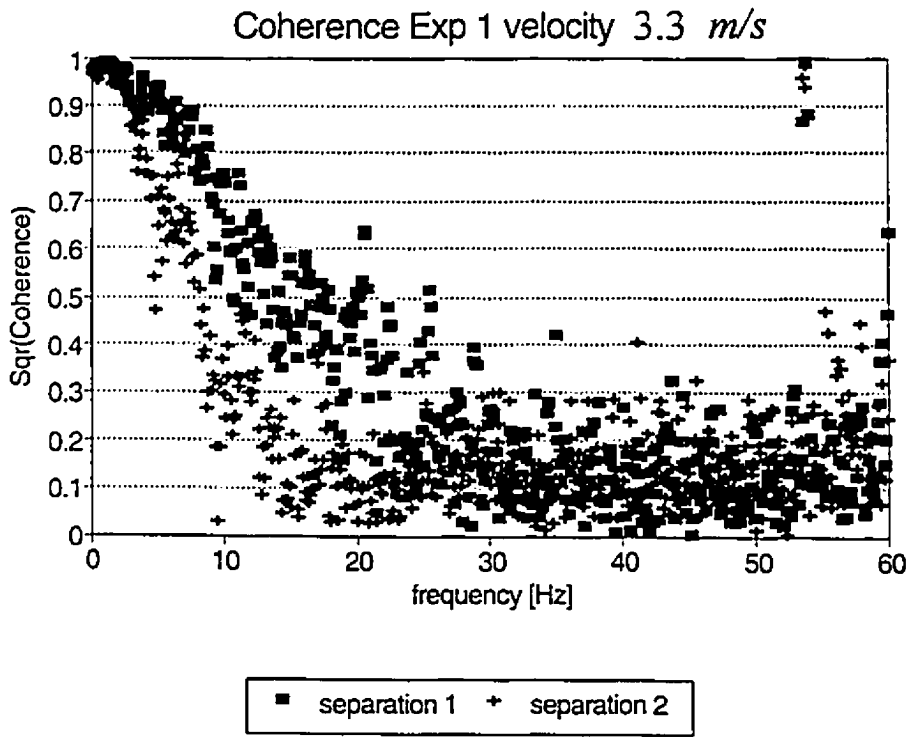

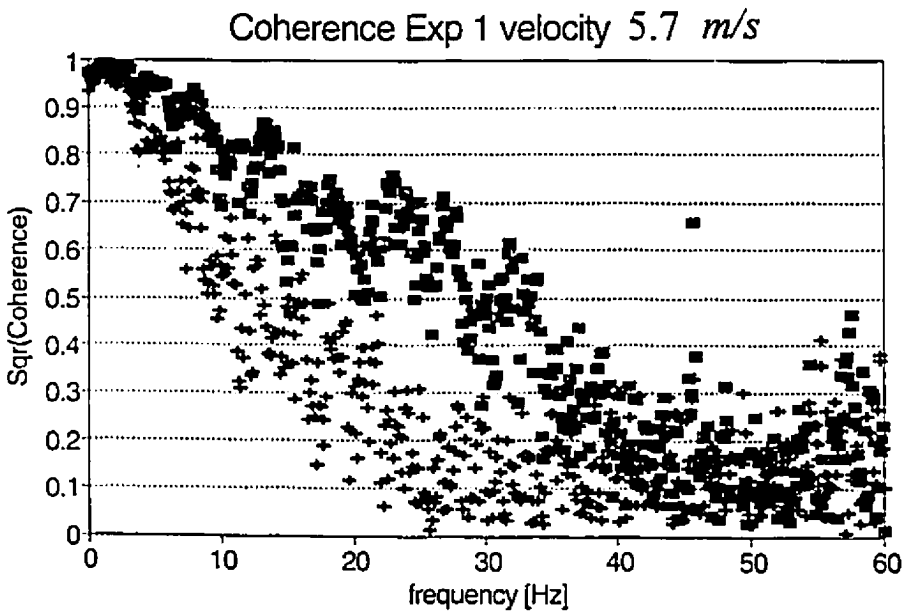

Figure 3.50 Square-root of coherence of drag forces at one cable extreme for the two separations tested and two velocities, for exposure 1.

3.5 Comparison with Ferraro's full-scale data

As one of the main purposes of this part is to develop a wind tunnel modelling technique for transmission line cables, it is important to check full-scale experimental data when available. From the measurements of Ferraro (1983), normalised power spectra of wind speed and transverse swing angle (which can be directly related to drag) are shown in Figs. 3.51 and 3.52 for the Ontario Hydro's Lambeth transmission line, and in figure 3.53 for the John Day-Grizzly line located in northern Oregon, USA, for different wind storms. The approximate characteristics of wind and cables are given in table 3.13. These lines do not relate directly to the models tested, but are typical lines and serve well for a qualitative comparison.

Table 3.13 Characteristics of wind and cables for full-scale transmission lines (approximate values).

Line	V [m/s]	d [m]	C_D [m]	m [kg/m]	S [m]	f_1 [Hz]
John Day	13.0	0.041	1.2	3.0	9.1	0.18
Lambeth	6.0	0.028	1.0	1.7	14.0	0.15

It can be seen that the spectra of Figs. 3.51 and 3.52 contain peaks corresponding to the natural frequencies of the cables and even a pronounced peak at higher frequencies corresponding to the tower natural frequency. The other line (John Day) did not have the peaks so pronounced. From table 3.13 we can infer a higher aerodynamic damping for this line in relation to the Lambeth line. At least qualitatively, the wind tunnel tests agree with Ferraro's full-scale data.

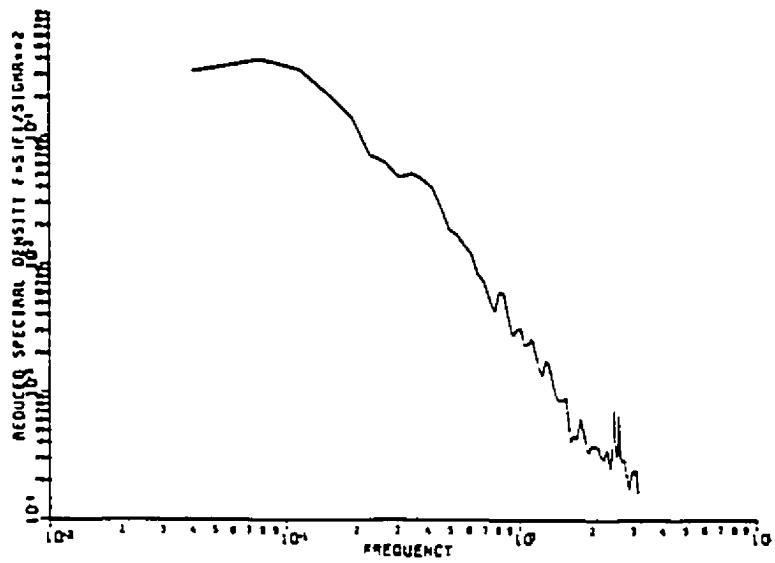

(a)

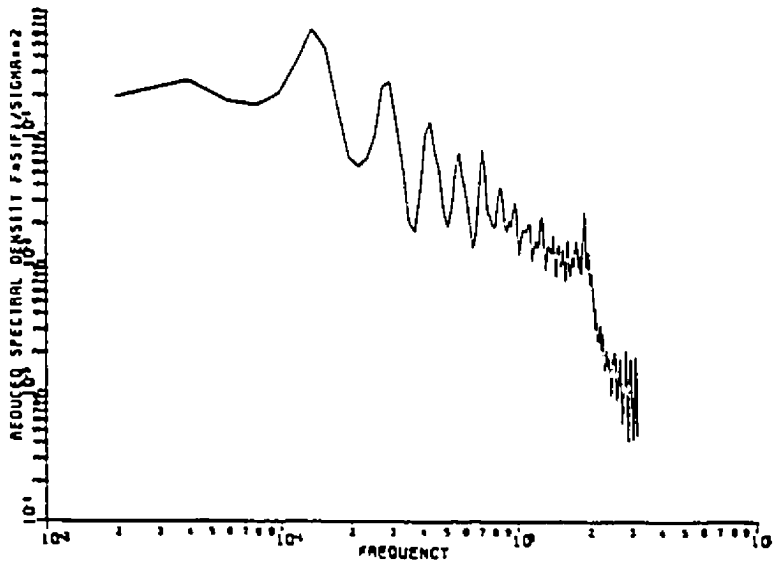

(b)

Figure 3.51 Normalised power spectra of (a) wind speed and (b) transverse swing angle for a full-scale transmission line - November 26, 1979 storm, Lambeth, Ontario (after Ferraro, 1983).

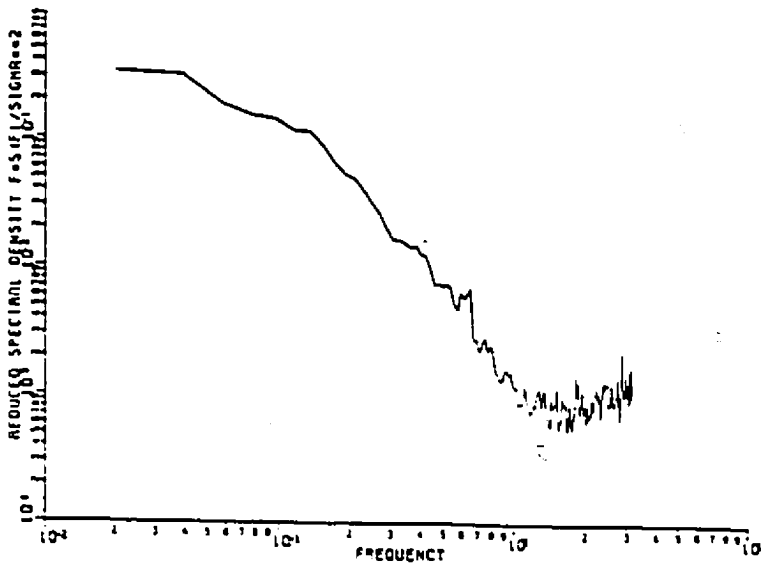

(a)

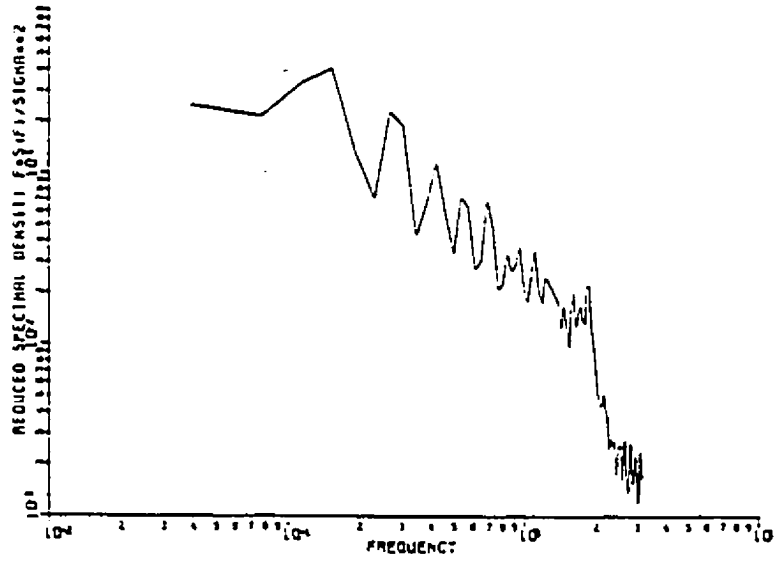

(b)

Figure 3.52 Normalised power spectra of (a) wind speed and (b) transverse swing angle for a full-scale transmission line - March 13, 1980 storm, Lambeth, Ontario (after Ferraro, 1983).

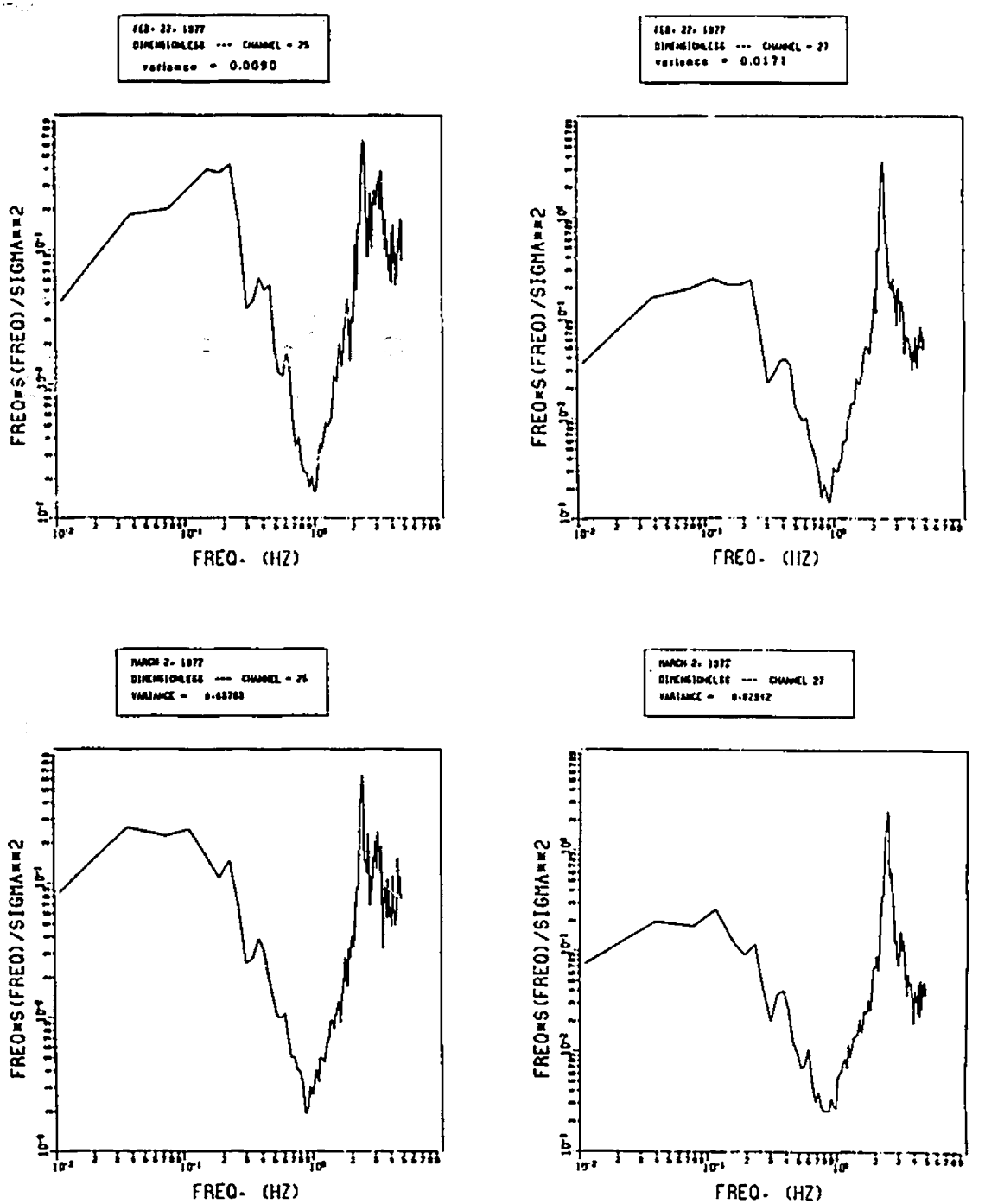

Figure 3.53 Normalised power spectral densities of transverse swing angle for John Day-Grizzly transmission line, Oregon, USA (after Ferraro, 1983).

CHAPTER 4

WIND FORCES ON TOWERS

4.1 INTRODUCTION

As already stated in chapter 1, transmission towers exist in many shapes and are made generally from steel or wood. The majority of transmission line networks, however, are supported by steel lattice towers, as shown in figures 1.1 to 1.3.

There are two ways of calculating the wind loads on lattice towers:

a) The first method is to determine the loading on each tower member separately and add them to determine the total load. For that, one need to know the geometric properties of each element as well as its aerodynamic force coefficient and design wind speed. For a typical tower, which is constituted of many structural elements, this is a very time consuming process.

b) The other way is to determine the loads on sections of the structure (including several elements) for which there are aerodynamic force coefficients available. The total force is also obtained from the summation of these partial loads, but it is a more practical and less time consuming procedure.

A fundamental concept is the solidity ratio ϕ, defined as the ratio between the total frontal area of all individual members (effective or solid area), A_s, and the frontal envelope area, A, i.e., the area of the limiting surface that includes all the individual members:

$$\phi = A_S / A \tag{4.1}$$

where the frontal areas are the areas projected in a plane perpendicular to the wind (shadow area). Solidity ratio must lie in the range $0 \leq \phi \leq 1$, with $\phi = 1$ representing a solid body.

The drag forces on the tower's sections are determined by putting models or full-scale sections of the tower in wind tunnels and measuring the loads induced by uniform or turbulent winds, through load cells at the base of the sections. The total force, F, obtained is then divided by the dynamic pressure, q, and by the effective area, A_S, and a drag coefficient is obtained:

$$C_D = \frac{F}{q A_S} \tag{4.2}$$

This drag coefficient is then associated with its corresponding solidity ratio, becoming suitable for codification purposes. The process automatically includes the effects of shielding caused by front elements on other elements located in their wakes. As an example, a comparison made by Blessmann (1990) of values of drag coefficients for a lattice tower of square cross-section given by some wind codes and researchers is shown in Fig. 4.1. NBR-6123 is the Brazilian wind code (1988), DIN4131 a German code (1969) and NV-65 a French code (1980).

There are many works dealing with wind forces on lattice towers. For more insight the works of Cook (1990) and Georgiou and Vickery (1979) are indicated. Data

and design indications can be obtained from appropriate codes and also from Walker (1975) and Bayar (1986).

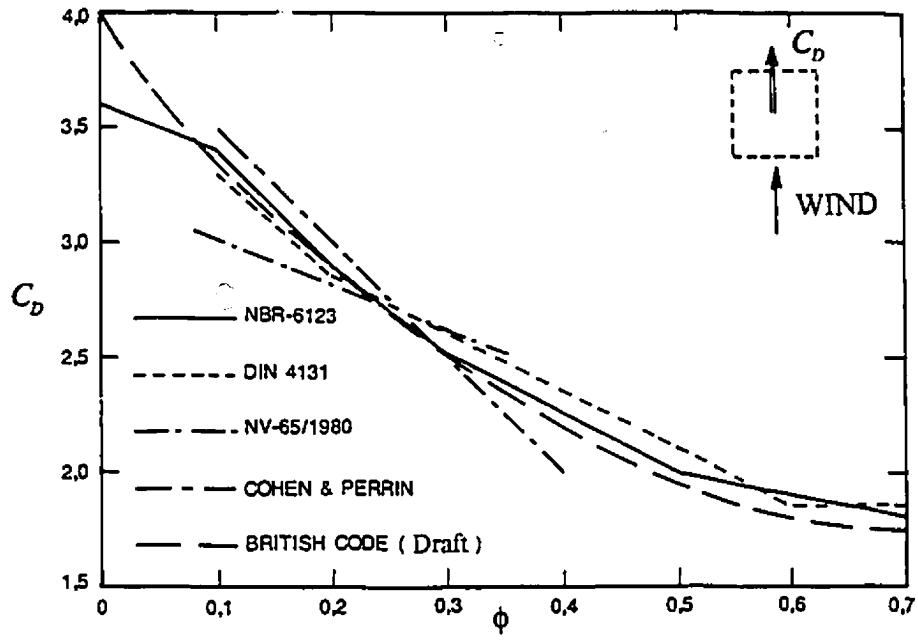

Figure 4.1 Drag coefficients of lattice towers of square cross-section (from Blessmann, 1990).

A more convenient form of drag coefficient, C_D', for the purpose of load analysis is based on the projected enclosed area of the front face, i.e.,

$$C_D' = A_s(solid) / A(enclosed) \quad C_D = \phi \quad C_D \tag{4.3}$$

Thus, there are two alternative ways of determining the drag:

$$F = 1/2\ \rho_a V^2 C_D'\ A(enclosed) = 1/2\ \rho_a\ V^2 C_D A_s(solid) \qquad (4.4)$$

However the solid (or effective) area at any section of the tower is difficult to estimate, whereas the enclosed area may be represented as a simple function of height.

The wind speed was assumed to be uniform in the example above just for simplification, but it is very well known that the variation of mean wind speed with height in the lower part of the atmospheric boundary layer follows a logarithmic law of the kind:

$$\overline{V}(z) = \frac{1}{k} u_* \ln \frac{z}{z_o} \qquad (4.5)$$

where $\overline{V}(z)$ is the mean speed at some height z from the ground, k = 0.40 is the Von Kármán constant, u_* the friction velocity and z_o the roughness length.

It is a fair approximation, however, to represent the mean velocity variation with height by a power law function:

$$\overline{V}(z) = \overline{V}_H \left(\frac{z}{H}\right)^{\alpha} \qquad (4.6)$$

where $\overline{V}_H$ is the mean wind speed at the reference height H, here chosen as the tower's height, and α is the power law exponent, a function of the terrain roughness.

A somewhat improved form of these laws can be obtained if the heights are measured not from the true ground but a false ground which varies with the height of the roughness elements of the terrain. This correction can be significant in densely developed areas where the effective ground plane tends to be nearer the average roof height (in case of buildings) rather than at true ground level. In general, transmission towers are located in open terrain and, for the purposes of this work, Eq. (4.6) will be adopted.

As already described in previous chapters an important tool in the analysis of the response is the use of influence lines or functions. Figure 4.2, extracted from Cook (1985), shows the influence function for axial tension, F_T, in a bracing member of a lattice tower of the Eiffel type, in which the lines of the main legs of the braced panel would intersect if produced upwards. The unit load at C, immediately above the braced panel, produces the maximum tension in the member. The unit load B at the intersection point of the legs has no effect on the bracing member, since the load is resisted wholly by the main legs. The unit load A at the top of the tower puts the bracing member into compression. The influence line is therefore positive in sign below B and negative above it. Such towers are frequently shaped so that the main legs intersect at the center of pressure of the mean wind loading profile with the objective of minimising the loads in the bracing members.

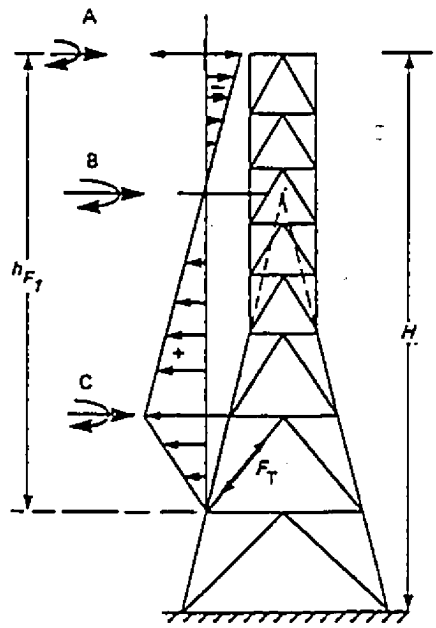

Figure 4.2 Tension in shear bracing member of lattice tower (after Cook, 1985).

Wind loading is by its nature a dynamic force, whose effect on a structure as a whole is to start it vibrating at its natural frequency and so inducing dynamic bending. This causes shear and bending stresses at all points, depending on the mass and acceleration of that point.

To obtain the natural frequencies and mode shapes of the towers a lumped-mass solution may be employed by dividing the tower height into a number of sections and lumping the mass of each section at discrete points. The stiffness properties between nodes can be obtained by considering the stiffness of individual members, and combining these into a local stiffness matrix. By assembling the contributions from all sections, a system of equations can be written as:

$$[M]\{\ddot{y}\} + [K]\{y\} = 0 \tag{4.7}$$

where $[M]$ = mass matrix;

$[K]$ = stiffness matrix;

$\{y\}$ = vector of horizontal deflections at each mass point.

By defining the circular frequency, ω, by the equation:

$$\omega^2 = \frac{K}{M} \tag{4.8}$$

we end up with:

$$([K] - \omega^2[M])\{y\} = 0 \tag{4.9}$$

The eigenvalues and eigenvectors give the free vibration natural frequencies and mode shapes for an undamped system. For more insight in dynamic analysis of structures and the introduction to other methods of analysis, the classical textbooks of Clough and Penzien (1993) and Thomson (1993) are recommended. A more common approach nowadays is to use a finite element method software and introduce the whole structure into the computer for analysis. Guidelines on computer use in transmission tower design are given by Lo et al. (1975).

Tower motion is generally dominated by structural damping, being also strongly influenced by damping of aerodynamic origin. Typical values of structural damping for transmission structures are given in table 4.1, which is extracted from ASCE (1991).

Table 4.1 Approximate dynamic properties for transmission structures.

Type of structure	Fundamental frequency f_T [Hz]	Damping ratio ζ_S
Lattice tower	2.0 - 4.0	0.04
H-frame	1.0 - 2.0	0.02
Pole	0.5 - 1.0	0.02

The aerodynamic damping for the tower can be estimated by using modal analysis as:

$$\zeta_{aj} = \frac{C_j^*}{C_{crit}} = \frac{C_j^*}{2\,\omega_j M_j} \tag{4.10}$$

where C_j^* is the modal damping at mode j, C_{crit} the critical modal damping and M_j the modal mass at the jth mode of vibration. The modal damping is given by:

$$C_j^* = \int_0^H C\,\mu_j^2(z)\,dz \tag{4.11}$$

with $C = \rho_a \bar{V}\, C_D\, w$. Recognizing that generally the mean velocity $\bar{V}$, the drag coefficient C_D and the tower's width w do vary with height, we have:

$$\zeta_{aj} = \left(\frac{\rho_a}{4\pi f_{Tj}}\right)\frac{\int_0^H \bar{V}(z)C_D(z)w(z)\mu_j^2(z)dz}{\int_0^H m(z)\mu_j^2(z)dz} \tag{4.12}$$

4.2 THEORETICAL APPROACHES

4.2.1 Statistical method using influence lines

Based on the considerations above and the statistical method described in 1.3.3 we can write the main equations assumed for the calculation of each of the three kinds of response of the tower. The load on a small cross-section of the structure will be:

$$d\bar{F}(z) = \frac{1}{2}\rho_a \bar{V}^2(z) C_D(z) \phi(z) w(z) dz \tag{4.13}$$

for the mean component, and

$$dF(z,t) = \rho_a \bar{V}(z)\, v(z,t)\, C_D(z)\, \phi(z)\, w(z)\, dz \tag{4.14}$$

for the fluctuating component. The three kinds of response are then:

4.2.1.1 Mean response

The mean response is given by:

$$\bar{r} = \int_0^H \frac{1}{2}\rho_a \bar{V}^2(z)\, \phi(z) C_D(z)\, w(z)\, i(z)\, dz \tag{4.15}$$

using Eq. (4.6) we have:

$$\bar{r} = \frac{1}{2}\rho_a \bar{V}_H^2 \int_0^H \left(\frac{z}{H}\right)^{2\alpha} \phi(z)\, C_D(z)\, w(z)\, i(z)\, dz$$

or,

$$\bar{r} = q_H \int_0^H \left(\frac{z}{H}\right)^{2\alpha} \phi(z)\, C_D(z)\, w(z)\, i(z)\, dz \tag{4.16}$$

4.2.1.2 **Background response**

The background response is given by:

$$\bar{r}_B^2 = \int_0^H \int_0^H \rho_a^2 C_D(z) C_D(z') \phi(z) \phi(z') \overline{[\bar{V}(z) v(z,t) i(z)] \left[\bar{V}(z') v(z',t) i(z')\right]} w(z) w(z') dz dz'$$

$$\bar{r}_B^2 = \rho_a^2 \int_0^H \int_0^H C_D(z) C_D(z') \phi(z) \phi(z') \bar{V}(z) \bar{V}(z') \sigma_v \sigma_{v'} R(v_z, v_{z'}) i(z) i(z') w(z) w(z') dz dz' \tag{4.17}$$

where $R(v_z, v_{z'})$ is the cross-correlation coefficient between v at the two heights z and z' and can be expressed by:

$$R(v_z, v_{z'}) = \frac{\overline{v(z,t) v(z',t)}}{\sigma_v \sigma_{v'}} = e^{-(\Delta z / {}^z L_v)} \tag{4.18}$$

where $\Delta z = \left| z - z' \right|$. Then:

$$\bar{r}_B^2 = \rho_a^2 \sigma_v^2 \bar{V}_H^2 \int_0^H \int_0^H C_D(z) C_D(z') \phi(z) \phi(z') \left(\frac{z}{H}\right)^{\alpha} \left(\frac{z'}{H}\right)^{\alpha} e^{-(\Delta z / {}^z L_v)} i(z) i(z') w(z) w(z') dz dz'$$

or,

$$\bar{r}_B^2 = (2 q_H I_v)^2 \int_0^H \int_0^H C_D(z) C_D(z') \phi(z) \phi(z') \left(\frac{z}{H}\right)^{\alpha} \left(\frac{z'}{H}\right)^{\alpha} e^{-(\Delta z / {}^z L_v)} i(z) i(z') w(z) w(z') dz dz' \tag{4.19}$$

4.2.1.3 **Resonant response**

The equation of motion in modal co-ordinates for a structural system subjected to a dynamic force can be written:

$$M_j \ddot{y}_j + C_j \dot{y}_j + K_j y_j = Q_j(t) \tag{4.20}$$

where y_j is the generalized co-ordinate or modal amplitude; M_j , C_j and K_j are, respectively, the generalized mass, damping and stiffness of the jth mode while $Q_j(t)$ is the generalized force given by:

$$Q_j(t) = \int_0^H F'(z,t)\mu_j(z)dz \tag{4.21}$$

The loading in this case is the wind and this may be expressed in terms of the fluctuating component of wind velocity by making use of Eq.(4.14). In practice , however, the presence of the structure tends to distort the turbulent flow and this applies particularly to the small high-frequency eddies. Davenport (1961) suggested the introduction of a correction factor to take account of this effect, which was termed Aerodynamic Admittance Function, $\chi(f)$. Then:

$$Q_j(t) = \chi(f)\int_0^H \rho_a \bar{V}(z)v(z,t)C_D(z)\phi(z)w(z)\mu_j(z)\,dz \tag{4.22}$$

The spectral density of the modal generalized force is then:

$$S_{Qj}(f_j) = \rho_a^2 \chi^2(f) \int_0^H \int_0^H C_D(z) C_D(z') \phi(z) \phi(z') \bar{V}(z) \bar{V}(z') S_v(z, z', f) \mu_j(z) \mu_j(z') w(z) w(z') dz\, dz' \tag{4.23}$$

where $S_v(z,z',f)$ is the cross spectral density of wind velocity, which is used in the calculation of the correlation of the individual frequency components of wind turbulence, or coherence:

$$\gamma^2(z, z', f) = \frac{\left| S_v(z, z', f) \right|^2}{S_v(f) S_v'(f)} \tag{4.24}$$

The square root of the coherence, when plotted against the reduced frequency, can be approximated by an exponential function of the form:

$$\gamma(\Delta z, f) \equiv e^{-\frac{C|\Delta z|f}{V(z)}} \tag{4.25}$$

A representative non-dimensional form of the power spectral density of the wind can be given by (Davenport, 1987):

$$\frac{f S_v(f)}{\sigma_v^2} = 0.045 \left(\frac{fz}{V(z)} \right)^{-2/3} \tag{4.26}$$

Although the wind spectra, and therefore the coherence, do vary with height, it is common to assume it constant and adopt a value of $\overline{V}(z) = \overline{V}_{Hz}$, i.e., to consider the mean velocity at mid-height in Eqs. (4.25) and (4.26). Therefore, the spectra of the generalized force becomes:

$$S_{Qj}(f) = \rho_a^2 \overline{V}_H^2 \chi^2(f) S_v(f) \int_0^H \int_0^H C_D(z) C_D(z') \phi(z) \phi(z') \left(\frac{z}{H}\right)^{\alpha} \left(\frac{z'}{H}\right)^{\alpha} \gamma(z, z', f) \mu_j(z) \mu_j(z') w(z) w(z') dz dz' \qquad (4.27)$$

or, multiplying by f_j:

$$f_j S_{Qj}(f_j) = (2 q_H I_v)^2 \frac{f_j S_v(f)}{\sigma_v^2} \chi^2(f) \int_0^H \int_0^H C_D(z) C_D(z') \phi(z) \phi(z') \left(\frac{z}{H}\right)^{\alpha} \left(\frac{z'}{H}\right)^{\alpha} e^{-C|\Delta z| f / \overline{V}_{Hz}} \mu_j(z) \mu_j(z') w(z) w(z') dz dz' \qquad (4.28)$$

The variance of the generalized modal co-ordinate, y_j, can be given approximately by:

$$\sigma_R^2(y_j) \approx \frac{\pi}{4(\zeta_{aj} + \zeta_S)} \frac{1}{K_j^2} f_j S_{Qj}(f_j) \qquad (4.29)$$

which is obtained by integrating the spectral density for modal response (displacement) over a narrow band in the vicinity of the natural frequency corresponding to mode j. $K_j = \omega_j^2 M_j$ is the modal stiffness, with the modal mass given by:

$$M_j = \int_0^H m(z) \mu_j^2(z) dz \qquad (4.30)$$

The resonant response for local effects (shear, bending moment, etc.) is obtained by multiplying the square root of Eq. (4.29) by the response participation factor:

$$\tilde{r}_{Rj} = \sigma_R(y_j)\int_0^H m(z)\omega_j^2\mu_j(z)i(z)dz \tag{4.31}$$

and therefore:

$$\tilde{r}_{Rj} = \sqrt{\frac{\pi}{4}\frac{f_j\, S_{Qj}(f_j)}{(\zeta_{aj}+\zeta_s)}}\,\frac{\int_0^H m(z)\,\mu_j(z)\,i(z)\,dz}{\int_0^H m(z)\,\mu_j^2(z)\,dz} \tag{4.32}$$

4.2.1.4 **Total response**

The total peak response $\hat{r}$ is given by:

$$\hat{r} = \bar{r} + g_s\tilde{r} \tag{4.33}$$

with the total fluctuating response $\tilde{r}$ (rms value) being:

$$\tilde{r} = \sqrt{\tilde{r}_B^2 + \Sigma\tilde{r}_{Rj}^2} \tag{4.34}$$

The statistical peak factor g_s is given by:

$$g_s = \sqrt{2\ln(\upsilon T)} + \frac{0.577}{\sqrt{2\ln(\upsilon T)}} \tag{4.35}$$

with the time T being around 1200 s to 3600 s and the crossing rate υ estimated by:

$$\upsilon^2 = \frac{\Sigma f_j^2 \tilde{r}_{Rj}^2}{\tilde{r}_B^2 + \Sigma \tilde{r}_{Rj}^2} \tag{4.36}$$

4.2.2 Current Procedures

4.2.2.1 Velocity gust factor

The current procedure for the design of transmission structures is largely based on the assumption of a static behaviour of the structure. A certain pattern of wind loading is assumed, generally a power law profile for velocities, the aerodynamic force coefficients are determined and the corresponding pressures calculated. The peak wind velocity used can be estimated by:

$$\hat{V} = \overline{V} + g_s \sigma_v$$

or,

$$\hat{V} = \overline{V}\left(1 + g_s \frac{\sigma_v}{\overline{V}}\right) = \overline{V}(1 + g_s I_v) \tag{4.37}$$

The hourly mean wind speed is multiplied by a gust factor and, therefore, the corresponding mean wind pressure by the square of it.

4.2.2.2 Gust response factor

An attempt to consider dynamic effects on the response of these structures is made through the Gust Response Factor (GRF) method suggested by Davenport (1979). This is incorporated in the ASCE (1991) guidelines for the loading of transmission structures, but with the resonant response component neglected. The approach is based on statistical methods which takes account of the spatial correlation and energy spectrum of the wind speed and the dynamic response of the transmission line system. The peak response is given by:

$$\hat{r} = \bar{F}_D \, i_r \, G_t \tag{4.38}$$

where $\bar{F}_D$ is the mean wind drag force, i_r an influence coefficient and G_t the gust response factor for the tower and is given by:

$$G_t = 1 + 0.75 g_s E_x \sqrt{B_t + R_t} \tag{4.39}$$

with the exposure factor E_x being:

$$E_x = \sqrt{24\kappa} \left(\frac{z_{ref}}{h_o} \right)^{\alpha} \tag{4.40}$$

where z_{ref} is the reference height, h_o the effective height (at the approximate center of pressure of the structure), α the power law exponent and κ the surface drag coefficient for which typical values are given in table 4.2.

Table 4.2 Typical values of the surface drag coefficient κ (Davenport, 1979).

Type of Terrain	Power Law Exponent α	Surface Drag Coefficient κ ($z_{ref} = 10\ m$)
Open country, flat shorelines	0.10	0.0015
Farmland, scattered trees and buildings	0.16	0.0050
Woodland, Suburbs	0.28	0.0150

The dimensionless resonant term R_t is:

$$R_t = 0.0123\left(\frac{f_T h_o}{\bar{V}_o}\right)^{-5/3}\frac{1}{\zeta} \tag{4.41}$$

where f_T is the tower's natural frequency, $\bar{V}_o$ the mean wind speed at effective height h_o and ζ the tower's total damping (structural plus aerodynamic).

The dimensionless response term corresponding to the quasi-static background wind loading on the tower, B_t, is given by:

$$B_t = \frac{1}{1+0.375H/L_v} \tag{4.42}$$

where H is the tower's height and L_v the transverse integral scale of turbulence.

There are, however, some simplifications in the GRF method. It does not account for unbalanced loading effects, or shear and axial loads, nor the effect of higher modes of vibration in the calculation of the response factors. A unified approach for a variety of structural responses is possible through the statistical method using influence lines, described in 4.2.1, which can easily incorporate all those factors.

4.3 CALCULATION OF THE RESPONSES

Several responses due to certain assumed wind characteristics were calculated for some typical transmission towers. These values were obtained considering transverse wind on the tower only. The consideration of the wind action on the conductors as well as the dead weight will increase the loads on the members. Also, the consideration of the conductors' masses will, in general, decrease the natural frequencies of the towers, therefore increasing the resonant response. The Aerodynamic Admittance Function was assumed to be equal to unity in the analyses.

4.3.1 Tower I

Shown in Fig. 4.3, this is a typical example of a suspension transmission tower, which was extracted from the example given by Zar and Arena (1979). In this reference, only the main members are given and, therefore, an assumption regarding the other members was made. From the characteristics of the structure the solidity ratio, $\phi(z)$, drag coefficient $C_D(z)$, mass distribution, $m(z)$, natural frequencies and mode shapes as well as influence lines for tension in some members were obtained (Figs. 4.4 to 4.10).

To initiate the investigation the following properties were assumed for the wind: mean wind speed of 35 *m/s* at the tower's height (H = 33.2 *m*), a terrain between open country and suburban, and therefore the power law exponent α = 0.16, vertical length scale of turbulence $^{z}L_{v}$ = 50 *m*, exponential decay factor for narrow band correlation C = 8. Different values of damping were used to study its influence on the resonant response.

24-16

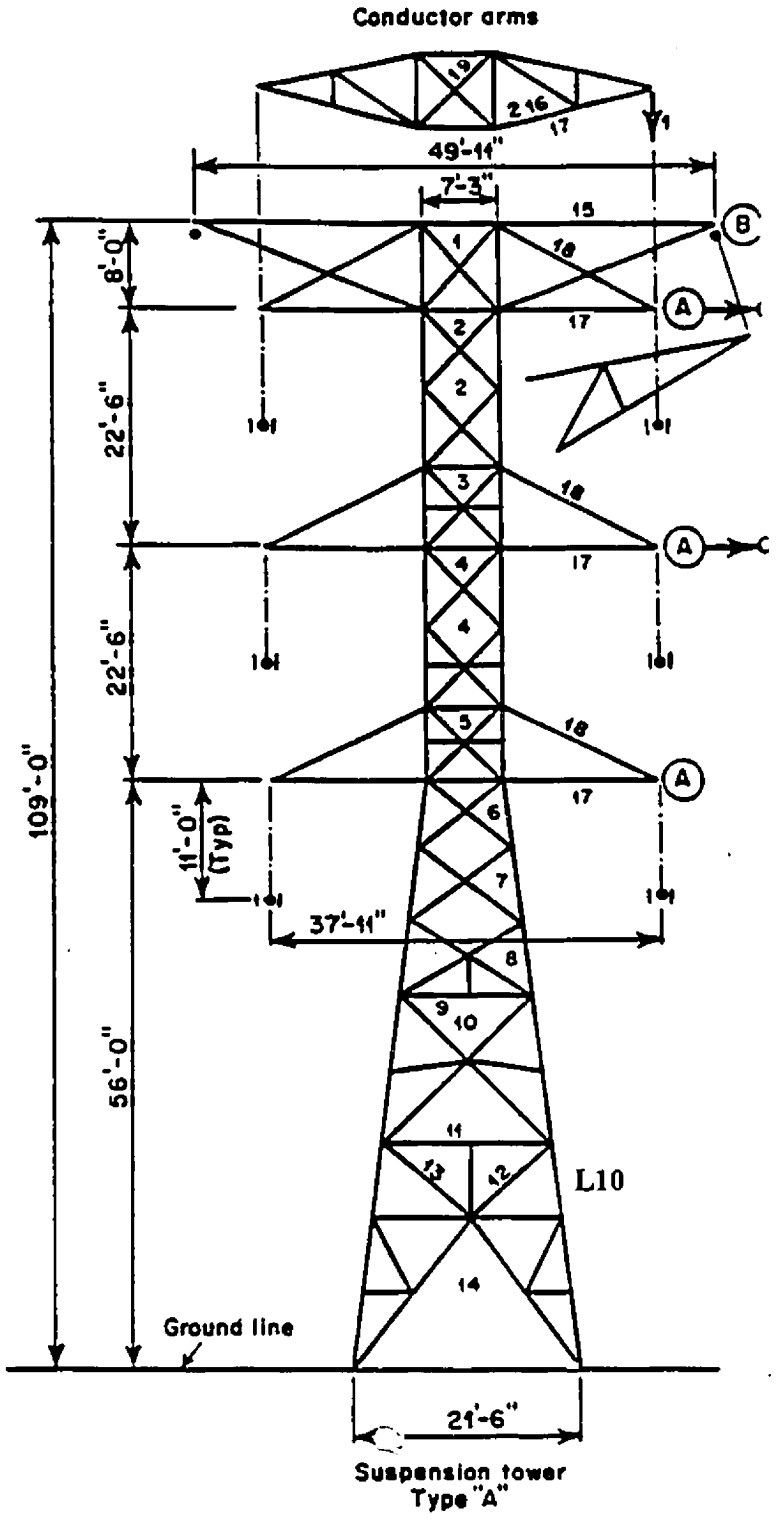

Figure 4.3 Transmission tower I .

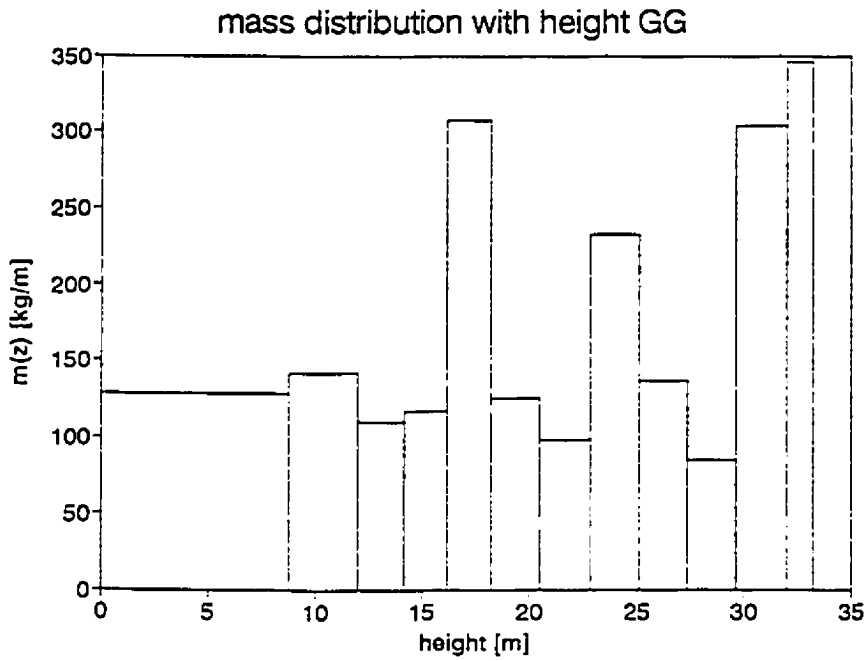

Figure 4.4 Distribution of mass with height for tower I.

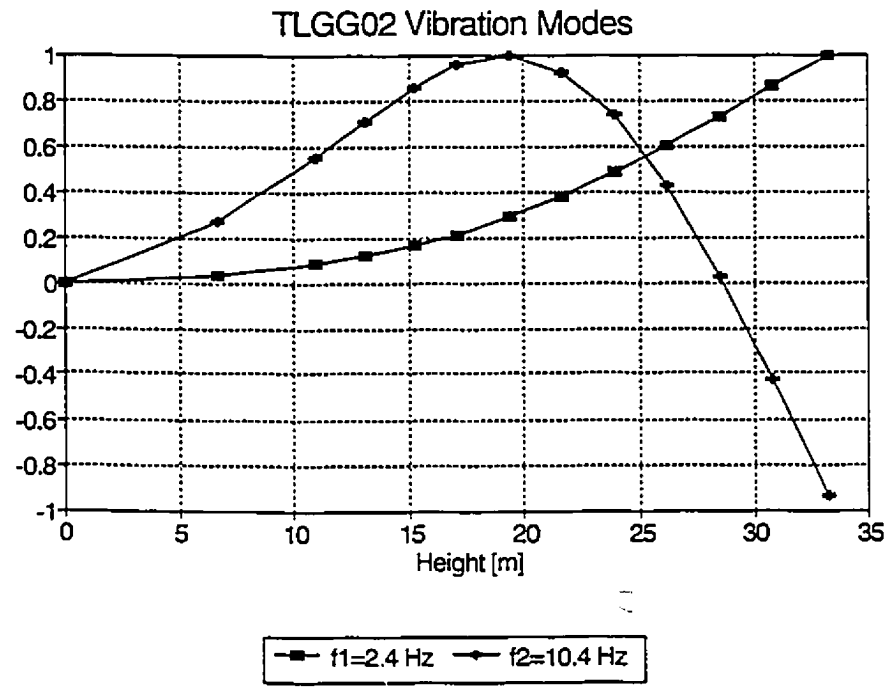

Figure 4.5 Natural frequencies and mode shapes for tower I.

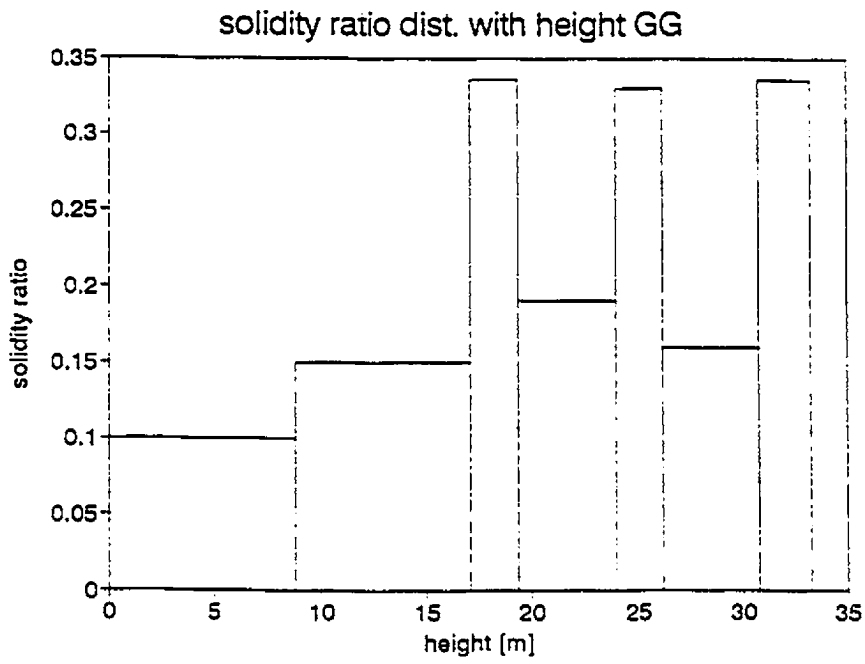

Figure 4.6 Distribution of solidity ratio with height for tower I.

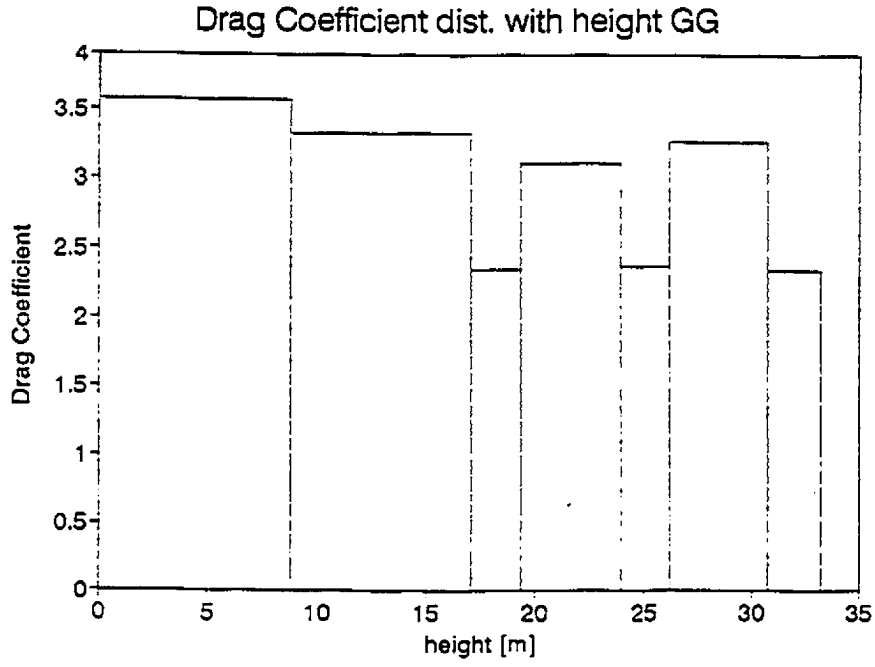

Figure 4.7 Distribution of drag coefficient with height for tower I.

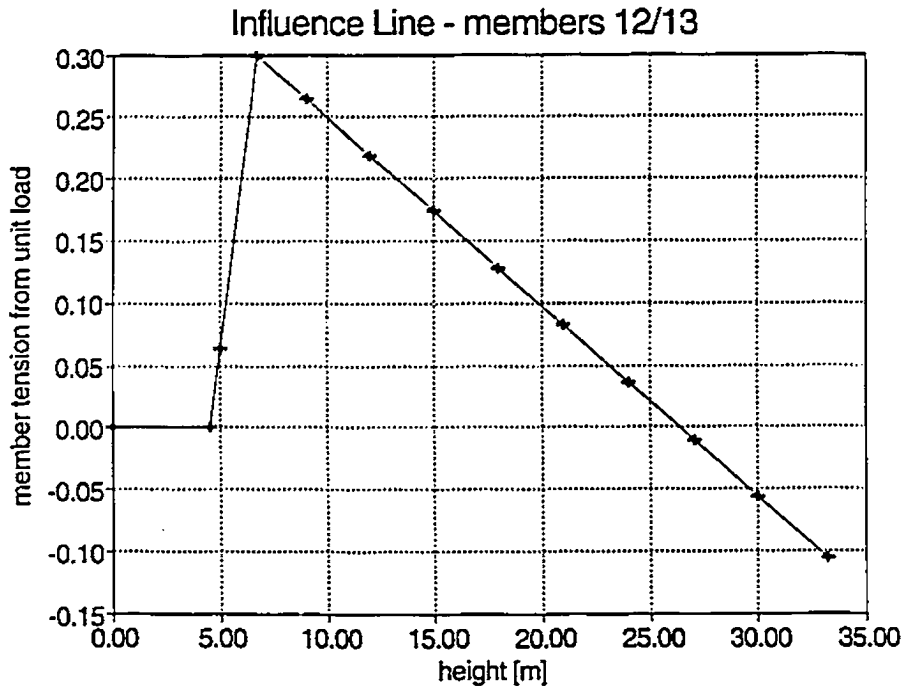

Figure 4.8 Influence line for tension in members 12/13 of tower I.

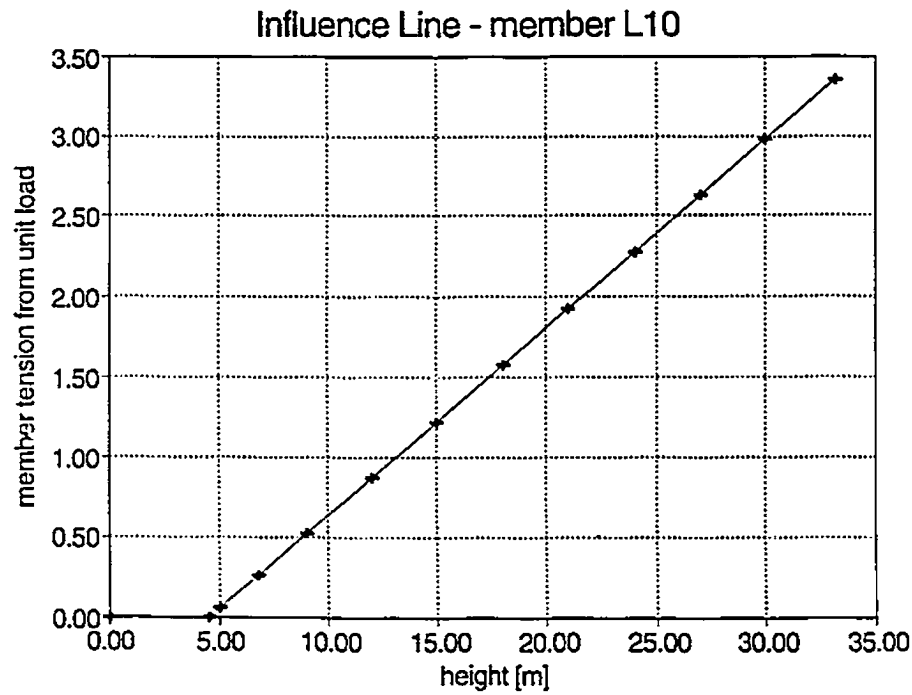

Figure 4.9 Influence line for tension in member L10 of tower I.

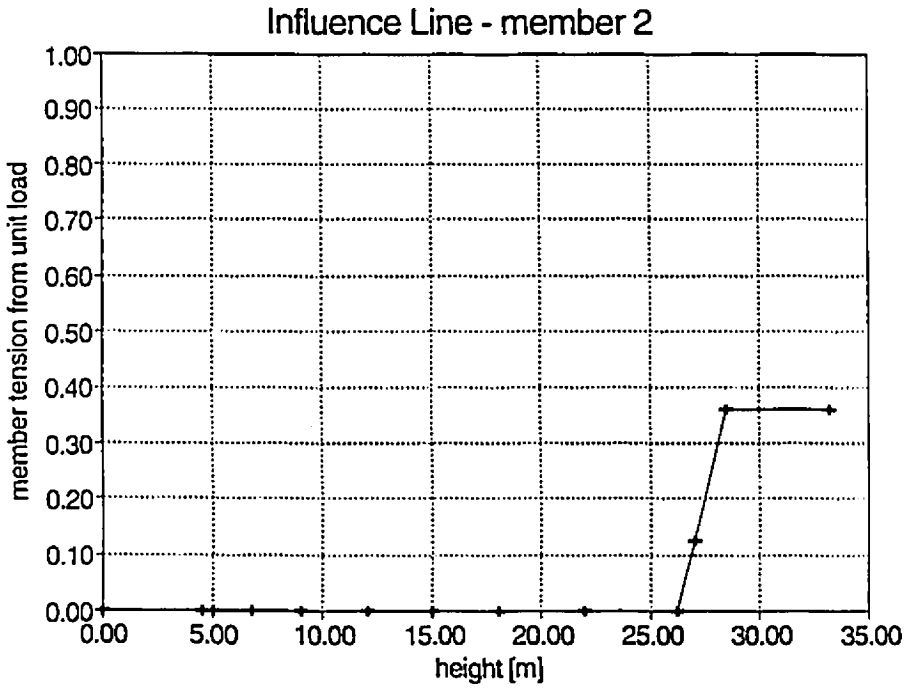

Figure 4.10 Influence line for tension in member 2 of tower I.

Table 4.3 shows the responses (tension) calculated for some members adopting the approach described in 4.2.1. In this example a structural damping ζ_s of 3% of the critical was assumed and the aerodynamic damping was considered as well. Using Eq. (4.12) the values were: $\zeta_{a1} = 0.039$ and $\zeta_{a2} = 0.013$. A statistical peak factor $g_s = 3.6$ was adopted.

Table 4.3 Forces in some members considering aerodynamic damping.

member	$\bar{r}$ [N]	$\tilde{r}_B$ [N]	$\tilde{r}_{R1}$ [N]	$\tilde{r}_{R2}$ [N]	$\tilde{r}$ [N]	$\hat{r}$ [N]	G
12/13	2484	944	9	87	948	5897	2.4
L10	46675	14719	3630	273	15162	101258	2.2
2	2154	685	285	60	744	4832	2.2

From the results given in table 4.3 it can be seen that for members 12/13, which have reversal in the forces depending on the load position, the resonant response in the second mode is bigger than the resonant response in the first mode of vibration. For the other two members the response in mode 1 was dominant. A response factor G was calculated by dividing the peak response by the mean response and is also shown in the table. These values were compared with the results given by the Gust Response Factor method presented in 4.2.2.2. The parameters adopted in the GRF method are: $\alpha = 0.16$, $H = 33.2\ m$, $V_H = 35\ m/s$, $z_{ref} = 10\ m$, $V_{10} = 28.9\ m/s$, $\kappa = 0.005$, $h_o = 22.15\ m$, $V_o = 32.8\ m/s$, $g_s = 3.6$, $L_v = 50\ m$, $f_T = 2.4\ Hz$ and $\zeta = 0.069$. The value of the gust response factor obtained was $G_t = 1.8$, which must be multiplied by the mean response to obtain the design value. It can be seen that the statistical method using influence lines gives larger (20-30%) peak responses than the GRF method.

Figure 4.11 shows the influence of the damping in the calculation of the resonant responses. The comparison is made for values of ζ ranging from 0.01 to 0.10 which are considered limit values. It can be seen that within this range the resonant responses can have their values doubled. As the correct structural damping is not easy to estimate, an allowance for the possibility of smaller values of ζ should be made since this means higher resonant loads. Although this influence sometimes may not be so big in terms of the total fluctuating component, increased resonant loads may lead to fatigue problems.

Unfortunately tower I did not have the design values due to "wind only" available. The results obtained however, instigated the necessity of going further in the analyses and work in a tower for which design values were available (from a Utility Company) and that is what is done next, for tower II.

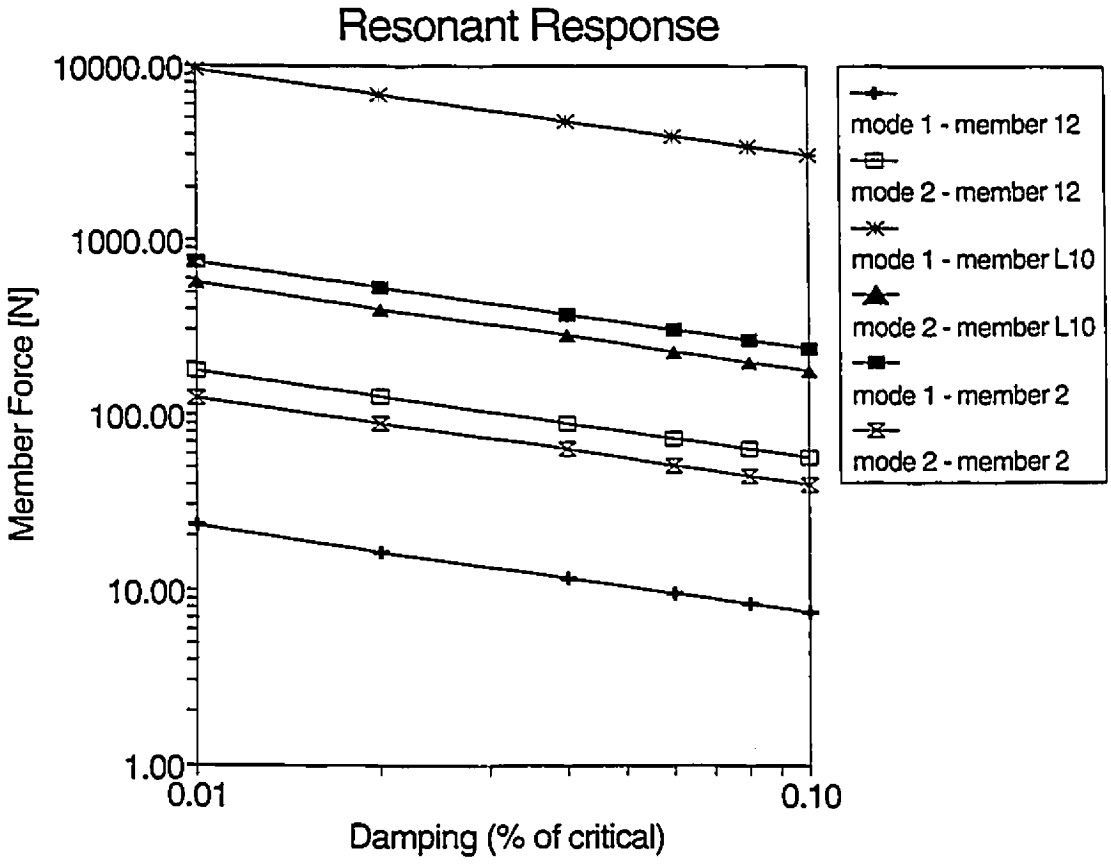

Figure 4.11 Influence of damping on the resonant responses (tension) for the first two modes of vibration of some members of tower I.

4.3.2 Tower II

This is shown in Fig. 4.12 and it is, again, an example of a suspension tower, but a slightly different configuration. The mass distribution, $m(z)$, natural frequencies and mode shapes, solidity ratio, $\phi(z)$, and drag coefficient distribution, $C_D(z)$, as well as influence lines for tension in certain members are shown in Figs. 4.13 to 4.20.

Initially the response (tension) due to wind action was calculated in member F3AT of the isolated tower. The mean, background and resonant components of the response were obtained following the formulation presented in 4.2.1.

As an example, the response in the member was calculated for two kinds of terrain (open country, $\alpha = 0.10$, and suburban exposure, $\alpha = 0.25$). An open country wind speed of 50 *m/s* at the tower's top, $H = 43.9$ *m*, was assumed, together with a corresponding velocity for the suburban exposure. The results are shown in Table 4.4 with the assumed parameters: turbulence length scale, $L_v = 50$ *m*, exponential decay factor for narrow band correlation, $C = 8$, tower damping $\zeta = 0.01$ and statistical peak factor g_s=3.6.

Table 4.4 Effect of different exposures in the response calculation.

V_H [m/s]	α	$\tilde{r}$ [N]	$\tilde{r}_B$ [N]	$\tilde{r}_{R1}$ [N]	$\tilde{r}_{R2}$ [N]	$\hat{r}$ [N]	G
35	0.25	2457	1441	108	440	7895	3.2
50	0.10	6310	1318	126	577	11510	1.8

The influence of the mean speed, $V(z)$, the power law exponent, α, the exponential decay factor for narrow band correlation, C, the vertical scale of the longitudinal component of turbulence, L_v, the mode shape and the damping ratio in the

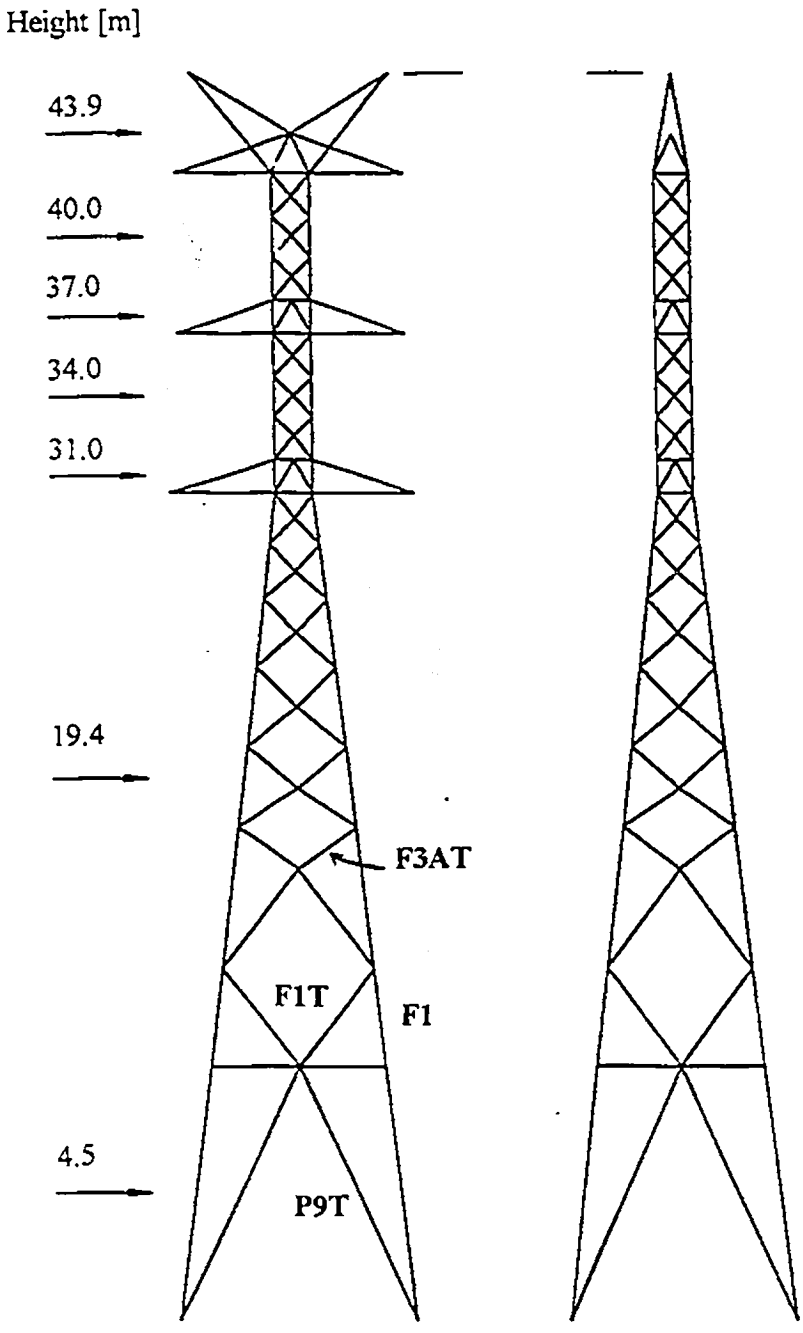

Figure 4.12 Transmission tower II .

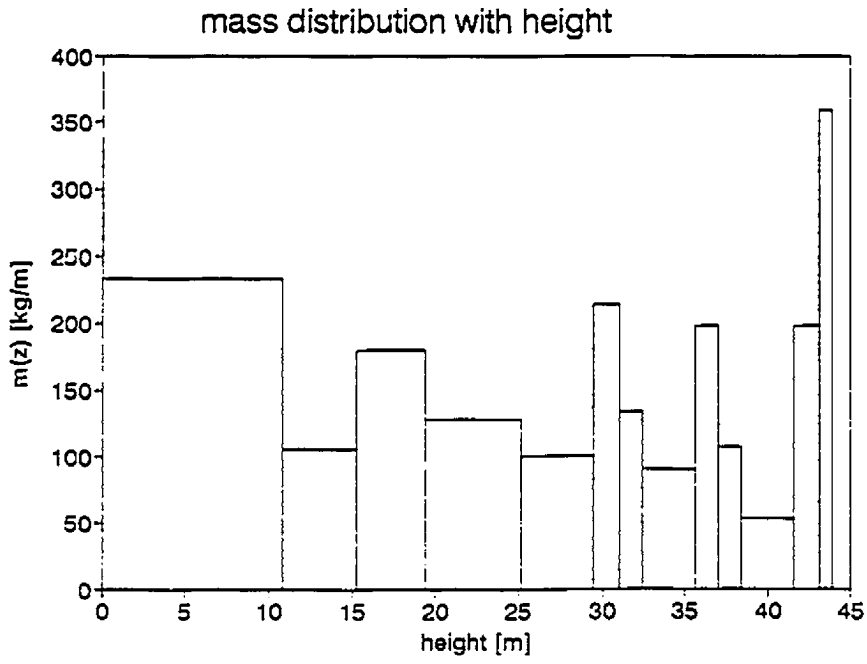

Figure 4.13 Distribution of mass with height for tower II.

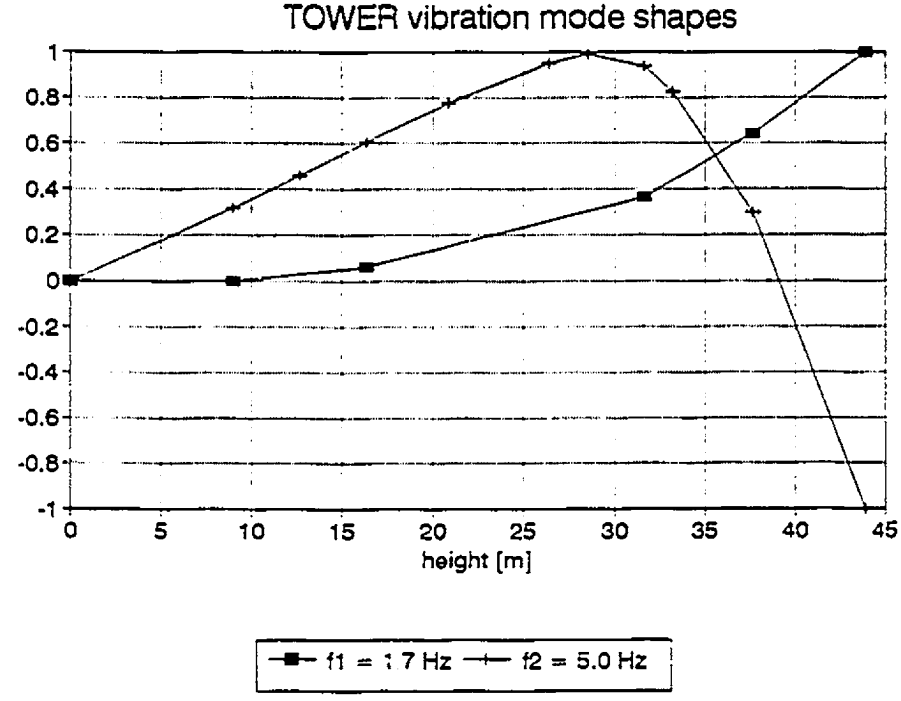

Figure 4.14 Natural frequencies and mode shapes for tower II.

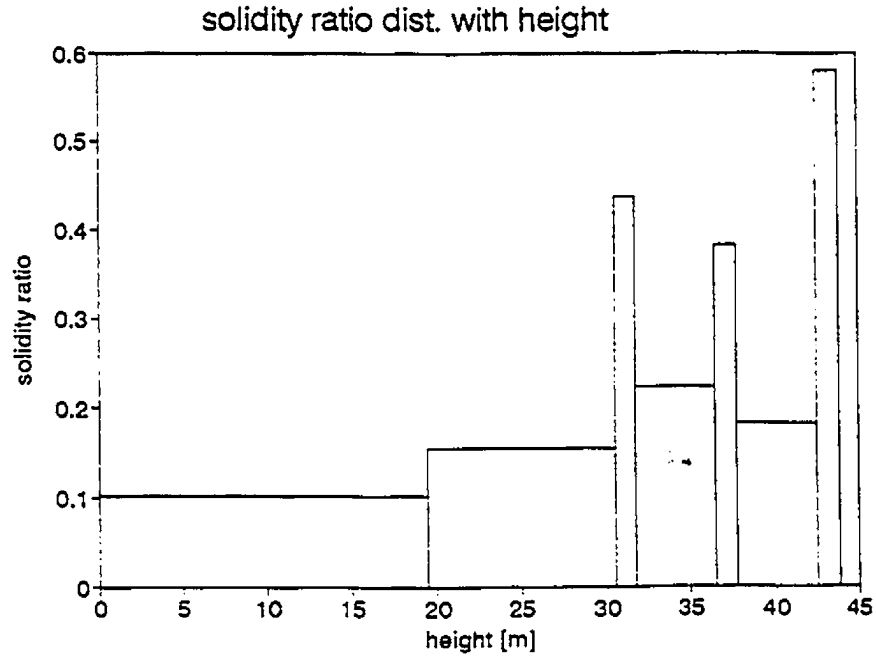

Figure 4.15 Distribution of solidity ratio with height for tower II.

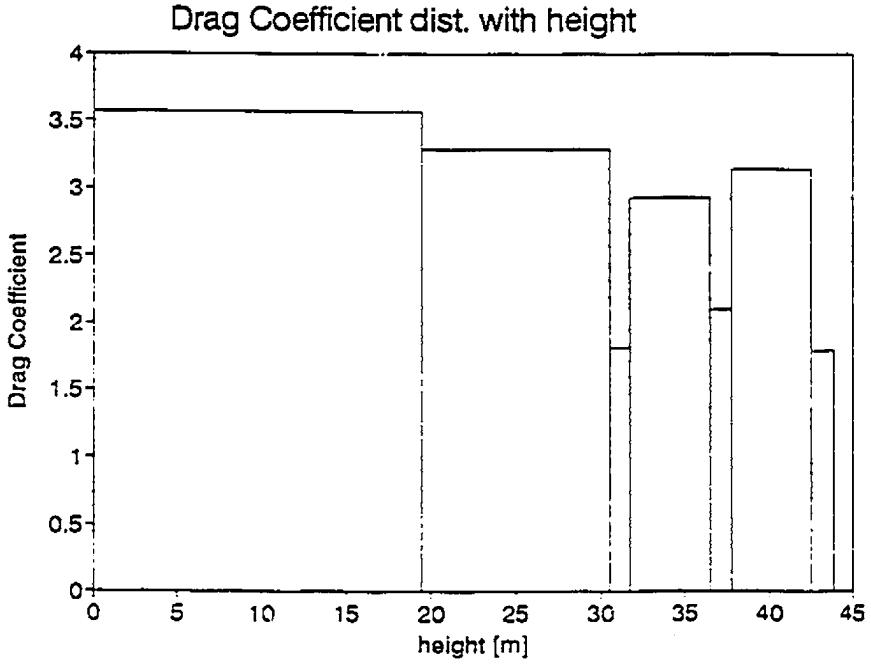

Figure 4.16 Distribution of drag coefficient with height for tower II.

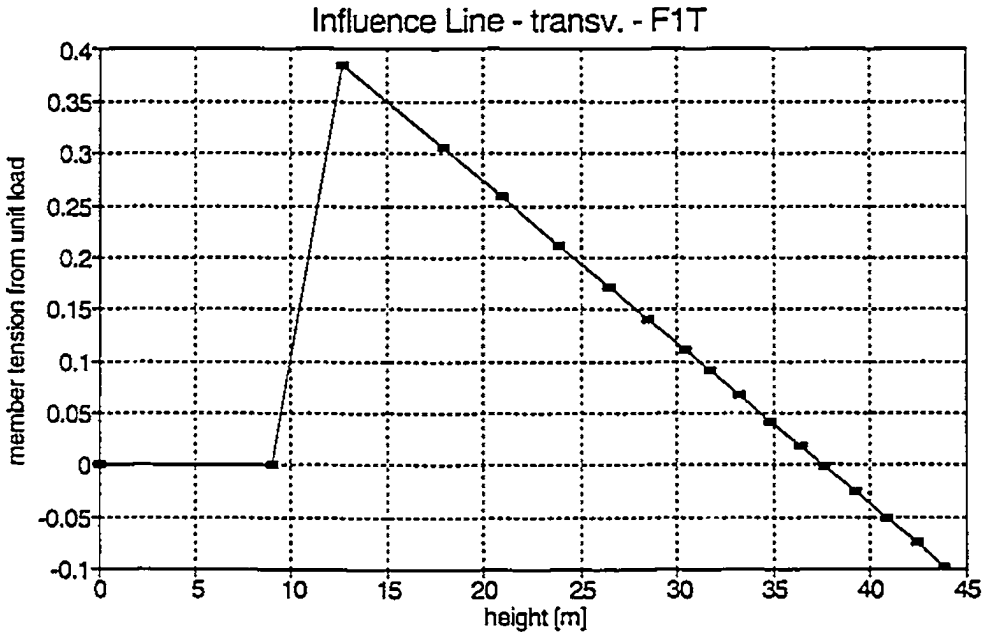

Figure 4.17 Influence line for tension in member F1T of tower II.

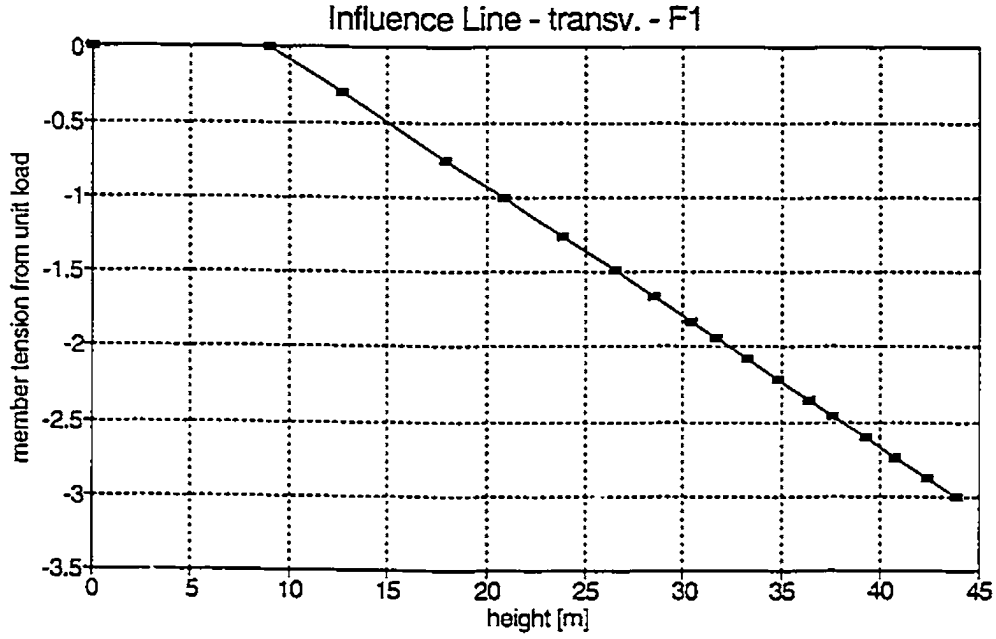

Figure 4.18 Influence line for tension in member F1 of tower II.

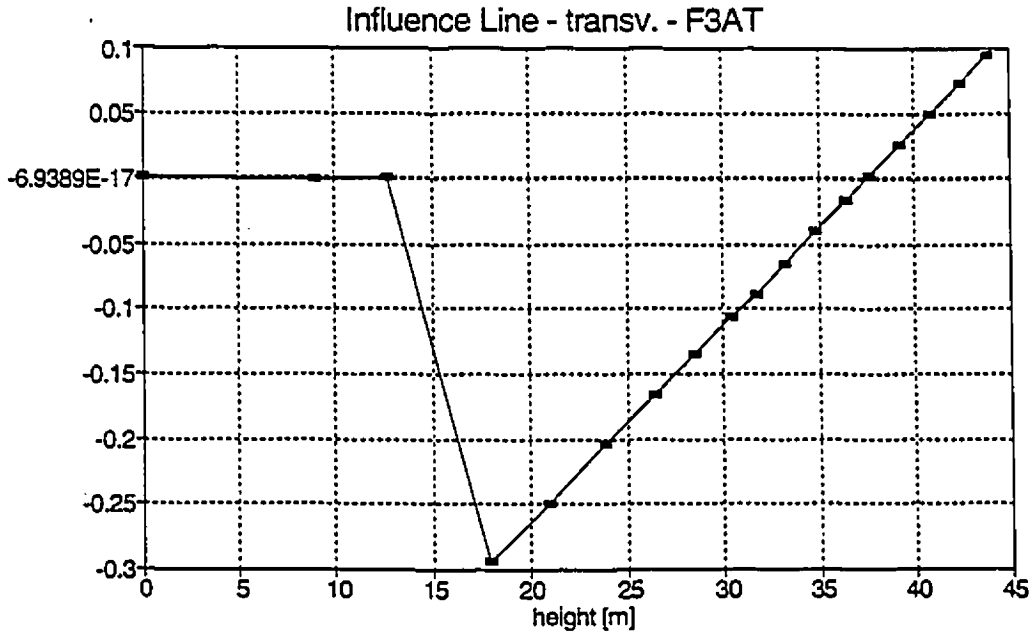

Figure 4.19 Influence line for tension in member F3AT of tower II.

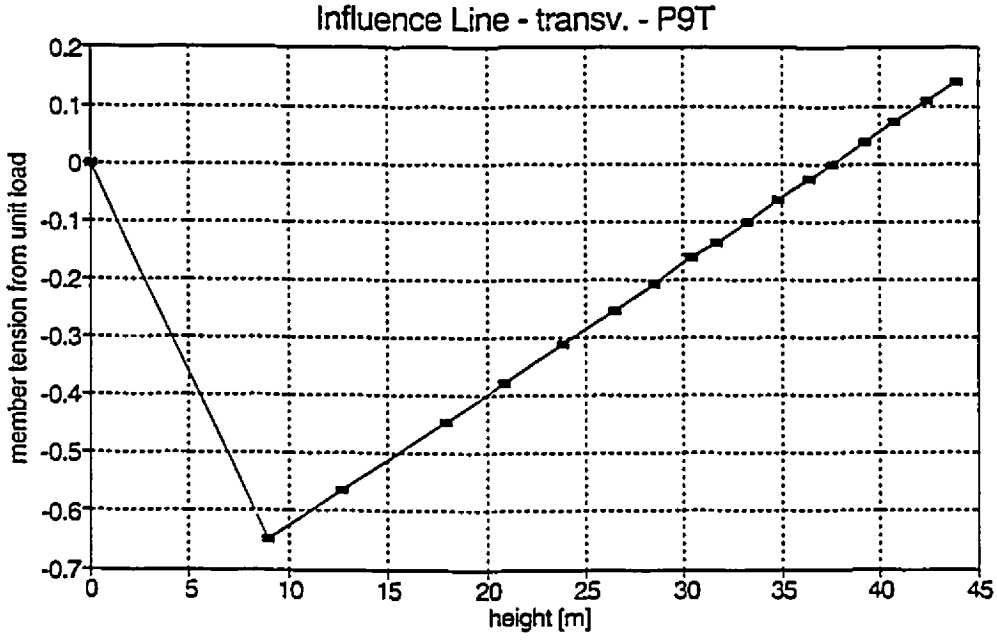

Figure 4.20 Influence line for tension in member P9T of tower II.

response was examined. Some results are given in table 4.5 (these values were determined using the same parameters as for table 4.4) and others shown in Figs. 4.21 to 4.24.

Fig. 4.21 shows the variation of the mean response with wind speed for three power law exponents. The response increases as $V(z)$ increases and α decreases, but the influence of the velocity is dominant.

Fig. 4.22 represents the variation of the background response with ${}^{c}L_{v}$ for two cases of wind speed and power law exponents. Again, the influence of the velocity is predominant but now an increase in α (and consequently an increase in the turbulence intensity I_{v}) causes an increase in the background response. A variation in L_{v} does not cause significant alteration in the response, at least in the range 30-60 m, which is the same order of magnitude as the tower's height.

Fig. 4.23 shows the variation of the root square of the spectrum of the generalized force at the natural frequency of the jth mode (SGF) with the exponential decay factor C and the mode shape, for two velocities and power law exponents. The value of SGF diminishes as C increases. It is bigger for mode 1 and increases with wind speed.

Fig. 4.24 is similar to Fig. 4.23 except that it shows the variation of the total resonant response varying with the same parameters as Fig. 4.23. Now, the combination of the influence line for member F3AT with the 2nd mode shape makes the ratio between the response participation factor and the generalized stiffness bigger than the corresponding ratio for the first mode, making the resonant response bigger in the 2nd mode. Also, an increase in the power law exponent causes an increase in the resonant

response. In reality, however, a bigger α comes together with a smaller wind speed and the smaller roughness terrain will still give the bigger response. A total damping of 0.01 was assumed and, of course, a lower value, although not likely, would increase the response.

Table 4.5 Influence of different wind speeds and exposure in the responses.

V_H [m/s]	30	30	50	50
α	0.25	0.10	0.25	0.10
$\bar{r}$ [N]	1805	2272	5015	6310
$\tilde{r}_B$ [N]	1059	474	2939	1318
$\tilde{r}_{R1}$ [N]	70	14	285	126
$\tilde{r}_{R2}$ [N]	285	137	1198	577
$\hat{r}$ [N]	5762	4049	16487	11510
G	3.2	1.8	3.3	1.8

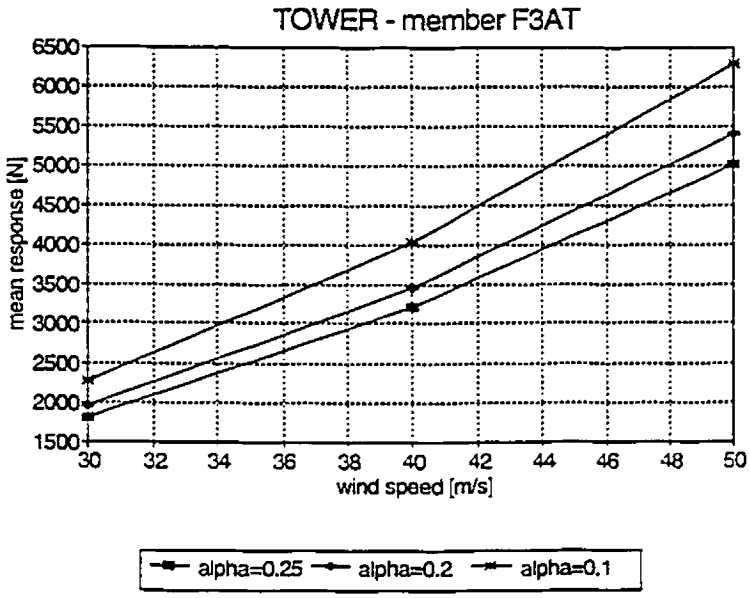

Figure 4. 21 Variation of mean response with wind speed and exposure.

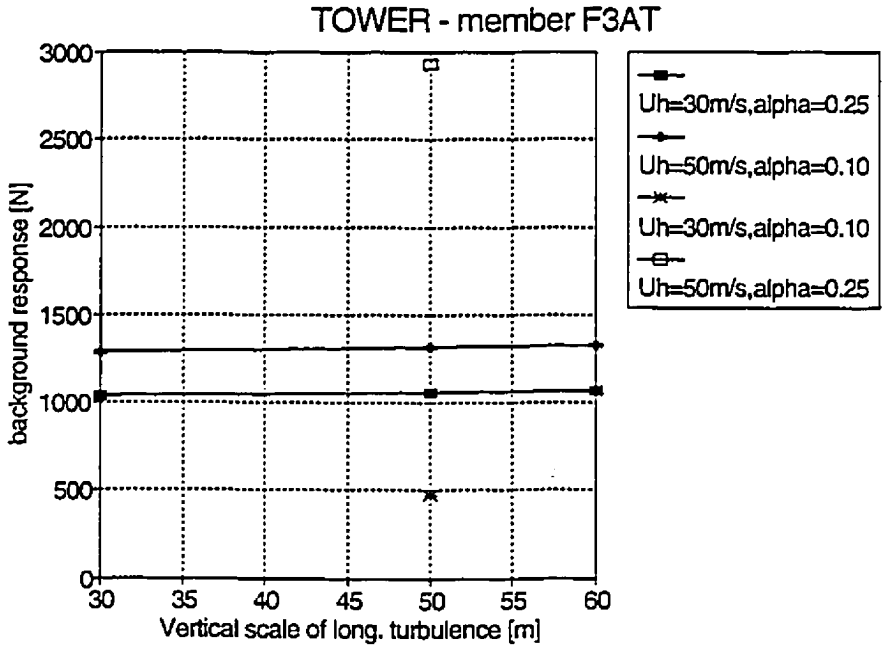

Figure 4.22 Variation of the background response with the vertical scale of longitudinal turbulence.

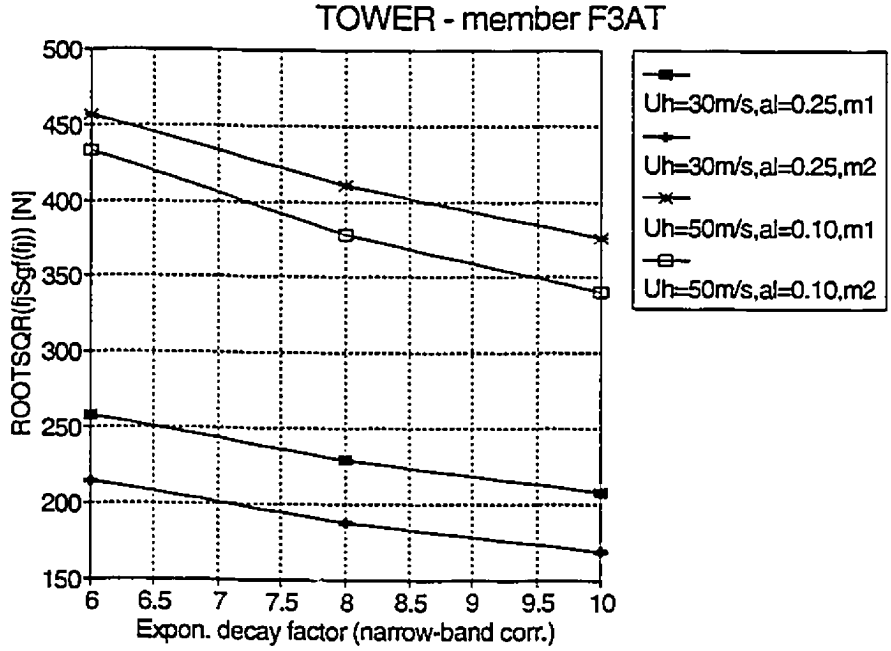

Figure 4.23 Variation of the root square of the spectrum of the generalized force with the exponential decay factor and mode shape.

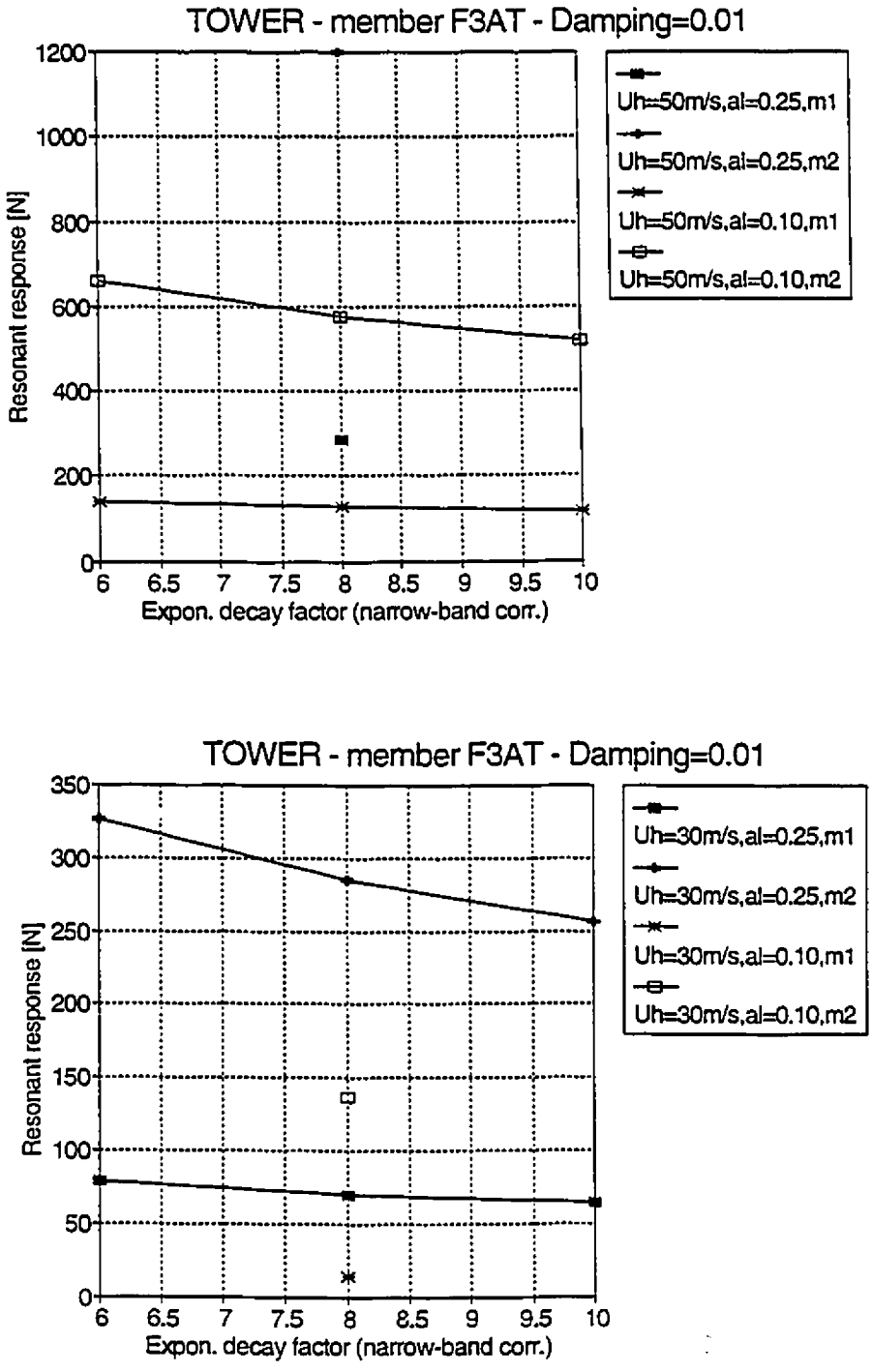

Figure 4.24 Variation of the resonant response with the exponential decay factor and mode shapes.

The method was then applied to other members and the responses calculated (tables 4.6 and 4.7). A third velocity value was included ($\overline{V}_H$= 42.4 m/s and α = 0.143) because that is the value adopted by the Utility Company from which the tower was obtained and the responses given by different methods will be compared for this value. From the analysis of these tables it can be observed that, for the members in which there is reversal in the efforts depending on the load position, the resonant response in the second mode of vibration was bigger, by four to five times, than the corresponding one in the first mode. Although this effect is not as severe in terms of resulting stresses when all the

Table 4.6 Member responses for: $L_s = 50m$, $C = 8$, $\zeta = 0.01$.

member	F1			F3AT		
V_H [m/s]	30	50	42.4	30	50	42.4
α	0.25	0.10	0.143	0.25	0.10	0.143
$\bar{r}$ [N]	27119	84073	58529	1805	6310	4248
$\tilde{r}_B$ [N]	13499	15865	16050	1059	1318	1312
$\tilde{r}_{R1}$ [N]	7606	13651	12090	70	126	112
$\tilde{r}_{R2}$ [N]	1397	2824	2413	285	577	493
$\hat{r}$ [N]	83125	160102	131387	5761	11509	9310
G	3.1	1.9	2.2	3.2	1.8	2.2
member	F1T			P9T		
V_H [m/s]	30	50	42.4	30	50	42.4
α	0.25	0.10	0.143	0.25	0.10	0.143
$\bar{r}$ [N]	2780	10176	6757	6041	24424	15725
$\tilde{r}_B$ [N]	1665	2125	2099	3836	5183	5035
$\tilde{r}_{R1}$ [N]	87	157	139	149	268	237
$\tilde{r}_{R2}$ [N]	368	743	635	698	1412	1206
$\hat{r}$ [N]	8927	18300	14668	20088	43787	34383
G	3.2	1.8	2.2	3.3	1.8	2.2

components are computed in the peak response, it can lead to fatigue problems and therefore decrease the nominal strength of the members in a shorter time than expected.

Table 4.7 Member responses for: $L_v = 50m$, $C = 8$, $\zeta = 0.02$.

member	F1			F3AT		
V_H [m/s]	30	50	42.4	30	50	42.4
α	0.25	0.10	0.143	0.25	0.10	0.143
$\bar{r}$ [N]	27119	84073	58529	1805	6310	4248
$\tilde{r}_B$ [N]	13499	15865	16050	1059	1318	1312
$\tilde{r}_{R1}$ [N]	5383	9661	8556	50	89	79
$\tilde{r}_{R2}$ [N]	989	1999	1708	202	408	349
$\hat{r}$ [N] 1st & 2nd modes	79558	151329	124294	5690	11287	9144
$\hat{r}$ [N] 1st mode only	79437	150943	124006	5622	11066	8980
G 1st & 2nd modes	2.9	1.8	2.1	3.2	1.8	2.2
G 1st mode only	2.9	1.8	2.1	3.1	1.8	2.1

member	F1T			P9T		
V_H [m/s]	30	50	42.4	30	50	42.4
α	0.25	0.10	0.143	0.25	0.10	0.143
$\bar{r}$ [N]	2780	10176	6757	6041	24424	15725
$\tilde{r}_B$ [N]	1665	2125	2099	3836	5183	5035
$\tilde{r}_{R1}$ [N]	62	111	98	105	190	168
$\tilde{r}_{R2}$ [N]	260	526	449	494	999	854
$\hat{r}$ [N] 1st & 2nd modes	8851	18067	14492	19970	43439	34120
$\hat{r}$ [N] 1st mode only	8778	17836	14322	19856	43095	33861
G 1st & 2nd modes	3.2	1.8	2.1	3.3	1.8	2.2
G 1st mode only	3.2	1.8	2.1	3.3	1.8	2.2

Table 4.8 presents response values (force on members) calculated from different methodologies. The design values (due to wind only) used by the Utility Company are compared with the Gust Response Factor method and the statistical method using influence lines (SIL). The parameters adopted in the GRF method are: $\alpha = 0.143$, H = 43.9 *m*, $V_H = 42.4$ *m/s*, $z_{ref} = 10$ *m*, $V_{10} = 34.3$ *m/s*, $\kappa = 0.004$, $h_o = 29.3$ *m*, $V_o = 40$ *m/s*, $g_s = 3.6$, $L_v = 50$ *m*, $f_T = 1.7$ *Hz* and $\zeta = 0.02$. The value of the gust response factor obtained was $G_t = 1.8$, which was multiplied by the mean response to obtain the design value. The Utility method does not consider any dynamic effects in its procedure.

From the analysis of the table it can be seen that the SIL gave always higher response values than the GRF method and also the Utility method. The results show that there can be an increase of more than 30% in the members' stresses by using SIL, in relation to the usual procedure. For the ratio SIL/GRF the difference was up to 20%. This figure can vary a great deal according to the properties and characteristics assumed for the wind and structure.

Table 4.8 Forces [*N*] on members obtained from different methodologies.

member	Utility method	GRF method $\zeta = 0.02$	statistical method using infl. lines		
			$\zeta = 0.01$ 1st & 2nd modes	$\zeta = 0.02$ 1st & 2nd modes	$\zeta = 0.02$ 1st mode only
F1T	12635	12163	14668	14492	14322
F3AT	6955	7646	9310	9144	8980
F1	109960	105352	131387	124294	124006
P9T	33070	28305	34383	34120	33861

4.4 FORCES ON THE TOWER-CABLES SYSTEM

When there are a number of conductors supported by a tower, it is usual to consider the maximum load exerted by each conductor and to apply it simultaneously at the appropriate points (Armitt et al., 1975). These loads are combined with the maximum insulator and tower loadings. For certain tower members, however, this practice can in fact constitute a reduction of its wind load. Lets take as an example the two towers studied earlier in this Chapter (Fig. 4.25).

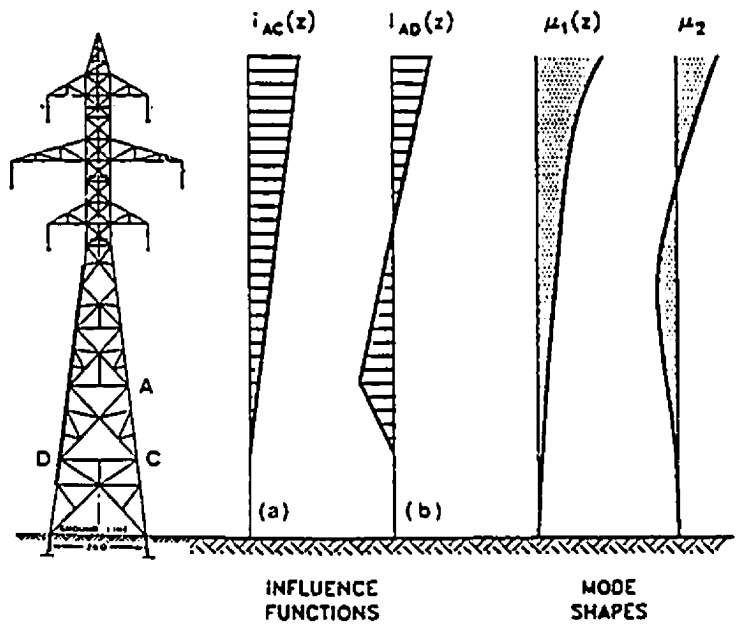

Figure 4.25 Influence lines for tension in tower members.

If we do not consider the loading due to the upper cable, the force on member (b) will be bigger than if we consider it. Regarding the middle cable, if the legs intercept

exactly at the height of the insulators' supports, no forces will be transmitted to member (b), but certainly will for member (a).

This measure could be regarded as too conservative. A good compromise would be to consider the correlation of loads existing among cables at different heights. This is not done in this work but is considered worth pursuing and a good tool for this study is the experimental approach described in Chapter 3.

The efforts in the tower members due to wind on cables can be obtained by employing a method as described in Chapter 2 and using influence coefficients from the influence lines of each member corresponding to the cables' heights. Those are then added to the efforts due to wind on the tower and the total wind effect determined.

As an example, table 4.9 presents the forces in some members of tower II due to wind on cables only. For this the wind velocity adopted was $V_H = 42.4$ *m/s* at $H = 43.9$ *m*, $\alpha = 0.143$, ${}^{x}L_v = 30$ *m*, $g_s = 3.6$. The cables were assumed to have a length $l = 400$ *m* and diameters of 0.04 *m* (conductors) and 0.01 *m* (ground-wires). Only the mean and background responses were calculated, following what was observed in Chapter 3.

Table 4.9 Forces in some members of tower II due to wind on cables only.

member	$\bar{r}$ [N]	$\tilde{r}_B$ [N]	$\hat{r}$ [N]	G
F1T	515	164	1105	2.15
F1	136752	43624	293798	2.15
P9T	614	196	1320	2.15
F3AT	526	168	1131	2.15

For the members in which there is reversal of forces according to the load position (Fig. 4.25b), the resultant cable loads are not too big. The contrary is true for the other members (Fig. 4.25a). A comparison with the values obtained from wind on the tower only can be seen in table 4.10. The loads on the tower dominate for members such as those in Fig. 4.25b. Loads on cables had the biggest share in the other case.

Table 4.10 Comparison of wind loads in members of tower II from cables and tower.

member	$\hat{F}$ [N] (cable)	$\hat{F}$ [N] (tower)	$\hat{F}$ [N] (total)	% cable	% tower
F1T	1105	14492	15597	7	93
F1	293798	124294	418092	70	30
P9T	1320	34120	35440	4	96
F3AT	1131	9144	10275	11	89

As a final observation, it should be mentioned:

Stress calculations in a transmission tower structure are generally based on a linear elastic analysis, normally assuming that members are axially loaded and pin-connected, with the stiffer main leg members considered as a continuous beam. Forces or stresses in the members are usually determined using a computer-aided method of analysis. There has been, however, some indication (EPRI, 1986 and Al-Bermani et al, 1992) that the linear elastic truss analysis method for transmission towers should be used with caution and that a more refined technique, meaning a non-linear analytical technique, would be preferable.

CHAPTER 5

SUMMARY AND CONCLUSIONS

5.1 OVERVIEW OF STUDY

The behaviour of transmission lines under severe boundary layer winds was examined. In this context, the thesis subject concerned two main topics:

Firstly, the examination of the effect of scale of turbulence on the response of a line-like structure (cable model) through wind tunnel tests and the comparison of experimental results with theoretical predictions made through the statistical method using influence lines. Consistency with theory allowed the development of a new modelling approach to conductor systems using a distorted horizontal length scale (span wise) to accommodate these systems in the wind tunnel. Transverse and oblique wind incidences were tested. Cables with different characteristics were simulated and correlations between drag forces at the cables' supports were obtained.

Secondly, from a theoretical approach, the design procedure for the establishment of wind loading on transmission towers was reviewed and current procedures, such as Davenport's Gust Response Factor, were compared with the statistical method using influence lines, which is considered more realistic. This latter approach can account for unbalanced loading effects, shear and axial loads and the effects of higher modes of vibration in the calculation of the response factors.

5.2 SUMMARY OF SIGNIFICANT RESULTS

From the results obtained in the experimental work, it is apparent that the new modelling approach to conductor systems in wind tunnels is a valid technique. It is necessary, however, that a correction be made in the values of the variance measured in the distorted model. Specifically, the findings were:

- Mean values measured from normal and distorted models agree fairly well among themselves and with those predicted from theory.

- The variance of the response measured from the distorted model was roughly double its corresponding value in the normal model. The horizontal distortion of the cable was $\gamma = 50\%$. In agreement with theory, the variance obtained from distorted models should be multiplied by γ, the horizontal geometric distortion of the cable model, to obtain the real values of the variance of the response.

- From the resulting spectra of the first models (low mass per unit length) it can be seen that, at the model design velocities, the response is all background. The theoretical predictions in this case overestimated a little bit the fluctuating response; but, due to the fact that there are uncertainties in the determination of the turbulence length scale, it can be said that the statistical method using influence lines is a good tool in the theoretical prediction of the cable responses.

- From the results of the other models (higher mass per unit length) it can be seen that the response has both components: background and resonant, for the design velocities. Comparison with theory was made and in this case the consideration of the resonant response of the first mode of vibration together with the background response were necessary to make the total predicted rms response match the measurements. Again, the same observation is valid: the theoretical method is a valid tool in the prediction.

- The results obtained demonstrate the effect of turbulence in the dynamic response. Theory says that the variance is directly proportional to the ratio between turbulence length scale and the structure's span, and that is exactly what is demonstrated in these experiments by modifying the structure and leaving the wind characteristics unchanged.

- Results obtained from the more massive cables demonstrated that the resonant response can be important in the total response. It depends on the characteristics of the structure and of the wind flow.

- Aerodynamic damping plays an important role in the dynamic behaviour of the cables. This was demonstrated in the experimental results obtained for the lines with different characteristics studied and also in full-scale experiments made by other researchers.

- The correlation coefficients of the drag force reactions at the two cables were found to be almost invariant with wind velocity and bigger for the smallest separation between cables. The values were slightly smaller for the more turbulent wind. The coherence between the forces was also found to be smaller for the larger separation between cables and to decrease with wind velocity.

- The model cables were always successful in qualitatively reproducing full-scale behaviour of transmission lines. Quantitative comparison was not possible for lack of similar data.

Several responses due to certain assumed transverse wind characteristics were calculated for some typical transmission towers. The statistical method using influence lines (SIL) was compared with the Gust Response Factor method (GRF) and with values given by Utility Companies (using other methodologies) when available. The main findings were:

- Peak loads calculated using SIL were larger than peak loads given by the GRF. The difference was around 20% to 30%. They were also larger than the values calculated by the Utility Company by up to around 30%.

- The dynamic response of transmission structures is strongly dependent on the turbulence intensity level and its spectrum. The assumed values of the vertical turbulence length scale, however, will not cause significant alteration in the response as long as they are of the same order of magnitude (or higher) than the tower's height.

- For members in which there is reversal in the forces depending on the load position, the resonant response in the second mode of vibration was bigger, even by four to five times, than the corresponding one in the first mode. Although this effect is not as severe in terms of resulting stresses when all the components are computed in the peak responses, it can lead to fatigue problems and therefore decrease the nominal strength of the members in a shorter time than expected.

- From the current results it can be concluded that the incorporation of the dynamic properties of transmission structures in the design methodologies is needed and that the statistical method using influence lines is a more correct approach since it allows for the inclusion of a larger number of factors in the design methodology.

5.3 RECOMMENDATIONS FOR FUTURE RESEARCH

Information regarding correlation among cable forces located at different heights (vertical separation), further horizontal separations and different types of terrain, as well as displacement of cables to verify if they can touch each other, are very important. The experimental technique developed can assist, in combination with the theoretical approach, in answering those questions.

The modelling can also be extended to several spans, located side by side, and to a possible joint modelling of cables and tower structure. In such case it must be remembered that velocity scaling laws for cables and towers are different: Froude number for cables and Cauchy number for towers.

It is very important for design procedures to try to establish boundary situations in which the consideration of the resonant response in the calculation is necessary, and how many modes of vibration should be considered. This is also possible to be done through the experimental technique developed.

For the towers, it would be interesting, although very difficult, to try to identify the exact tower members that have failed in wind related accidents and make a detailed investigation to see if the statistical method using influence lines can predict any extra load not taken into account in the design, and this can include the problem of fatigue. Further investigation in non-linear analysis of the towers and a possible inclusion of that in the theoretical method would also be useful.

APPENDIX A

STATIC AND DYNAMIC BEHAVIOUR OF A SINGLE CABLE UNDER UNIFORMLY DISTRIBUTED LOAD

A.1 - STATIC BEHAVIOUR (from Zetlin and Lew, 1979)

The cable will assume a parabolic configuration under uniform load (Fig. A.1), so the initial curve is assumed to be a parabola.

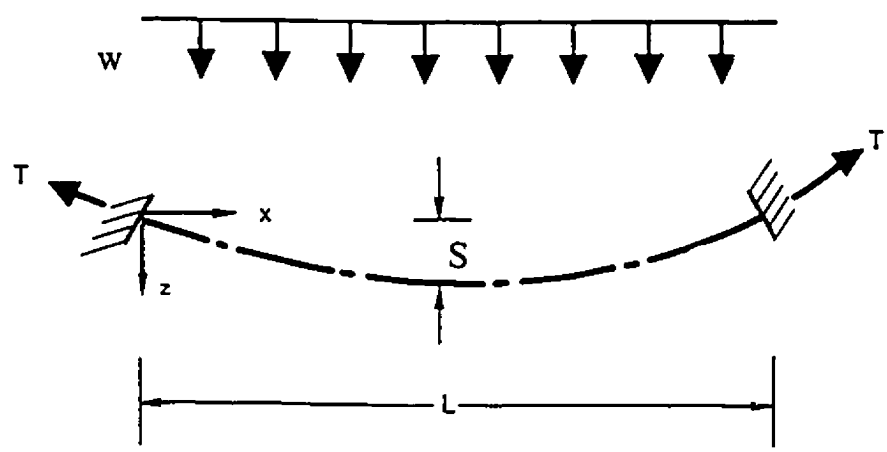

Figure A.1 Cable hanging in a shallow parabola.

The problem is to find:

a) the deflected configuration;

b) the force in the cable;

c) the forces on the supports.

It is assumed that the uniformly distributed load acts vertically and that the supports at each end of the cable are on the same horizontal line.

The initial length l of the cable can be expressed accurately enough for design purposes by:

$$l = L\left[1 + \frac{8}{3}\left(\frac{S}{L}\right)^2\right] \tag{A.1}$$

The tension T is given by:

$$T = \frac{wL^2}{8S}\sqrt{1 + 16\left(\frac{S}{L}\right)^2} \tag{A.2}$$

The approximate elastic elongation of the cable is:

$$\Delta l = \frac{T l}{E A_c} \tag{A.3}$$

The increase in sag is:

$$\Delta S = \frac{\Delta l}{(16/15)(S/L)\left[5 - 24(S/l)^2\right]} \tag{A.4}$$

The angle β is given by:

$$\tan\beta = \frac{4(S + \Delta S)}{L} \tag{A.5}$$

The vertical and horizontal reactions are:

$$U = T\sin\beta$$
$$H_t = T\cos\beta \qquad \text{(A.6)}$$

A.2 - DYNAMIC BEHAVIOUR : The Linear Theory of Free Vibrations of a Suspended Cable.

This part is mainly based on the works of Blevins(1979), Irvine (1981) and Simpson (1965). It assumes small sag to span ratios (<1/8).

If the cable is given a small arbitrary displacement from static equilibrium, the resulting vibrations will have three components (Fig. A.2): (1) horizontal motion in the plane of the catenary, X(x,t); (2) vertical motion in the plane of the catenary, Z(x,t); and (3) transverse motion out of the plane of the catenary, Y(x,t). The spatial form of the free vibrations associated with each of these components is given by the mode shapes $\bar{x}(x)$, $\bar{z}(x)$and $\bar{y}(x)$, respectively.

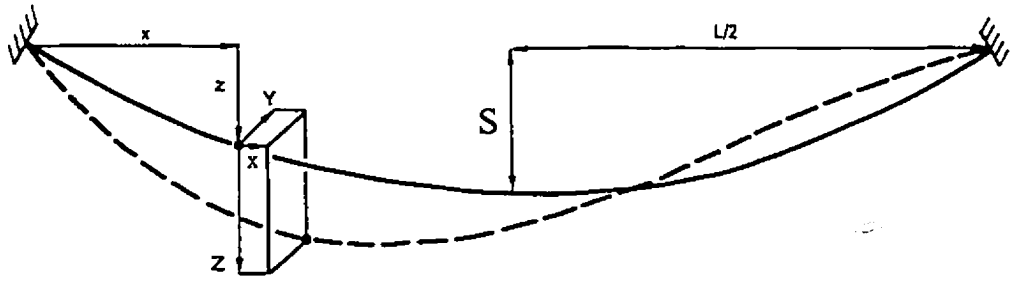

Figure A.2 Definition diagram for cable dynamic deflections X, Y and Z.

In our case $\tilde{x}(x)$ has no practical importance and only the other two will be given. The natural frequencies (all frequencies given in Hertz) and normalised mode shapes are then:

a) Out-of-plane (pendulum) mode:

$$f_{oj} = \frac{j}{2L}\sqrt{\frac{T}{m}} \tag{A.7}$$

$$\tilde{y}_j(x) = (\mu_j(x)) = \sin\left(j\frac{\pi x}{L}\right) \tag{A.8}$$

where j=1,2,3,... signify the first, second, third modes, respectively, and so on. The frequency of the first out-of-plane mode is the first of any given flat-sag suspended cable.

b) In-plane (vertical) motion:

It is now necessary to separate the in-plane modes in *antisymmetric* and *symmetric*. The form of typical symmetric and antisymmetric in-plane modes of sagging cables is shown in Fig. A.3.

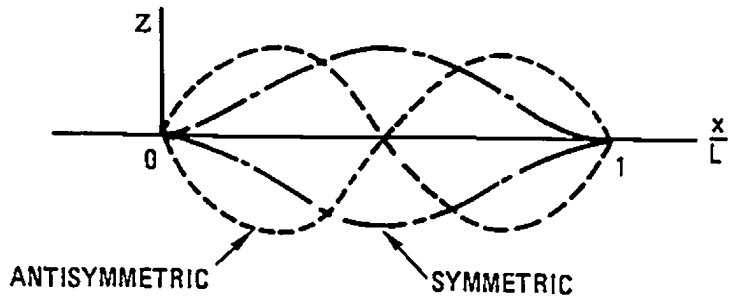

Figure A.3 First symmetric and antisymmetric in-plane cable modes.

In the case of *antisymmetric* in-plane modes:

$$f_{oj} = \frac{j}{L}\sqrt{\frac{T}{m}} \tag{A.9}$$

$$\bar{z}_j(x) = (\mu_j(x)) = \sin\left(2j\frac{\pi x}{L}\right) \tag{A.10}$$

Again j=1,2,3...but now signify the first, second, and so on *antisymmetric* modes.

For an elastic catenary with spring-restrained ends, the effects of cable elasticity are confined to the in-plane symmetric modes of oscillation. In this case, additional tension is induced and is substantially constant with the span. The natural frequencies and mode shapes of the *symmetric* in-plane modes are given by:

$$f_{oj} = \frac{\varepsilon_j}{2L}\sqrt{\frac{T}{m}} \tag{A.11}$$

$$\bar{z}_j(x) = (\mu_j(x)) = 1 - \tan\left(\frac{\pi\varepsilon_j}{2}\right)\sin\left(\frac{\pi\varepsilon_j x}{L}\right) - \cos\left(\frac{\pi\varepsilon_j x}{L}\right) \tag{A.12}$$

where j=1,2,3,... represent the first, second,.... *symmetric* modes. The nondimensional frequency parameter ε_j may be found from the positive nonzero roots of the following transcendental equation:

$$\tan\left(\frac{\pi\varepsilon}{2}\right) = \left(\frac{\pi\varepsilon}{2}\right) - \frac{4}{\lambda^2}\left(\frac{\pi\varepsilon}{2}\right)^3 \tag{A.13}$$

where $\lambda^2 = (mgL/H)^2 L / (Hl/EA)$, being L is the span length, H the horizontal component of cable tension, m the mass per unit length, l the cable length, E the modulus of elasticity and A the cable cross-sectional area. Equation (A.13) is of fundamental importance in the theory of cable vibrations and its solution is expressed graphically in Fig. A.4 for a certain range of values for the parameter λ^2. Table A.1 gives the frequencies of the first eight symmetric in-plane modes for a wide range of values of the parameter involving cable elasticity and geometry.

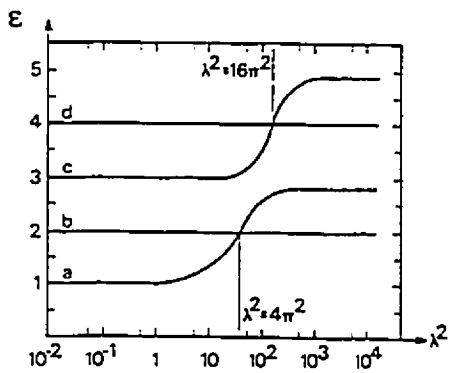

Figure A.4 General dimensionless curves for the first four natural frequencies of a flat-sag suspended cable: (a) first symmetric in-plane mode, (b) first antisymmetric in-plane mode, (c) second symmetric in-plane mode, (d) second antisymmetric in-plane mode.

As a general rule it can be said that if λ^2 is much greater than $256\pi^2$,

$$\varepsilon_1 = 2.861$$

$$\varepsilon_2 = 4.9181$$

$$\varepsilon_3 = 6.9418$$

$$\varepsilon_j = 2j + 1 \qquad ; \qquad j = 4, 5, 6, \ldots$$

and if λ^2 is much less than 1.0,

$\varepsilon_j = 2j - 1 \qquad ; \qquad j = 1, 2, 3, \ldots$

In the case of the first modes three important ranges may be established:

1. If $\lambda^2 < 4\pi^2$, the frequency of the first symmetric mode is less than the frequency of the first antisymmetric mode. If $\lambda^2 \cong 0$, then the natural frequencies and mode shapes approach those for a straight cable. The vertical component of the first symmetric mode has no internal nodes (Fig. A.5a).

2. If $\lambda^2 = 4\pi^2$, the first symmetric and first antisymmetric in-plane modes have the same natural frequencies and the vertical modal component is tangential to the profile at the supports (Fig. A.5b). This value of λ^2 gives the first modal crossover.

3. If $\lambda^2 > 4\pi^2$, the natural frequency of the first symmetric in-plane mode is now greater than the natural frequency of the first antisymmetric in-plane mode and two internal nodes appear (Fig. A.5c).

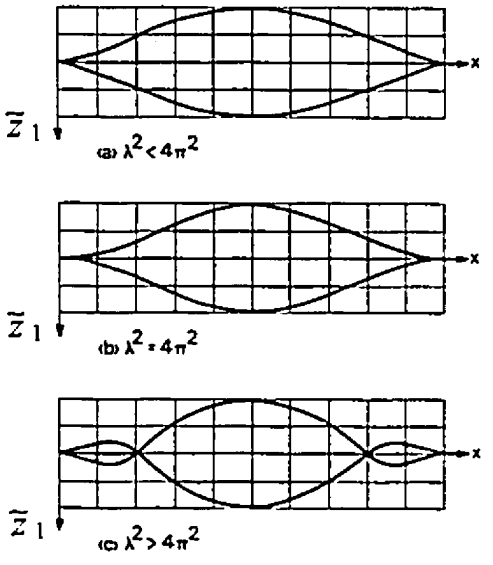

Figure A.5 Possible forms for the vertical component of the first symmetric in-plane mode.

An undesirable property of shallow catenaries is that the lateral and in-plane antisymmetric normal modes occur in corresponding pairs and have nearly equal natural frequencies (in the extreme case of a stretched string, corresponding lateral and in-plane modes have equal frequencies). Add to this the fact that in some cases there is also the possibility of coupling (or "tripling") with one of the symmetrical in-plane modes. There is no simple means of detuning these modes except to increase the sag to span ratio of the catenary, which is not always possible.

Table A.1 Natural frequencies of the first eight symmetric in-plane modes as a function of λ^2:

λ^2	ε_1	ε_2	ε_3	ε_4	ε_5	ε_6	ε_7	ε_8
∞	2.86	4.92	6.94	8.95	10.96	12.97	14.97	16.98
$256\pi^2$	2.86	4.91	6.93	8.93	10.93	12.91	14.81	16.00*
$196\pi^2$	2.85	4.91	6.92	8.92	10.91	12.81	14.00*	15.15
$144\pi^2$	2.85	4.90	6.91	8.90	10.81	12.00*	13.15	15.05
$100\pi^2$	2.85	4.89	6.89	8.80	10.00*	11.15	13.04	15.02
$64\pi^2$	2.84	4.87	6.79	8.00*	9.14	11.04	13.02	15.01
$36\pi^2$	2.82	4.78	6.00*	7.14	9.04	11.02	13.01	15.01
$16\pi^2$	2.74	4.00*	5.12	7.03	9.01	11.01	13.00	15.00
100	2.60	3.48	5.05	7.01	9.01	---	---	---
80	2.48	3.31	5.04	7.01	9.01	---	---	---
60	2.29	3.18	5.03	7.01	---	---	---	---
$4\pi^2$	2.00*	3.09	5.02	7.01	---	---	---	---
20	1.61	3.04	5.01	7.00	---	---	---	---
10	1.35	3.02	5.00	---	---	---	---	---
8	1.28	3.01	---	---	---	---	---	---
6	1.22	---	---	---	---	---	---	---
4	1.15	---	---	---	---	---	---	---
2	1.08	---	---	---	---	---	---	---
1	1.04	---	---	---	---	---	---	---
0	1.00*	3.00*	5.00*	7.00*	9.00*	11.00*	13.00*	15.00*

APPENDIX B

ESTIMATED NATURAL FREQUENCIES OF CABLES

In this appendix the estimated natural frequencies [*Hz*] for the cables tested and corresponding full-scale values are given. They were calculated using the methodology indicated an Appendix A and, therefore, consider the effects of cable elasticity in the symmetric in-plane modes. The frequencies were calculated by considering two situations: (a) a "no wind" condition, or tension due to the cables' own weight, and (b) resultant cable tension obtained by assuming a wind load corresponding to the mean wind speed used for test. Situation (a) is expected to serve as a lower limit, below which the frequencies are not expected to be.

Table B.1a Estimated natural frequencies for cables 1 & 2 and full-scale for a "no wind" condition.

	full-scale				cable 1			cable 2		
		in-plane								
mode	out of plane	antisym	symmetric E [Pa] 7E10	symmetric E [Pa] 2E11	out of plane	in-plane antisym	in-plane symm	out of plane	in-plane antisym	in-plane symm
1	0.2	0.41	0.58	0.58	1.44	2.89	4.13	1.48	2.97	4.24
2	0.41	0.82	1	1	2.89	5.77	7.1	2.97	5.93	7.3
3	0.61	1.23	1.41	1.42	4.33	8.66	10.02	4.45	8.9	10.3
4	0.82	1.63	1.82	1.83	5.77	11.55	12.92	5.93	11.87	13.28
5	1.02	2.04	2.23	2.24	7.22	14.44	15.82	7.42	14.84	16.26
6	1.23	2.45	2.62	2.65	8.66	17.32	18.72	8.9	17.8	19.24
7	1.43	2.86	2.86	3.06	10.11	20.21	21.61	10.39	20.77	22.21
8	1.63	3.27	3.09	3.47	11.55	23.1	24.51	11.87	23.74	25.19
9	1.84	3.68			12.99	25.99		13.35	26.71	
10	2.04				14.44			14.84		
11	2.25				15.88			16.32		
12	2.45				17.32			17.8		
13	2.65				18.77			19.29		
14	2.86				20.21			20.77		
15	3.06				21.66			22.25		
16	3.27				23.1			23.74		
17	3.47				24.54			25.22		
18	3.68				25.99			26.71		

Table B.1b Estimated natural frequencies of cables 1 & 2 and full-scale for a wind speed of 45 m/s (6.4 m/s model).

	full-scale				cable 1			cable 2		
		in-plane								
mode	out of plane	antisym	symmetric E [Pa] 7E10	symmetric E [Pa] 2E11	out of plane	in-plane antisym	in-plane symm	out of plane	in-plane antisym	in-plane symm
1	0.2	0.41	0.58	0.58	1.44	2.89	4.13	1.48	2.97	4.24
2	0.41	0.82	1	1	2.89	5.77	7.1	2.97	5.93	7.3
3	0.61	1.23	1.41	1.42	4.33	8.66	10.02	4.45	8.9	10.3
4	0.82	1.63	1.82	1.83	5.77	11.55	12.92	5.93	11.87	13.28
5	1.02	2.04	2.23	2.24	7.22	14.44	15.82	7.42	14.84	16.26
6	1.23	2.45	2.62	2.65	8.66	17.32	18.72	8.9	17.8	19.24
7	1.43	2.86	2.86	3.06	10.11	20.21	21.61	10.39	20.77	22.21
8	1.63	3.27	3.09	3.47	11.55	23.1	24.51	11.87	23.74	25.19
9	1.84	3.68			12.99	25.99		13.35	26.71	
10	2.04				14.44			14.84		
11	2.25				15.88			16.32		
12	2.45				17.32			17.8		
13	2.65				18.77			19.29		
14	2.86				20.21			20.77		
15	3.06				21.66			22.25		
16	3.27				23.1			23.74		
17	3.47				24.54			25.22		
18	3.68				25.99			26.71		

Table B.2a Estimated natural frequencies of cables 3 & 4 (sag=0.2m) and full-scale for a 'no wind' condition.

	----> full-scale				---------->cable 3			------>cable 4		
		in-plane								
mode	out of plane	antisym	symmetric E [Pa] 7E10	symmetric E [Pa] 2E11	out of plane	in-plane antisym	in-plane symm	out of plane	in-plane antisym	in-plane symm
1	0.18	0.35	0.47	0.5	1.26	2.52	3.6	1.26	2.52	3.6
2	0.35	0.7	0.66	0.84	2.52	5.04	6.2	2.52	5.04	6.2
3	0.53	1.06	0.89	1.07	3.78	7.56	8.74	3.78	7.56	8.74
4	0.7	1.41	1.23	1.27	5.04	10.08	11.27	5.04	10.08	11.27
5	0.88	1.76	1.58	1.59	6.3	12.6	13.8	6.3	12.6	13.6
6	1.06	2.11	1.93	1.94	7.56	15.11	16.33	7.56	15.11	16.33
7	1.23	2.46	2.29	2.29	8.82	17.63	18.85	8.82	17.63	18.85
8	1.41	2.81	2.64	2.64	10.08	20.15	21.39	10.08	20.15	21.39
9	1.58	3.17			11.34	22.67		11.34	22.67	
10	1.76				12.6			12.6		
11	1.93				13.85			13.85		
12	2.11				15.11			15.11		
13	2.29				16.37			16.37		
14	2.46				17.63			17.63		
15	2.64				18.89			18.89		
16	2.81				20.15			20.15		
17	2.99				21.41			21.41		
18	3.17				22.67			22.67		

Table B.2b Estimated natural frequencies of cable 3 (sag=0.2m) and full-scale for a wind speed of 40 m/s (5.7 m/s model).

	----> full-scale				---------->cable 3			------>		
		in-plane								
mode	out of plane	antisym	symmetric E [Pa] 7E10	symmetric E [Pa] 2.1E11	out of plane	in-plane antisym	in-plane symm	out of plane	in-plane antisym	in-plane symm
1	0.2	0.41	0.45	0.56	1.46	2.93	4.17			
2	0.41	0.82	0.64	0.82	2.93	5.85	7.18			
3	0.61	1.23	1.03	1.05	4.39	8.78	10.12			
4	0.82	1.64	1.43	1.44	5.85	11.7	13.04			
5	1.02	2.05	1.84	1.84	7.31	14.63	15.89			
6	1.23	2.45	2.25	2.25	8.78	17.56	18.14			
7	1.43	2.86	2.66	2.66	10.24	20.48	19.87			
8	1.64	3.27	3.07	3.07	11.7	23.41	22.09			
9	1.84	3.68			13.17	26.33				
10	2.05				14.63					
11	2.25				16.09					
12	2.45				17.56					
13	2.66				19.02					
14	2.86				20.48					
15	3.07				21.94					
16	3.27				23.41					
17	3.48				24.87					
18	3.68				26.33					

Table B.3 Estimated natural frequencies for cable 3 (sag=0.3m) for a "no wind" condition and a wind speed of 5.7 m/s (40m/s full-scale).

	----> full-scale (no wind)				---------->cable 3 (no wind)			------>cable 3 (wind = 5.7 m/s)		
		in-plane				in-plane			in-plane	
mode	out of plane	antisym	symmetric E [Pa] 7E10	symmetric E [Pa] 2E11	out of plane	antisym	symm	out of plane	antisym	symm
1					1.05	2.1	3	1.23	2.45	3.51
2					2.1	4.2	5.16	2.45	4.9	6.03
3					3.15	6.29	7.28	3.68	7.35	8.51
4					4.2	8.39	9.39	4.9	9.81	10.97
5					5.25	10.49	11.5	6.13	12.26	13.43
6					6.29	12.59	13.61	7.35	14.71	15.9
7					7.34	14.69	15.7	8.58	17.16	18.35
8					8.39	16.79	17.81	9.81	19.61	20.81
9					9.44	18.88		11.03	22.06	
10					10.49			12.26		
11					11.54			13.48		
12					12.59			14.71		
13					13.64			15.93		
14					14.69			17.16		
15					15.74			18.39		
16					16.79			19.61		
17					17.83			20.84		
18					18.88			22.06		

REFERENCES

Al-Bermani, F. G. A. and Kitipornchai, S. (1992) Nonlinear analysis of transmission towers. Eng. Struct., Vol. 14, No. 3. pp. 139-151.

American Society of Civil Engineers (1987) Wind Tunnel Model Studies of Buildings and Structures. ASCE Manuals and Reports on Engineering Practice No. 67. New York.

American Society of Civil Engineers (1991) Guidelines for Electrical Transmission Line Structural Loading. ASCE Manuals and Reports on Engineering Practice No. 74. New York.

American Society of Civil Engineers (1992) Design of Latticed Steel Transmission Structures. ASCE Standard 10-90. New York.

Armitt, J., Cojan, M., Manuzio, C. and Nicolini, P. (1975) Calculation of wind loadings on components of overhead lines. Proc. I.E.E., Vol. 122, No. 11, November. pp. 1247-1252.

Bachmann, H. et al (1995) Vibration Problems in Structures: Practical Guidelines. Birkhäuser Verlag Basel.

Ball, N. G., Rawlins, C. B. and Renowden, J. D. (1992) "Wind Tunnel Errors in Drag Measurements of Power Conductors". Journal of Wind Engineering and Industrial Aerodynamics, 41-44 (1992) 847-857. Elsevier.

Bayar, D. C. (1986) Drag Coefficients of Latticed Towers. Journal of Structural Engineering. ASCE. Vol. 112, No.2, February. p. 417-430.

Billinton, R. and Allan, R. N. (1986) Probabilistic Methodologies Used in the Assessment of Power System Reliability Evaluation. Proceedings of the First International Symposium on Probabilistic Methods Applied to Electric Power Systems. Toronto, Canada, 11-13 July. pp. 3-16.

Blessmann, J. (1986) Acidentes causados pelo vento. 3 ed. rev. ampl. Porto Alegre: Ed. Universidade / UFRGS. 8lp. (Série Engenharia Estrutural, 2).

Blessmann, J. (1990) Tópicos de Normas de Vento 2ed. Porto Alegre, Ed. da Universidade Federal do Rio Grande do Sul. (Série Engenharia Estrutural, 6).

Blessmann, J. (1995) O vento na engenharia estrutural. Porto Alegre: Ed. Universidade / UFRGS.

Blevins, R. D. (1979) Formulas for natural frequency and mode shapes. Van Nostrand Reinhold Company. New York.

Boudreaux, T. P. (1962) Hurricane Carla vs. Transmission Lines. Civil Engineering. April. pp. 70-72.

Brazilian wind code: NBR-6123 (1988). "Wind Forces on Buildings". Associação Brasileira de Normas Técnicas, Rio de Janeiro (In Portuguese).

British Code (1978) Code of Practice. Lattice Towers Loading. Third Draft.

Canadian Standards Association (1987) CAN/CSA-C22.3 No. 1-M87 Overhead Systems. April. 127 pages.

Castanheta, M. N. (1970) Dynamic Behaviour of Overhead Power Lines Subject to the Action of the Wind. CIGRE International Conference on Large High Tension Electric Systems. Paris. 24 August - 2 September. 15p. 22-08.

Clough, R. W. and Penzien, J. (1993) Dynamics of Structures. 2nd. Edition. McGraw-Hill, Inc.

Cojan, M. (1973) Étude de l'action du vent sur les conducteurs des lignes aériennes. R.G.E. - Tome 82 - No. 2 - Février. pp. 111-115.

Cohen, E. and Perrin, H. (1957) Design of multi-level guyed towers: wind loading. Proceedings of the ASCE. Journal of the Structural Division. September. No. 5. 29p.

Cook, N. J. (1985) The designer's guide to wind loading of building structures. Part 1. (Building Research Establishment). London, UK.

Cook, N. J. (1990) The designer's guide to wind loading of building structures. Part 2: Static Structures. (Building Research Establishment). London, UK.

Cooper, K. R. and Wardlaw, R. L. (1970) Preliminary wind tunnel investigation of twin bundle sub-conductor oscillations. National Aeronautical Establishment. Laboratory Tech. Report LTR-LA-41. Ottawa. 35p.

Cornell, C. A. (1986) Probabilistic Methods in Structural Design and Analysis. Proceedings of the First International Symposium on Probabilistic Methods Applied to Electric Power Systems. Toronto, Canada, 11-13 July. pp. 19-28.

Davenport, A. G. (1961) The Application of Statistical Concepts to the Wind Loading of Structures. Institution of Civil Engineers. Proceedings. Vol. 19, August. pp. 449-472.

Davenport, A. G. (1962) The response of slender, line-like structures to a gusty wind. In: ICE Proceedings, v. 23, Paper No. 6610, November. pp. 389-408.

Davenport, A. G. (1979) Gust response factors for transmission line loading. Proceedings of the Fifth International Conference on Wind Engineering. Colorado State University. July. Pergamon Press.

Davenport, A. G. (1987) "The Response of Slender Structures to Wind" In: The Application of Wind Engineering Principles to the Design of Structures. Lausanne, Switzerland, February 23-27, 1987.

Davenport, A. G. (1988) The response of tension structures to turbulent wind: the role of aerodynamic damping. In: 1st International Oleg Kerensky Memorial Conference on Tension Structures. June 20-22. London, England.

Davenport, A. G. (1993) "How Can We Simplify and Generalize Wind Loads?" Presented at the Third Asia-Pacific Symposium on Wind Engineering, Dec. 13-15, 1993, Hong Kong - Keynote Lecture.

Davenport, A. G. (1994) A simple representation of the dynamics of a massive stay cable in wind. Proceedings of the International Conference on Cable-Stayed and Suspension Bridges. Deauville, France. October 12-15. Vol. 2. pp. 427 - 438.

Davenport, A. G. and Isyumov, N. (1967) The Application of the Boundary Layer Wind Tunnel to the Prediction of Wind Loading. In: Proceedings of the International Research Seminar: Wind Effects on Buildings and Structures. Ottawa, Canada. September 11-15. Vol. 1. pp. 201-230.

Davenport, A. G., Surry, D., Georgiou, P. N. and Lythe, G. (1984). The response of transmission towers in hilly terrain to typhoon winds. Hurricane Alicia: one year later, Proceedings of the Specialty Conference, ASCE. Galveston, Texas. August 16-17. pp. 124-134.

Davis, D. A., Richards, D. J. W. and Scriven, R. A. (1963) Investigation of conductor oscillation on the 275kV crossing over the Rivers Severn and Wye. Proceedings I.E.E., vol. 110, No. 1, January. pp. 205-219.

Deutsches Institut für Normung (1969) Antennentragwerke aus Stahl. DIN 4131. Berlin. März.

Elashkar, I. and Novak, M. (1983) Wind tunnel studies of cable roofs. Proceedings of the Sixth International Conference on Wind Engineering. Gold Coast, Australia, March 21-25, Auckland, New Zealand, April 6-7.

Electric Power Research Institute (1979) Transmission Line Reference Book / Wind-Induced Conductor Motion. EPRI Research Project 792. Palo Alto, California.

Electric Power Research Institute (1986) Structural development studies at the EPRI transmission line mechanical research facility. Interim Report No.1: EPRI EL-4756, August. Sverdrup Technology, Inc. Tullahoma, Tennessee.

Engineering News-Record (1996) "Power market evolves". Cover Story. McGraw-Hill. ENR/March 11. pp.26-30.

Engineering Science Data Unit (1974) Characteristics of atmospheric turbulence near the ground. Data Item 74031. October.

Ferraro, V. (1983) Transverse Response of Transmission Lines to Turbulent Wind. Master of Engineering Thesis. The University of Western Ontario. London, Canada.

Georgiou, P. N. and Vickery, B. J. (1979) Wind loads on buildings frames. Proceedings of the Fifth International Conference on Wind Engineering, Fort Coolings, Colorado, USA, July. vol. 1. p. 421-433.

Goel, A. P. (1994) "Fatigue Problems in Power Transmission Lines" Canadian Civil Engineer, p. 7. February 1994.

Griffing, K. L. and Leavengood, D. C. (1973) Transmission Line Failures, Part I. Meteorological Phenomena - Severe Winds and Icing. Proceedings, IEEE Winter Power Meeting, Paper No.73 CH0816-9-PWR, pp. 5-14.

Groupe de Coordination des Textes Techniques (1980) Règles définissant les effets de la niege et du vent sur les constructions. Règles NV.65. Paris, Ed. Eyrolles, Juin.

Holdø , A. E. (1993). Reynolds number effects on lattice structures forming part of a wind tunnel model. Journal of Wind Engineering and Industrial Aerodynamics, 45. pp. 229-238.

Holmes, J. D. (1993a) Wind Engineering - AS1170 Review and ESAA Standards; Wind Velocities and Pressure. A Short Course on Design of Transmission Line Structures - Foundations. Centre for Transmission Line Structures. The University of Queensland, Australia. July 5-9. Vol. 2.

Holmes, J. D. (1993b) "Dynamic along-wind response of free-standing lattice towers" Proceedings of the 1st IAWE European and African Regional Conference. Guernsey, September 20-24, 1993.

Irvine, H. M. (1981) "Cable Structures". The Massachusetts Institute of Technology.

Jancauskas, E. D. and Sankaran, R. (1992) " The Coherence of Cross-Wind Velocity and Pressure on Two-Dimensional Rectangular Cylinders in Turbulent Flows". In: Proceedings of the 8th International Conference on Wind Engineering. London, Ontario, Canada. July. pp. 809 - 810.

Katoh, T., Momomura, Y., Izawa, K., Okamura, T. and Okhuma, T. (1995) Full-Scale Measurements of Wind-Induced Vibration of Transmission Line System in Mountaineous Area. Proceedings of the Ninth International Conference on Wind Engineering. New Delhi, India. January 9-13. Vol. I. pp. 433-444.

Kempner Jr., L., Stroud, R. C. and Smith, S. (1981) Transmission Line Dynamic/Static Structural Testing. Journal of the Structural Division, ASCE, Vol. 107. No.ST10, October. p. 1895-1906.

Kempner Jr., L. and Laursen, H. I. (1981) Measured Dynamic Response of a Latticed Transmission Line Tower and Conductors to Wind Loading. In: Pre-prints of the Fourth U.S. National Conference on Wind Engineering. Seattle, Washington. July 27-29. pp.348-355.

Kobayashi, H., Tomita, M., Kobayashi, M. and Koyama, M. (1994) "Wind Tunnel Test on 500KV Transmission Tower with Solid Web Brackets" (In Japanese) Journal of Wind Engineering. No. 58 January. p. 54-60.

Krishna, P. (1978) Cable-suspended roofs. McGraw-Hill, Inc.

Krishnasamy, S. (1981) Wind and Ice Loading on Overhead Transmission Lines. In: Pre-prints of the Fourth U.S. National Conference on Wind Engineering. Seattle, Washington. July 27-29. pp.356-364.

Larose, G. L. (1992) The Response of a Suspension Bridge Deck to Turbulent Wind: the Taut Strip Model Approach. Master of Engineering Science Thesis. The University of Western Ontario. London, Canada.

Leibfried, W. and Mors, H. (1964) The Hornisgrinde Testing Station (in German).

Liew, S. H. and Norville, H. S. (1989) Frequency Response Function of a Transmission Tower Subjected to Multiple Loadings. In: Proceedings of the Sixth U.S. National Conference on Wind Engineering. Houston, Texas. March 8-10. Vol. I. pp.B3-27 to B3-35.

Lo, D. L. C., Morcos, A. and Goel, S. K. (1975) Use of Computers in Transmission Tower Design. Journal of the Structural Division, Proceedings of the ASCE, Vol.101, No. ST7, July. pp. 1443-1453.

Lummis, J. and Fiss, R. A. (1971) Designing Power Lines for Flexible Supports. ASCE National Structural Engineering Meeting. Baltimore, Maryland. April 19-23.

Mac Donald, A. J. (1975) "Wind Loading on Buildings London, Applied Science Publishers, 1975.

Manuzio, C. (1967) Wind effects on suspended cables. Proceedings of the Second International Conference on Wind Engineering. Ottawa, Canada. September 11-15. V.1. p. 337-370.

Manuzio, C. and Paris, L. (1964) Statistical determination of wind loading effects on overhead line conductors. In: Conférence Internationale des Grands Réseaux Électriques à Haute Tension, CIGRE 64. Paris. June 1-10. paper 231.

Marjerrison, M. (1967) Electric Transmission Tower Design. ASCE Structural Engineering Conference. Seattle, Washington. May 8-12.

Marsh, C. (1968) A Guide to the Design of Aluminum Transmission Towers. ASCE Annual Meeting and National Meeting on Structural Engineering. Pittsburgh, Pa. September 30 - October 4.

Matheson, M. J. and Holmes, J. D. (1981) Simulation of the Dynamic Response of Transmission Lines in Strong Winds. Engineering Structures, Vol. 3. pp. 105-110.

Mehta, K. C. and Kadaba, R. (1989) Field Data Analysis of Electrical Conductor Response to Winds. Proceedings of the Sixth U.S. National Conference on Wind Engineering. Houston, Texas. March 8-10. Vol. I. pp. C2-1 to C2-9.

Mehta, K. C. and Norville, H. S. (1985) Electrical Transmission Line Structure Response to Wind. Proceedings of the First Asia Pacific Symposium on Wind Engineering. December 5-7. Roorkee, India. pp. 59-64.

Melbourne, W. H. (1982) "Comparison of Model and Full-Scale Tests of a Bridge and Chimney Stack". In: Proceedings of International Workshop on Wind Tunnel Modelling Criteria and Techniques in Civil Engineering Applications. Gaithersburg, Maryland, USA. April 14-16. pp. VI-6.

Monk, P. E. (1980) Structural Failure of Transmission Towers Under High Wind Loads. Dept. Mech. Eng. University of Canterbury. Christchurch, New Zealand. Master of Engineering Project Report.

Mounla, H. M. (1995) Shielding Forces on Structural Arrays in Turbulent Boundary Layers. PhD Thesis. University of Western Ontario. London, Canada.

Petersen, W. O. (1962) Design of EHV Steel Tower Transmission Lines. Journal of the Power Division, American Society of Civil Engineers, Vol. 88, No. PO1, May. pp. 39-65.

Praca, J. C. G. and Schilling, M. T. H. (1986) Brazilian Experience on Probabilistic Methods Applied to Network Planning. Proceedings of the First International Symposium on Probabilistic Methods Applied to Electric Power Systems. Toronto, Canada, 11-13 July. p. 231-240.

Randall, R. B. (1987) Frequency Analysis. Brüel & Kjær. Denmark.

Roberts, J. B. and Surry, D. (1973) Coherence of Grid Generated Turbulence. In: Journal of the Engineering Mechanics Division, ASCE, vol. 99, No. EM6. December. pp. 1227-1245.

Sachs, P. (1978) Wind forces in engineering. 2nd edition. Pergamon Press.

Saffir, H. S. (1991) Hurricane Hugo and Implications for Design Professionals and Code-Writing Authorities. Journal of Coastal Research, SI #8, 25-32. Fort Lauderdale, Florida.

Schlichting, H. (1979) Boundary-Layer Theory. McGRAW-HILL, INC. Seventh Edition.

Scruton, C. and Rogers, E.W.E. (1971) "Steady and Unsteady Wind Loading of Buildings and Structures", Phil. Trans. Roy. Soc. London, A269, pp. 353-383.

Shan, L., Jenke, L. M. and Cannon Jr., D. D. (1992) Field Determination of Conductor Drag Coefficients. Journal of Wind Engineering and Industrial Aerodynamics, 41-44. p. 835-846.

Shichiri, Y. (1971) Wind withstanding design for transmission line tower. Proceedings of the Third International Conference on Wind Engineering. Tokyo, Japan. pp. 451-456.

Simpson, A. (1965) Aerodynamic instability of long-span transmission lines. Proceedings I.E.E., Vol. 112, No. 2, February.

Smith, J. W. (1988) Vibration of Structures: applications in civil engineering design. Chapman and Hall Ltd.

Sparling, B. F. (1995) The Dynamic Behavior of Guys and Guyed Masts in Turbulent Winds. PhD Thesis. The University of Western Ontario. London, Canada.

Tabatabai, M., Krishnasamy, S. G., Meale, J. and Cooper, K. R. (1992) Response of smooth body, trapezoidal wire overhead (compact) conductors to wind loading. Journal of Wind Engineering and Industrial Aerodynamics, 41-44. p. 825-834.

Tanaka, H. (1988) Similitude and Modelling in Wind Tunnel Testing of Bridges. International Colloquium on Bluff Body Aerodynamics and its Applications. Kyoto, Japan. Japanese Journal of Wind Engineering. No. 37. October. pp.429-446.

Thomson, W. T. (1993) Theory of vibration with applications. 4th Edition. Prentice-Hall.

Tracy, T. M. and McDonald, J. R. (1989) "Mitigation of Damages to Electric Utilities due to High Winds". ASCE Journal of Aerospace Engineerin„ Vol. 2, No. 2, April. pp. 97-101.

Vickery, B. J. (1981) Wind induced vibrations of elevator cables in a partially enclosed shaft. In: "Designing With the Wind". Symposium at C.S.T.B., Nantes, June 1981. pp. VII-3-1, 19.

Vickery, B. J. (1982) The aeroelastic modelling of chimneys and towers. Workshop on Wind Tunnel Modeling, Gaithersburg, Maryland, April 14-16. pp. IV-2.

Vickery, B. J. (1992) Advanced Structural Dynamics I. (Engineering Science 610) Course Notes. The University of Western Ontario, London, Canada.

Vickery, B. J. (1995) The response of chimneys and tower-like structures to wind loading. A State of the Art in Wind Engineering. Ninth International Conference on Wind Engineering. New Delhi, India. Davenport Sixtieth Birth Anniversary Volume. pp. 205-233.

Vilar, J. I. and López, A. (1995) Terrain Related Parameters for the Evaluation of Turbulence and their Application to the Response of Transmission Structures. Proceedings of the Ninth International Conference on Wind Engineering. New Delhi, India. January 9-13. Vol. I. pp.15-26.

Walker, H. B. (Ed.) (1975) "Wind Forces on Unclad Tubular Structures" CONSTRADO, Vol.1, Jan. 1975. 19p.

Wardlaw, R. L., Cooper, K. R., Ko, R. G. and Watts, J. A. (1975) Wind Tunnel and Analytical Investigations into the Aeroelastic Behaviour of Bundled Conductors. IEEE Transactions on Power Apparatus and Systems, vol. PAS-94, no.2, March/April.

Wen, Y. K. (1968) Dynamic Response of Transmission line system to turbulent wind load. The University of Western Ontario, Engineering Science Research Report. BLWT - 9 -68.

Whitbread, R. E. (1979) The influence of shielding on the wind forces experienced by arrays of lattice frames. Proceedings of the Fifth International Conference on Wind Engineering, Fort Collins. Colorado, USA, July, vol. 1. p. 405-420.

Wind Engineer (1994) Periodical publication of the Wind Engineering Research Council, Inc. Notre Dame, IN, USA. Summer edition. p. 5.

Yu, P., Desai, Y. M., Shah, A. H. and Popplewell, N. (1993a) "Three-Degree-of-Freedom Model for Galloping. Part I: Formulation". ASCE Journal of Engineering Mechanics, Vol. 119, No. 12, December. pp. 2404-2425.

Yu, P., Desai, Y. M., Shah, A. H. and Popplewell, N. (1993b) "Three-Degree-of-Freedom Model for Galloping. Part II: Solutions". ASCE Journal of Engineering Mechanics, Vol. 119, No. 12, December. pp. 2426-2448.

Zar, M. and Arena, J. R. (1979) "Towers and Transmission Pole Structures". Structural Engineering Handbook, Section 24. Edited by E. H. Gaylord, Jr. and C. N. Gaylord. McGraw-Hill Book Co.

Zetlin, L. and Lew, I. P. (1979) "Suspension Roofs". Structural Engineering Handbook, Setion 21. Edited by E. H. Gaylord, Jr. and C. N. Gaylord. McGraw-Hill Book Co.